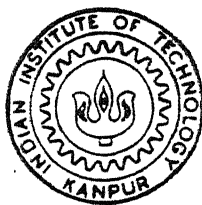


STUDIES ON NON PARALLEL AND NON CIRCULAR TWIN JETS

by
A. SOLAIAPPAN



DEPARTMENT OF AEROSPACE ENGINEERING
INDIAN INSTITUTE OF TECHNOLOGY KANPUR
MAY, 1994

AE
1994
M
SOL
STU

STUDIES ON NON PARALLEL AND NON CIRCULAR TWIN JETS

A thesis submitted
in partial fulfilment of the requirements
for the degree of

MASTER OF TECHNOLOGY

by

A. SOLAIAPPAN

to the

Department of Aerospace Engineering,
Indian Institute of Technology, Kanpur, India.

May, 1994

TH
629.120072
Sv 412

AE-1994-M-SEL-STV

26 MAY 1994/AE
CENTRAL LIBRARY
I. I. T., KANPUR


Acc. No. A. 117799

CERTIFICATE

It is certified that the work contained in the thesis entitled "**STUDIES ON NON PARALLEL AND NON CIRCULAR TWIN JETS** ", by **A. Solaiappan**, has been carried out under my supervision and that this work has not been submitted elsewhere for a degree.

Kanpur

May, 1994


(**E. Rathakrishnan**)
Thesis Supervisor
Department of Aerospace Engineering
Indian Institute of Technology
Kanpur-208 016, India

to my beloved father

ABSTRACT

This thesis consists of experimental studies on flow field of twin jets issuing from two kinds of devices, namely twin axisymmetric nozzles and sharp edged elliptic slots.

The first part of the thesis describes studies on non parallel axisymmetric twin jets. The nozzles of exit diameter (D) 3.2 mm are set on a common end wall with their axes intersecting each other at half angles (α) of 0° , 5° , 10° and 15° . The centre to centre spacing (S) of the nozzles, non dimensionalized, as S/D , is around 3.1. The jet exit Mach numbers (M_e) studied are 0.2, 0.4, 0.6, 0.8 and 1.0. The nozzles are operated at under-expansion ratios (r) ranging from 1.4 to 2.0. The results indicate that the near field characteristics are strongly influenced by α , M_e and r . However, the potential core of the individual jets are only marginally influenced by these parameters. The far field characteristics of the twin jet flow field appear to be almost independent of α , M_e and r . The merging and combining of the jets are influenced by these parameters. The cross section of the jet just downstream of the combining point is approximately elliptic and the axis switching phenomenon normally associated with non circular jets is observed in the combined jet flow. Entrainment of the ambient fluid is found to be more in the case of twin parallel jets ($\alpha = 0^\circ$). The entrainment decreases with increasing α .

The second part of the thesis describes experimental studies on twin elliptic jets issuing from sharp edged elliptic slots with non dimensional centre to centre spacing (S/D_e) of 1.0. The aspect ratio (defined as the ratio of major axis to minor axis of the elliptic slots) of the jets studied are 1:1, 2:1, 2.5:1 and 4:1. The jet exit Mach numbers studied are 0.1, 0.2, 0.4 and 0.6. The results indicate that the initial region of the flow field is strongly influenced by the jet exit Mach number M_e and the aspect ratio of the elliptic slot. The potential core length of the individual jets decreases with increasing aspect ratio. The cross section of the jet just downstream of the combining point has a diamond like shape which gradually transforms into elliptic shape with increasing downstream distance. For all the cases studied the entrainment is found to be almost the same.

ACKNOWLEDGEMENT

I wish to acknowledge with sincere gratitude the invaluable guidance rendered by Dr. E. Rathakrishnan during the course of this thesis work. I would like to thank Mr. S. Elangovan, for his multifarious help in literature survey, experiments and for patiently answering many of my questions (some of them silly); without whose helpful discussions this work would not have been a success.

I gratefully acknowledge the interest and helpful comments of my friends ksri, ignatius, himanshu and akhilesh raghuvanshi during my thesis work. My special thanks to venky and ramesh for their help while preparing this report. I want to express my special thanks to thalaivar, immi, kasi, ragu, uma, palani, rajesh, arumugam, guru, victor, siva, periappa, justin thomas, kuppi, whiteford and subiksha who made my stay in this institute enjoyable.

I would also like to thank Mr. Chauhan, Mr. Shishupal and Mr. Bhantu of the High Speed Laboratory, and Mr. Bhattacharya of the work shop for all their help during the experimental work.

Finally, I owe a debt of gratitude to all my family members for their encouragement, support, love, affection and blessing showered on me throughout my studies.

A. Solaiappan

Contents

I STUDIES ON NON PARALLEL TWIN CIRCULAR JETS

xii

1	INTRODUCTION	1
1.1	Free jets	1
1.1.1	Single jet	1
1.1.2	Non parallel twin jets	3
1.2	Literature review	4
1.3	Applications	7
1.4	Aim of the present investigation	8
2	EXPERIMENTAL FACILITY AND PROCEDURE	10
2.1	Experimental apparatus	10
2.2	Experimental procedure	12
2.2.1	Data accuracy	13
3	RESULTS AND DISCUSSIONS	15
3.1	Non dimensionalization	16
3.2	Equations of motion	16
3.3	Centreline velocity decay	17
3.3.1	General features of the centreline velocity/pressure decay	19
3.4	Mean velocity profiles	22

3.5	Potential core length for under-expanded jets	23
3.6	Merging and Combining points	26
3.6.1	Subsonic jets	26
3.6.2	Sonic and Under-expanded sonic jets	26
3.7	Similarity profile	28
3.8	Iso Mach lines	29
3.9	Spread rate	30
3.10	The Integral momentum equation	30
3.11	Variation of entrainment with axial distance	32
3.12	Constant velocity contours	32
4	SUMMARY AND CONCLUSIONS	34
4.1	Suggestions for future work	36
II	STUDIES ON PARALLEL TWIN ELLIPTIC JETS	69
5	INTRODUCTION	71
5.1	Literature review	72
5.2	Applications	74
5.3	Aim of the present investigation	75
5.4	Experimental set-up and procedure	75
6	RESULTS AND ANALYSIS	76
6.1	Length scale and Velocity scale	76
6.2	Centreline jet decay	77
6.3	Mean axial velocity profiles	78
6.3.1	Potential core	79
6.4	Shear layers	80

6.5	Three dimensional half width spread	81
6.6	Conservation of momentum	81
6.7	Entrainment	81
6.8	Mixing flow cross sectional Contours	82
6.9	Jet width	82
6.10	Iso Mach lines	83
6.11	Similarity profiles	83
7	CONCLUSIONS	84
7.1	Suggestions for future work	85

List of Figures

I STUDIES ON NON PARALLEL TWIN CIRCULAR JETS

1.a	Experimental set-up	39
1.b	Notation for the Flow field Co-ordinate System	40
1.c	Under-expanded Jets	41
1.d	Pitot Probe	41
2.a1	Centreline Velocity Decay ($\alpha = 0^\circ$)	42
2.a2	Centreline Pressure Decay ($\alpha = 0^\circ$)	42
2.b1	Centreline Velocity Decay ($\alpha = 5^\circ$)	43
2.b2	Centreline Pressure Decay ($\alpha = 5^\circ$)	43
2.c1	Centreline Velocity Decay ($\alpha = 10^\circ$)	44
2.c2	Centreline Pressure Decay ($\alpha = 10^\circ$)	44
2.d1	Centreline Velocity Decay ($\alpha = 15^\circ$)	45
2.d2	Centreline Pressure Decay ($\alpha = 15^\circ$)	45
3.a1	Mean Velocity profiles at various X/D ($\alpha = 5^\circ$) in XZ plane	46
3.a2	Mean Velocity profiles at various X/D ($\alpha = 5^\circ$) in XY plane	46
3.b1	Isometric View of Velocity profiles in XZ plane [$M_e = 0.2, \alpha = 10^\circ$]	47
3.b1	Isometric View of Velocity profiles in XY plane [$M_e = 0.2, \alpha = 10^\circ$]	48
3.c	Mean Velocity profiles at various X/D ($\alpha = 15^\circ$)	49

4.a	Velocity profiles in the Potential Core Region ($\alpha = 0^\circ$)	50
4.b	Velocity profiles in the Potential Core Region ($\alpha = 10^\circ$)	50
4.c	Velocity profiles in the Potential Core Region ($\alpha = 15^\circ$)	51
4.d	Velocity profiles in the Potential Core Region (Single jet)	51
5.a1	Similarity profiles (parallel jet) in XY plane [$X/D = 30.0$]	52
5.a2	Similarity profiles (parallel jet) in XZ plane [$X/D = 30.0$]	52
5.b1	Similarity profiles ($\alpha = 5^\circ$) in XZ plane [$M_e = 0.2$]	53
5.b2	Similarity profiles ($\alpha = 5^\circ$) in XZ plane [$M_e = 0.6$]	53
5.c1	Similarity profiles ($\alpha = 5^\circ$) in XZ plane [$r = 1.1$]	54
5.c2	Similarity profiles ($\alpha = 5^\circ$) in XZ plane [$r = 1.7$]	54
5.d1	Similarity profiles ($\alpha = 5^\circ$) in XZ plane [$X/D = 30.0$]	55
5.d2	Similarity profiles ($\alpha = 5^\circ$) in XZ plane [$X/D = 40.0$]	55
5.e	Similarity profiles ($\alpha = 10^\circ$) in XZ plane [$M_e = 0.2$]	56
5.f	Similarity profiles ($\alpha = 15^\circ$) in XZ plane [$M_e = 0.2$]	56
6.a1	Iso Mach Number profiles [$\alpha = 5^\circ, M_e = 0.2$]	57
6.a2	Iso Mach Number profiles [$\alpha = 5^\circ, M_e = 1.0$]	58
6.a3	Iso Mach Number profiles [$\alpha = 5^\circ, r = 1.7$]	59
6.b	Iso Mach Number profiles [$\alpha = 10^\circ, M_e = 0.2$]	60
6.c	Iso Mach Number profiles [$\alpha = 15^\circ, M_e = 0.2$]	61
7.a	Variation of Half Width with X/D for $M_e = 0.2$ in XZ plane	62
7.a	Variation of Half Width with X/D for $M_e = 0.2$ in YZ plane	62
8.	Momentum Flux along the Axial Direction ($M_e = 0.2$)	63
9.	Variation of Entrainment with Axial Distance ($M_e = 0.2$)	63
10.a	Constant Velocity Contours ($\alpha = 5^\circ$)	64
10.b	Constant Velocity Contours ($\alpha = 10^\circ$)	65
10.c	Constant Velocity Contours ($\alpha = 15^\circ$)	66
11	Schlieren Photographs	67

II STUDIES ON PARALLEL TWIN ELLIPTIC JETS 65

1.a	Twin Elliptic Orifice - Photograph	90
1.b	Centreline Velocity variation ($AR = 2.5$)	91
1.c	Centreline Velocity variation ($M_e = 0.2$)	91
2.a1	Mean axial Velocity profiles in XY plane ($AR = 2, M_e = 0.2$)	92
2.a2	Mean axial Velocity profiles in XZ plane ($AR = 2, M_e = 0.2$)	92
2.b1	Mean axial Velocity profiles in XY plane ($AR = 2.5, M_e = 0.1$)	93
2.b2	Mean axial Velocity profiles in XZ plane ($AR = 2.5, M_e = 0.1$)	93
2.b3	Mean axial Velocity profiles in XY plane ($AR = 2.5, M_e = 0.6$)	94
2.b4	Mean axial Velocity profiles in XZ plane ($AR = 2.5, M_e = 0.6$)	94
2.c1	Mean axial Velocity profiles in XY plane ($AR = 4, M_e = 0.2$)	95
2.c2	Mean axial Velocity profiles in XZ plane ($AR = 4, M_e = 0.2$)	95
3.a1	Growth of Iso spread lines in XZ plane ($AR = 2, M_e = 0.2$)	96
3.a2	Growth of Iso spread lines in XY plane ($AR = 2, M_e = 0.2$)	96
3.b1	Growth of Iso spread lines in XZ plane ($AR = 2.5, M_e = 0.2$)	97
3.b2	Growth of Iso spread lines in XY plane ($AR = 2.5, M_e = 0.2$)	97
3.b3	Growth of Iso spread lines in XZ plane ($AR = 2.5, M_e = 0.4$)	98
3.b4	Growth of Iso spread lines in XY plane ($AR = 2.5, M_e = 0.6$)	98
3.c1	Growth of Iso spread lines in XZ plane ($AR = 4, M_e = 0.2$)	99
3.c2	Growth of Iso spread lines in XY plane ($AR = 4, M_e = 0.2$)	99
4.a	Three Dimensional half width spread ($AR = 2, M_e = 0.2$)	100
4.b1	Three Dimensional half width spread ($AR = 2.5, M_e = 0.2$)	101
4.b2	Three Dimensional half width spread ($AR = 2.5, M_e = 0.4$)	102
4.b3	Three Dimensional half width spread ($AR = 2.5, M_e = 0.6$)	103
4.c	Three Dimensional half width spread ($AR = 4, M_e = 0.2$)	104
5.a	Momentum flux for all Mach numbers ($AR = 2.5$)	105
5.b	Momentum flux for all aspect ratios	105

6.a	Variation of entrainment with axial location ($AR = 2.5$)	106
6.b	Variation of entrainment with axial location ($M_e = 0.2$)	106
7.a	Constant velocity contours ($AR = 2, M_e = 0.2$)	107
7.b1	Constant velocity contours ($AR = 2.5, M_e = 0.2$)	108
7.b2	Constant velocity contours ($AR = 2.5, M_e = 0.4$)	109
7.b3	Constant velocity contours ($AR = 2.5, M_e = 0.6$)	110
7.c	Constant velocity contours ($AR = 4, M_e = 0.2$)	111
8.a1	Comparison of half width velocity in XY plane	112
8.a2	Comparison of half width velocity in XZ plane	112
8.b	Half spread lines in XZ and XY plane	113
9.a	Iso Mach profiles ($AR = 2, M_e = 0.2$)	114
9.b1	Iso Mach profiles ($AR = 2.5, M_e = 0.1$ & 0.6)	115
9.b2	Iso Mach profiles ($AR = 2.5, M_e = 0.2$)	116
9.c	Iso Mach profiles ($AR = 4, M_e = 0.2$)	117
10.a	Similarity profiles for AR 1:1	118
10.b	Similarity profiles for AR 2:1	118
10.c	Similarity profiles for AR 2.5:1	119
10.d	Similarity profiles for AR 4:1	119

Part I

**STUDIES ON NON PARALLEL
TWIN CIRCULAR JETS**

NOMENCLATURE

$C.P$	Combining point of the jets	X	Coordinate perpendicular to exit plane
D	Nozzle exit diameter	X_{cp}	Axial location of combining point (C.P)
$G.P$	Geometric intersection point	X_{gp}	Location of geometric intersection point
J_o	Momentum flux at nozzle exit	X_p	Location of peak pressure along the
J	Momentum flux at jet cross section		centreline
M	Mach number in the flow field	X_l	$X_{gp} - X_{cp}$
M_e	Nozzle exit Mach number	X_{mp}	Location of merging point
$M.P$	Merging point	Y	Transverse co-ordinate parallel to
Q_o	Mass flow rate at nozzle exit		plane of symmetry
Q	Mass flow rate in the X-direction	$Y_{0.5}$	Half width of jet in Y direction
p_a	Ambient pressure	Z	Spanwise co-ordinate perpendicular
p_c	Total pressure along centreline		plane of symmetry
p_e	Static pressure at nozzle exit	$Z_{0.5}$	Half width of jet in Z direction
p_m	Peak total pressure along the centreline		
p_t	Total pressure in the flow field		
p_{tm}	Centreline total pressure	α	Half angle of intersection
p_o	Stagnation pressure	γ	Specific heat ratio of fluid
r	Degree of underexpansion = p_e/p_a	ν	Kinematic viscosity of fluid
r_p	Stagnation pressure ratio = p_o/p_a	η_y	Similarity length scale $\frac{Y}{Y_{0.5}}$
S	Nozzle spacing (centre to centre)	η_z	Similarity length scale $\frac{Z}{Z_{0.5}}$
U	Streamwise mean velocity	ρ	Mass density of fluid
U_c	Velocity along centreline		
U_m	Local maximum velocity		
U_o	Velocity at nozzle exit		

move on !

*limitless is the universe in which we live. there still are
discoveries to be made, beauty to be created, secrets to be probed.
what part are you going to play in the ever-unfolding cosmic plan?*

Chapter 1

INTRODUCTION

“turbulent motion. It remains to call attention

to the chief outstanding difficulty of our subjects”

– Horace Lamb, Hydrodynamics, 1932.

1.1 Free jets

Jet is a free shear layer driven by means of favourable pressure gradients spreading at a half angle of around 12° . In the case of jet there exists a flow field establishment region immediately downstream of the nozzle exit where the flow experiences a sudden change in boundary conditions from a confined flow to a free shear layer flow. The emerging jet carries with it some of the surrounding fluid which was originally at rest, because of the velocity gradient at the interface between the jet and the surroundings. This addition of dragged mass from the surroundings is called **entrainment**.

1.1.1 Single jet

The basic feature of the free jet is that the momentum is conserved at any cross section, since while the velocity keeps on decreasing, mass is added to the system keeping the mo-

momentum constant. The following regions are classified based on the flow field development of a free jet.

- **Potential core** The region close to the nozzle exit where the exit velocity is preserved is known as the potential core. The jet mixes with the surrounding fluid forming turbulent shear layer all around. The turbulence created by the jet penetrates inward in to the core region, thereby reducing the thickness of the central region of potential flow. The end of potential core of the jet is situated at that axial section where the inner boundary of the annular shear layer meets the jet axis.
- **Transition decay** The region, where the velocity decay is dependent upon orifice configuration.
- **Fully developed decay** The region, where the flow field becomes independent of the orifice geometry.

The jet Mach number (M_e) is defined as the ratio between the nozzle exit velocity to the ambient sound speed. Based on M_e , jet issuing from circular convergent nozzles may be divided in to three main classes, namely, (a). Subsonic, for which the jet exit Mach number (M_e) is less than unity. (b). Correctly expanded sonic, for which $M_e = 1$. This corresponds to the critical stagnation pressure ratio r_p of 1.89. and (c). Under-expanded sonic jet, where the exit static pressure (p_e) is higher than the back pressure (p_a). This corresponds to r_p values greater than 1.89. The jet Mach number M_e remains constant at unity. Since the expansion inside the nozzle is insufficient to reach the back pressure, expansion fans form at the nozzle exit plane. Under expanded jets are often encountered in practical situations, such as industrial applications and the rocket exhaust at higher altitudes.

1.1.2 Non parallel twin jets

Turbulent mixing of two jets issuing from two nozzles at different intersecting angles is one of the most important problems of turbulent shear flows. The above mechanism of turbulent mixing, although studied for over thirty years, has recently received a good deal of attention. The main objectives in the jet flow studies are (1) Understanding of jet propagation and (2) Control of jets. One of the main objectives of jet flow control is mixing enhancement. This can be achieved either actively or passively. Passive control techniques do not require any auxiliary energy for jet control, and may be achieved using three dimensional nozzles namely Rectangular, Square, Triangular, Diamond, Elliptic *etc.* The present study is an attempt at passive control of axisymmetric jets.

Why do we go for Nonparallel twin axisymmetric jets ?

- * axisymmetric jets are easy to fabricate and most commonly found.
- * twin jets (Multi jets) are used for increasing the entrainment and noise reduction. The increased circumferential area of the twin jet compared to an equivalent single jet leads to increased entrainment.
- * in many practical applications like combustors, furnaces etc, early combining and mixing of two different streams close to the nozzle exit is the primary requirement. This type of jet mixing is best described by non parallel jet flow field.

The twin turbulent jets are characterized by three distinct regions along the X - axis. These regions are shown in Fig 1.b and classified as follows.

1. **Converging region :** The individual jets entrain the ambient fluid which leads to subatmospheric conditions between the inner shear layers of the jets. Due to this the jets are attracted towards each other and the inner layers start merging. This merging process is influenced by the intersecting angle α .

2. **Mixing region :** In this region, the inner layers mix up thoroughly and the individual axes of the jets shift to the nozzle centreline. The two jets combine completely and the axis of the combined jet coincides with the nozzle centreline.
3. **Combined flow region :** In this region, the combined jet propagates attaining self similarity. The combined jet need not be axisymmetric.

1.2 Literature review

Many investigators have studied twin parallel jets. But studies on non parallel jets are very limited.

Becker *et. al.* [1] studied the mixing in the interaction zone of two round free jets with nozzle axes intersecting at half angles of 15, 30 and 45 deg, by smoke scattered light technique. The correlation function between the concentration fluctuations associated with the two nozzle streams was determined. The fields of mean concentration and concentration fluctuation intensity were mapped. The implications of the results for the process involving chemical reactions were examined.

Elbanna *et. al.* [2] studied experimentally the flow field generated by two equal two-dimensional turbulent plane parallel jets issuing from parallel slot nozzles. The centre line velocity decayed at the same rate as for a single jet, but with higher values of U_m/U_o . The maximum shear stress had nearly the same value as that in the single jet. They also examined [3] the interception of two two-dimensional jets. Four interception angles of 30, 60, 80 and 100 deg were studied. The static pressure in the combined jet was found to be negative and increased gradually with down stream distance. The distribution of the three components of turbulent velocity fluctuations showed different behaviour than that for a single jet.

Murai *et. al.* [4] studied the confluence of two two-dimensional jets issuing from a common wall. Their work was confined to the calculation of axial momentum and energy

flux.

Okamoto *et. al.* [5] presented an experiment of investigation on the intersection of twin turbulent circular jet. The position of maximum velocity of the twin jet shifted from the nozzle axis to the mid point between the jets. The decay of the maximum velocity of the twin jet agreed with that of a single jet. The static pressure recovered to the ambient pressure faster than that of a single jet. The twin jet interacted and joined in the form of an ellipse at the down stream distance and became close to a circle at far down stream distance.

Rajaratnam *et. al.* [7] presented the results of an experimental study on intersecting circular turbulent jets of equal momentum flux, with the angle of intersection increasing from 30 to 120 degrees. The effect of increased pressure near the geometric intersection point was studied in the development zone. They found the growth rate of the resulting jet in the vertical direction was about three times that in the transverse direction in the combined flow. In the far region, the resulting jet tended to become axisymmetric but still grew at about 1.5 times the rate of the corresponding single circular jet. They also developed some useful correlations for the velocity and pressure.

Rho *et. al.* [8] measured the turbulent characteristics of a cross jet mixing flow after the geometric cross point of the centrelines of the two nozzles. The (ventilated) flow was generated by two circular nozzles and the cross angle of the jets was fixed at 45° with respect to each other. The flow field was strongly influenced by cross point stagnation region, which created an elliptical jet region with unusual turbulent properties (major axis was along 'Y' direction). They correlated the mean velocity profiles with semiempirical equations based on the local half-widths of the jet. Rho *et. al.* [9] conducted another experiment on the structure of a turbulent cross jet corresponding to cross angle variation. In this experimental study, emphasis was placed on the measurement of the structure of a turbulent mixing flow depending upon the cross angle ($2\alpha = 35^\circ$ to 55°). The mean and fluctuating velocities and Reynolds stress distributions were analyzed and compared with

semi-empirical equation for free jets. The cross jet of the mixing flow after collision was formed as an ellipse near the cross point and the contour of the section agreed well with their modified formula. The intensities of turbulence on the centerline were quite high. The maximum value of u' was 28% and 20% for v' and w' respectively.

Tanaka *et. al.* [10], [11] investigated the flow field of a dual jet issuing from two parallel slot nozzles set on a common end wall. The effect of distance between the nozzles on the combined flow region of the dual jet was investigated by measuring the static pressure, mean and fluctuating velocities of the flow. The individual jets attracted each other and the axis of each jet coincided with the arc of a circle. A relation involving the radius of arc, nozzle width and the nozzle distance was established. Decay of the velocity was stronger than that of a single jet, and the rate of decrease was lesser for larger values of S/D . The velocity profiles of the combined flow were similar and agreed well with the single jet, but the turbulence intensities showed a different property from those of a single jet. The width of the combined jet spread linearly in the downstream direction and increased with the distance between the two nozzles. The momentum flux ($\rho U^2 D$) of the combined jet at each section was conserved for $S/D < 8.5$ but decreased with $S/D > 8.5$. This decrease of momentum was due to the static pressure recovery from negative to the atmospheric pressure. But the total momentum was nearly constant in each cross section.

A perusal of the available literature on parallel and non-parallel twin jets shows that most of them are on low subsonic jets ($M = 0.1$ to 0.2). Studies on high speed jets, particularly, on intersecting twin jets is almost absent. With the increasing interest in scramjets and supersonic combustion, mixing of high speed jets assumes lot of importance. Moreover the shock shear layer interaction involved in this type of flow fields is too complicated to be studied analytically. Another important aspect of high speed jets is the shock induced noise. studies have been made on nozzle geometry effects on supersonic jet interaction [14] with particular emphasis on nozzle spacing and screech noise (high intensity narrow-band noise) suppression. Apart from nozzle spacing, non parallel nature of the jets also may be

expected to influence such flow fields.

Further, no previous study has been reported on the combined effect of intersecting angle and pressure ratio on the twin jet flow field. In many practical situations the flow field is generated by jets issuing from nozzles set on a common end wall (unventilated) as in the case of cluster nozzles in Rocket exhaust systems and multi jet configurations in V/STOL aircrafts. The multi jet arrangements in V/STOL aircrafts are designed to minimize suck down, induced moments and reingestion of hot exhaust into the engine intake. Sherrieb [15] made an extensive study on various configurations and concluded that four jet arrangement was an attractive solution. He also observed that deflecting the jets toward and away from each other was beneficial. Thus the practical importance of non parallel jets, particularly, of unventilated jets needs no further emphasis. The suppression of screech in the case of jet engine exhausts is one problem which has attracted many researchers. The nozzle spacing has found to be an important parameter [14] in such problem. Hence it is surprising that no systematic study has been made on unventilated intersecting jets. For such flow fields the description of mean flow field itself can be a much rewarding exercise. Hence it was felt that, the study of intersecting twin jet propagation for various pressure ratios would yield many interesting results and the measurements would serve as a data base for future modelling studies.

1.3 Applications

Jet flow systems are essential components in many industrial flow circuits. Jet flows are used for heat and mass exchange, for aerodynamic stabilization of strips, plates, blocks etc, boundary layer control in aerofoil sections, jet spray painting at low velocities, removal of thin surface layers.

The interaction of parallel and non parallel jets are of great importance in engineering field. While some of the best known and most challenging applications lie in the field of

Aerospace engineering. They find application in many other fields also. Some of these applications are listed below.

- ⊙ In the process industry where the mixing of two or more gases are encountered frequently.
- ⊙ To mix the dry cooling air with the wet air in a hybrid cooling tower to avoid the condensation plume of the cooling tower.
- ⊙ Jet flows from the nozzle exhaust of jet engines, rocket engines (with cluster nozzle), missiles and boosters.
- ⊙ Mixing of fuel and oxidiser in the combustion chambers and wherever the mixing of two fluid streams are required.

1.4 Aim of the present investigation

An experimental study of two circular jets issuing from contoured convergent nozzles at different angles, emanating from a common end plate have been carried out. Three interception angles of $\alpha = 5^\circ$, 10° and 15° are studied. This preliminary investigation has been carried out for different Mach numbers ($M = 0.2, 0.4, 0.6, 0.8, 1.0$) and various under-expansion ratios ($r = 1.0, 1.1, 1.4, 1.7$)

The present investigation is mainly aimed at studying the following aspects of the twin jet flow field.

1. effect of Mach number on the distribution of mean velocity,
2. effect of under-expansion ratio on the distribution of mean velocity,
3. centreline velocity decay for different cross angles and Mach numbers,
4. centreline pressure decay in the case of under-expanded jets,

5. shift of combining point from geometric intersection point for different Mach numbers and angles,
6. change in the value of centerline maximum pressure with Mach number, and angle,
7. spread rate after the combining point in the Z and Y directions,
8. similarity profiles in the combined flow region,
9. influence of angle of intersection on entrainment,
10. verification of the conservation of momentum in the case of twin intersecting jets,
11. location of attainment of axisymmetry of the combined flow.

Chapter 2

EXPERIMENTAL FACILITY AND PROCEDURE

Mankind will not remain on the earth forever, but in the pursuit of light and space, we will, timidly at first, overcome the limits of the atmosphere and then conquer all the area around the Sun

– Tsiolkovsky's letter to an Engineer, 1911

2.1 Experimental apparatus

The experimental apparatus used for this study is shown schematically in figure 1.a Cross jet experiments were carried out with jet issuing from two axisymmetric, contoured, circular nozzles of 3.2 mm exit diameter with centre to centre nozzle spacing (S) of 10 mm. The nozzles were drilled in 22 mm thick perspex plate (nozzle block) with smooth surface finishing. The nozzle axes are coplanar and intersect in the downstream direction; that is, the jets are obliquely oriented towards each other. Different nozzle blocks were fabricated for each angle of intersection (α) studied. The half angles (α) chosen for the present study are 5, 10 and 15 degrees.

The nozzles were made at the workshop of Aerospace Engineering Department and the experiments were carried out using internal flow facility at the High speed aerodynamics laboratory, IIT Kanpur. The compressed air supply system was driven by a 3-phase 150 hp induction motor. This air was cooled by passing through an after cooler and then fed to a prefilter to remove solid contaminants and oil droplets. The prefilter consists of porous stone candles which perform the filtering action. After passing through an activated carbon filter the compressed air was dried in a dual tower air dryer using silica gel as desiccant. Air was stored in three tanks with total capacity of 3000 ft^3 at a pressure of 250 psi ($250 \text{ lb/in}^2 = 17.0 \text{ kg/cm}^2$). As shown in figure 1.a, the compressed air was ducted through a control valve and a pressure regulating valve to a settling chamber, where the air was brought to an equilibrium stagnant condition. In order to minimize the disturbance level and fluctuations at the nozzle inlet, the air was passed through three fine mesh screens in the settling chamber, set 3 cm apart. This undisturbed air from the settling chamber was accelerated through the two nozzles made in the nozzle block, which was fitted perfectly at the end of the settling chamber using O-ring, so as to ensure no leakage even at very high pressures. The air was released into the ambient still atmosphere in the form of dual free jet.

A long column 'U' tube mercury manometer and a water manometer were used for pressure measurements. The total pressures in the jet field were measured using Pitot probe of 0.8 mm inner diameter. The schematic of the probe employed is shown in figure 1.d. The probe was mounted on a traversing mechanism having 6 degrees of freedom; and having a least count of 0.1 mm in linear and 0.5 degree in angular motion.

The half angle of interception α has been restricted to 15° due to the limitations of total pressure probe which measures the correct reading with in 2% error up to 15° misalignment from the flow direction. The static pressure in the jet was assumed to be that of atmosphere since in all subsonic free jet fields, the variation reported in literature [7] is within 3%. However, the static pressure variation in the shock cell; in the case of under-expanded jets

show considerable variation. But measurement of such pressure calls for special probes like disc probe. In spite these precautions, even the disc probe is capable of measuring the static pressure accurately only when the local streamline is exactly aligned to the flat surface of the disc. This is possible only along the centreline of a single jet. Therefore, it was felt that it will be misleading if disc probe measurements are made in the fields like the present one. At every nodal point of the field, if the disc has to be properly aligned, the alignment itself will call for a separate investigation. Hence such attempts were not made, since that was not the aim of the present work.

2.2 Experimental procedure

Different jet flow Mach number and under-expansion ratio at the nozzle exit were achieved by controlling the pressure regulating valve, thereby changing stagnation pressure in the settling chamber. The temperature in the settling chamber was measured by a mercury thermometer and the stagnation pressure was measured by mercury manometer and a bourdon type pressure gauge.

A long column 'U' tube water-in-glass type manometer was used for measurements upto Mach number (M) 0.4. For all other pressure ratios ($M > 0.4$), 'U' tube mercury-in-glass type manometer was used for near field and water-in-glass type manometer for far field measurements.

For every angle of intersection studied, the nozzle axisymmetric line (centreline) was aligned longitudinally and the nozzle blocks were fixed at the end of the settling chamber. The traverse was aligned parallel to the longitudinal X-axis. The experimental data were acquired in one quarter plane of the jet flow field atarting from the nozzle centreline. The probe mounted on the traverse was moved parallel to the Z axis in steps of 1 or 2 mm upto a point where the manometer reading becomes zero. At a given axial location, this is repeated for various Y locations. Thus the measurements were made in the form of a grid

with a uniform step of 1 mm in the near field and 2 mm in the far field. This step had been chosen in order not to have significant changes in the manometer readings with the step increment. These grid measurements were made at various axial locations starting from a point close to the nozzle exit upto an axial distance of about 50 D . The measurements taken for one quadrant were extended to the whole flow field assuming symmetry of the flow field about Y and Z axes. This manometer readings were noted manually on the data sheet and these data were keyed in a computer for data processing. The data reduction and calculations were performed on HP-9000 supermini computer systems of IIT Kanpur.

The stagnation pressure ratio r_p was varied from 1.03 to 3.84. The jet Reynolds number based on D was varied from 1.48×10^4 to 8.79×10^4 . The Mach number of the jet at nozzle exit was varied from 0.2 to 1.0. The sonic jet was studied for various degrees of under-expansion (r).

Schlieren technique was used to visualize the wave pattern in the jet flow field. In this technique, a source of light at the focus of a concave mirror, sends parallel rays of light through jet flow field. A second mirror focuses the on-coming rays to a knife edge which controls the intensity of light on the screen. When there is no flow, all the rays emanating from the source converge at the knife edge, thereby producing a uniform illumination on the screen. But, when there is underexpanded flow, there are shock waves and expansion waves in the near field, producing regions of higher and lower density. The rays passing through the jet flow field undergo different orders of refraction and regions of dark and bright patches appear on the screen representing the shock and expansion waves.

2.2.1 Data accuracy

The possible sources of error of the present investigation are:

- * the linear movement of the traverse along X , Y and Z directions.
- * the settling chamber stagnation pressure measuring manometer

- * the error in the measurement of total pressure at the grid points in the jet field

The traverse is provided with a vernier scale with a resolution of 0.1 mm. Hence all the length scales measured were accurate upto ± 0.1 mm. The pressure measuring manometers were provided with graduations with a resolution of 1 mm. All the pressure measurements in liquid column were accurate upto ± 1 mm, and all the measurements were found to be repeatable within ± 3 %. The variation of temperature throughout one set of experimental run was around ± 5 %.

Chapter 3

RESULTS AND DISCUSSIONS

The most important thing for India first is to get into space, rather than establishing space stations or space power stations using photon energy.

– U. R. Rao, 1994

The atmospheric pressure is measured using a mercury barometer. The measured data consists of the distances along X, Y, Z directions, the settling chamber pressure p_o and the total pressure p_t at various nodal points in the jet field. For presentation of results, the measured total pressures have been converted to Mach number using the isentropic relation

$$\frac{p_t}{p} = \left(1 + \frac{\gamma - 1}{2} M^2\right)^{\gamma/(\gamma-1)} \quad (3.1)$$

where p_t is the local total pressure of the fluid after it is slowed down isentropically to zero velocity and p is the local static pressure of the fluid, which is assumed to be a constant equal to ambient pressure and γ is the specific heat ratio of the fluid. Velocities at the nodal points are obtained from the computed M values using the relation $V = M a$. Where $a = \sqrt{\gamma RT}$ is the local speed of sound.

3.1 Non dimensionalization

The results are presented after normalizing the local velocity U in the flow field by jet exit velocity U_o . The axial distance X along the twin jet centreline is normalized by the diameter D of the single jet. The lateral (Z) and transverse (Y) locations of the probe have been normalized by the centre to centre space S of the nozzles. This spacing S has been chosen as the normalizing parameter for presenting the lateral and transverse spread of the jet of the jet because for a given diameter D , the spacing between the nozzles greatly affects the jet spread. In the following discussions wherever the various parameters like local velocity (U), centreline local velocity (U_m), total pressure (p_t) etc are mentioned, it may be assumed that only the normalized parameters are referred to.

3.2 Equations of motion

The Reynolds equation in the Cartesian system is written as (Schlichting [19])

$$\rho \left(\frac{\partial u}{\partial t} + u \frac{\partial u}{\partial x} + v \frac{\partial u}{\partial y} + w \frac{\partial u}{\partial z} \right) = -\frac{\partial p}{\partial x} + \mu \left(\frac{\partial^2 u}{\partial x^2} + \frac{\partial^2 u}{\partial y^2} + \frac{\partial^2 u}{\partial z^2} \right) - \rho \left(\frac{\overline{\partial u'^2}}{\partial x} + \frac{\overline{\partial u'v'}}{\partial y} + \frac{\overline{\partial u'w'}}{\partial z} \right) \quad (3.2)$$

the continuity equation is

$$\frac{\partial u}{\partial x} + \frac{\partial v}{\partial y} + \frac{\partial w}{\partial z} = 0 \quad (3.3)$$

where u, v, w and u', v' and w' are the turbulent mean and fluctuating velocities in the X, Y and Z co-ordinate directions, p is the pressure at any point and t is the time variable.

For steady flow, the equation of motion reduces to the form

$$\rho \left(u \frac{\partial u}{\partial x} + v \frac{\partial u}{\partial y} + w \frac{\partial u}{\partial z} \right) = -\frac{\partial p}{\partial x} + \mu \left(\frac{\partial^2 u}{\partial x^2} + \frac{\partial^2 u}{\partial y^2} + \frac{\partial^2 u}{\partial z^2} \right) - \rho \left(\frac{\overline{\partial u'v'}}{\partial y} + \frac{\overline{\partial u'w'}}{\partial z} + \frac{\overline{\partial u'^2}}{\partial x} \right) \quad (3.4)$$

the last term in the above equation is smaller than the other terms and could be dropped.

$$\rho \left(u \frac{\partial u}{\partial x} + v \frac{\partial u}{\partial y} + w \frac{\partial u}{\partial z} \right) = -\frac{\partial p}{\partial x} + \mu \left(\frac{\partial^2 u}{\partial x^2} + \frac{\partial^2 u}{\partial y^2} + \frac{\partial^2 u}{\partial z^2} \right) - \rho \left(\frac{\overline{\partial u'v'}}{\partial y} + \frac{\overline{\partial u'w'}}{\partial z} \right)$$

$$= -\frac{\partial p}{\partial x} + \frac{\partial(\tau_l + \tau_t)}{\partial y}$$

where τ_l and τ_t are, respectively, the laminar and turbulent shear stresses. In the free turbulent flows due to the absence of solid boundaries, τ_t is much larger than τ_l and hence it is reasonable to neglect τ_l . Further the pressure gradient in the axial direction is negligibly small (subsonic) and can be set $\frac{\partial p}{\partial x} = 0$, becomes

$$\rho \left(u \frac{\partial u}{\partial x} + v \frac{\partial u}{\partial y} + w \frac{\partial u}{\partial z} \right) = \frac{\partial(\tau_t)}{\partial y} \quad (3.5)$$

$$\left(u \frac{\partial u}{\partial x} + v \frac{\partial u}{\partial y} + w \frac{\partial u}{\partial z} \right) = - \left(\frac{\overline{\partial u'v'}}{\partial y} + \frac{\overline{\partial u'w'}}{\partial z} \right) \quad (3.6)$$

$$\frac{\partial u}{\partial x} + \frac{\partial v}{\partial y} + \frac{\partial w}{\partial z} = 0 \quad (3.7)$$

for two dimensional flows the above equations can be written as

$$\begin{aligned} \rho \left(u \frac{\partial u}{\partial x} + v \frac{\partial u}{\partial y} \right) &= \frac{\partial \tau_t}{\partial y} \\ \frac{\partial u}{\partial x} + \frac{\partial v}{\partial y} &= 0 \end{aligned} \quad (3.8)$$

3.3 Centreline velocity decay

The overall characteristics of a jet flow field are best described by the variation of mean centreline velocity U_m of the jet along the jet axis. In the case of single jets it can be seen that centreline mean velocity U_m remains constant at U_o upto the end of potential core region and then starts decreasing monotonically due to the exchange of momentum with the entrained mass. In other words, the non dimensionalized velocity U/U_o decreases from a maximum value of 1.0 to almost zero with increasing non dimensional axial distance X/D . Hence in the case of twin jets the centreline between the two jets is taken as axis of the twin jet flow field.

Figure 2.a1 shows the variation of mean centreline velocity U_c with axial distance for twin parallel jets ($\alpha = 0^\circ$) for various jet exit Mach numbers M_e . It can be seen that

all the plots almost merge indicating that the decay U_m is nearly the same for all Mach numbers. The value of U_c is zero upto $X/D \approx 6.0$ (merging point) beyond which it starts increasing steeply and reaches a maximum at around $X/D = 15.0$. Then it starts decreasing very gradually.

Figure 2.a2 shows the variation of U_c for various under-expanded jets (degree of under-expansion r varying from 1.0 to 1.82). As the static pressure varies in the under-expanded jets, conversion of total pressure into velocity is not possible. Hence centreline total pressure (p_c) decay is shown instead of decay of U_m . p_m is normalized as $\frac{p_c - p_a}{p_o - p_a}$. It is interesting to note that the point of maximum centreline pressure shifts downstream as r increases. The decay of p_c beyond this point is more rapid compared to sonic and subsonic jets and is almost the same for all values of r .

Figures 2.b1 and 2.b2 show similar plots for non parallel ($\alpha = 5^\circ$) jets. It is interesting to note that as the Mach number increases, the peak centreline pressure (p_m) increases. For all Mach numbers this maximum value decreases more rapidly compared to an equivalent parallel jet and the peak centreline velocity is more than that of parallel jets. The plots almost merge beyond $X/D = 40.0$. Similarly the peak centreline pressure p_m decreases with increasing r and the decay is same for the under-expanded jets and sonic jet beyond 40 D. The merging of the jets occurs earlier than parallel jets (around 3.5 D) and is almost same for all Mach numbers, whereas the merging point is shifted upstream with increasing r .

Figures 2.c1 and 2.c2 show similar plots for $\alpha = 10^\circ$. For the incompressible jets ($M_e = 0.2$), the rate of increase of U_m after merging is much steeper compared to the compressible jets. With increasing M_e , the maximum value of U_c marginally decreases. But the plots merge for all subsonic jets after this maximum point indicating that the decay of U_c is almost independent of M_e . But sonic jet has a slightly lesser decay rate compared to subsonic jets. The maximum U_c occur around 9 D for all M_e . The merging point is independent of M_e , as before but merging occurs earlier than in the case of $\alpha = 5^\circ$, at

around 3.4 D. In the case of under-expanded jet the peak centreline pressure p_m is more for sonic jet ($r = 1$) than that under-expanded jets and is almost the same for all under-expanded jets and the initial decay of p_c is almost same for all the jets except $r = 1.98$, but beyond 40.0 D the plots merge indicating the flow field is totally independent of M_e and r , beyond this. The peak value of p_c (p_m) occurs earlier as r decreases.

Similar plots for $\alpha = 15^\circ$, as illustrated by figures 2.d1 and 2.d2, indicate that the rate of increase of U_m with axial distance marginally decreases as the Mach number increases. The location (X_p) at which peak value p_c (p_m) occurs is shifted downstream with increasing Mach number. The initial decay of subsonic jet is less than that of supersonic jets but, as before, beyond $X/D = 40.0$ the plots merge. The merging of twin jets occurs at around 2.5 D for all M_e and the location of maximum U_c varies from around 8 for $M_e = 0.2$ to around 11.0 D for $M_e = 1.0$. In the case of under-expanded jets the value of p_m decreases with increasing r , but X_p does not vary significantly with r . The decay of p_c appears to be faster in the case with $r = 1.83$ compared to lower degrees of under-expansion. But the plots merge beyond 40.0 D as in other cases of α . The merging of the jet occurs earlier as r increases. The point C.P shifts downstream with increasing r .

3.3.1 General features of the centreline velocity/pressure decay

A comparison of all these plots show that with increasing half angle α , the merging of individual jets is advanced and the value of maximum U_c or p_m increases. The rate of decay of U_c or p_c beyond this maximum point with axial distance increases with increasing α . In all the cases the plots are flatter in the region of maximum U_c or p_m indicating that this maximum value is not confined to a single point but it occurs over a region. This flatter portion decreases with increasing α . Another interesting aspect is that the axial distance X_{cp} is less than the location of geometric intersecting point X_{gp} in the case of $\alpha = 0^\circ$ and $\alpha = 5^\circ$. In the case of $\alpha = 10^\circ$, X_{cp} is almost equal to X_{gp} . This may be explained

as follows: In the case of parallel jets and intersecting jets of very small half angle α , ($\alpha = 5^\circ$) the region between the inner layers of the merging jets is comparatively more and consequently the subatmospheric zone is increased. This results in the bending of the jet towards each other beyond the core region (where the inertial forces are predominant). This leads to shifting of the axes of the individual jets to the nozzle centreline. The point C.P on the centreline almost coincides with the merging of the individual axes. Beyond this point the individual jets are combined into a single jet and the combined jet propagates as a single jet. Due to the bending of axes C.P is shifted upstream of G.P. In the case of jets with higher α ($\alpha = 10^\circ$ and 15°), the subatmospheric zone is reduced and hence the bending of axes is insignificant, the axes of the individual jets almost follow their geometric axes. Hence in the case of $\alpha = 10^\circ$, C.P almost coincides with G.P. The shifting of C.P downstream of G.P in the case of $\alpha = 15^\circ$ may be due to the following reasons:

The individual jets impinge upon each other quite close to the nozzle almost at X_{gp} which is around $6D$ for $\alpha = 15^\circ$. In this region the inertial forces are still predominant and the collision of individual jets leads to quasi stagnant conditions in the zone of impingement leading to reduced values of peak U_c or p_m . Then the flow gets accelerated till it attains a maximum and then starts decelerating thus pushing C.P downstream of G.P.

The reduced values of maximum U_c or p_m with decreasing α may be due to the fact that the combining of jets occurs farther from the nozzle exit for lower values of α . At these farther locations the twin jet would have entrained more ambient fluid and hence the maximum centreline values of velocity and pressure get reduced.

The reason for early merging of individual jets with increasing α is obvious. The inner layers of the individual jets tend to merge earlier as the angle of inclination (α) towards each other increases. This merging of jets appears to depend purely upon the level of expansion at the nozzle exit for a given α . In the case of subsonic and correctly expanded sonic jets, it appears that the opposite effects of increased inertial forces and consequent increased activeness of the subatmospheric zone nullify each other which results in the near

independent of merging point location of jet exit Mach number.

However, in the case of underexpanded jets with increased degree of under-expansion r , the nozzle exit static pressure p_e increases. The higher value of p_e as compared to the ambient pressure p_a , results in diverging of jet flow in all directions. This explains the early merging of under-expanded jets with increasing degree of under-expansion.

It may be observed that for a given Mach number M_e , the rate of increase of U_c or p_c with axial distance increases with increasing α in the merging region. This may be explained as follows:

The inner layer, in an individual jet in general, is a region of steeper velocity gradients compared to the outer layer. This is due to the fact that the inner layer has to develop in a limited space unlike the outer layer and this leads to inhibited growth of inner layer. This limitation in space increases with increasing α and also the early merging of the jets close to the nozzle exit requires that the velocities have to decrease sharply from a higher value of velocity/pressure at the jet axis to zero at the boundary of inner layer within a short distance. These steep velocity gradients lead to intense interaction of inner layers after merging, the intensity increasing with increased α . The flatness of the centreline velocity/pressure decay profile around the maximum point decreases with increasing α due to the higher intense mixing of inner layers in the combining region.

The flatness of the profile itself indicates that the combining of the jets is not limited to a single point but spread over a range of axial distance; this trend getting more pronounced as α decreases.

In all the cases, the plots merge beyond an axial location of 40.0 D, indicating that the far field region beyond 40 D is independent of the initial geometric and flow conditions of the twin jet. The combined jet propagates just as any incompressible jet.

3.4 Mean velocity profiles

The mean velocity profile in the Y and Z direction are presented in figures 3.a1 and 3.a2 for $M_e = 0.2$ in the case of $\alpha = 5^\circ$. Mean velocity profiles give certain finer details of the flow field both in the near field and far field. The length of the potential core of individual jets in the case of twin jets can not be determined from the centreline velocity decay presented in the previous section. In the case of single jets by traversing the probe along the jet axis, from the nozzle exit to the location upto which exit velocity U_o is preserved, the core length can be determined as the axial distance of this location. In twin jets, the axes of individual jets bend toward each other and hence moving the probe along the individual jet axis is difficult. At each axial location grid measurements are to be made and only from the mean velocity profiles obtained through these measurements potential core length can be determined. Now the question may arise, why potential core length is to be determined, at all. The length of potential core is a measure of the growth and penetration of the turbulent shear layer that starts growing along the periphery of the jet as soon as the jet issues out the nozzle. A shorter potential core length implies faster growth and penetration of the shear layer. In the case of single axisymmetric jets issuing from smooth contoured nozzle, the length of potential core generally varies from 4 D to 5 D in the Mach number range of 0.2 to 1.0. The length of potential core increases with Mach number.

From figures 3.a1 and 3.a2, it can be seen that the velocity profiles are flatter close to the nozzle exit indicating the presence of potential core. The gradual decrease of the flatter region with increasing axial distance may be observed. At around 4 D, the potential core ends and downstream of this location the local maximum velocity (U_m) starts decreasing with increasing downstream distance. The radial (Z) location of this maximum velocity falls on the individual jet axis. The shifting of this peak towards the nozzle centreline indicates the shifting of the jet axes to the centreline. At around 12 D, this peak occurs at the centreline and downstream of this location the velocity profiles are similar to a single

jet with a single peak velocity at the centreline. With increasing downstream distance the profile becomes flatter, *ie.* the velocity gradients are very gradual, indicating thorough mixing of jet fluid with ambient fluid. The merging of the inner layers close to the nozzle exit is indicated by the joining of individual jet profiles. Which is around 3.0 D as seen from the figures 3.a.

Figures 3.b1 and 3.b2 present similar profiles for $\alpha = 10^\circ$ in 3-dimensional form for $M_e = 0.2$. Here again the end of potential core occurs around 4 D and shifting of peak velocity to the centreline occurs around 9 D.

Figures 3.c1 and 3.c2 show similar profiles for $\alpha = 15^\circ$ for $M_e = 0.2$. For this case also, the potential core ends at around 4 D and peak velocity shifts to centreline at around 10 D.

Comparison of all these profiles, show that the general features of the flow field are not altered much by the half angle of intersection α . The merging and combining of the jets are strongly influenced by α whereas the length of the potential core appears to be independent of α .

3.5 Potential core length for under-expanded jets

When the convergent nozzle is operated at stagnation pressure ratio (r_p) higher than the critical pressure ratio ($r_p = 1.89$) under-expanded jets are produced. Donaldson *et al* [13] give a vivid description of under-expanded sonic jets which is worth reproducing here. When critical pressure ratio is reached, a very weak normal shock forms at the exit. This shock changes rapidly with increasing pressure ratio, however, at around $p_e/p_a = 1.1$, the familiar pattern of “shock diamonds” or “cells” composed of intersecting oblique shocks is established in the core (see fig 1.c). The term “moderately under-expanded” is used to denote jets within the pressure ratio interval ($1.1 \leq p_e/p_a \leq 2$). Because of the additional expansion required in the unconfined jet flow beyond the nozzle, the boundaries of what

was the potential core in the subsonic case are now determined by the requirement of pressure equilibrium between the outermost portion of the flow within the shock structure and the surrounding ambient air. The inverted diffusion of the mixing region, however, continues and ultimately results in the dissipation of the core. Downstream of the core, after the jet has become subsonic, the spread and decay would be expected to be similar to that of a totally subsonic jet. At a pressure ratio $p_e/p_a \approx 2$, the form of the shock structure in the initial cell begins to change. Along the jet centreline, where the expansion is maximum, the pressure becomes so low relative to ambient pressure that the recompression in the remainder of the cell reaches the limiting value for conical shocks and the required compression takes place through an observable normal shock disc. Once this disc forms, the jet is said to be “highly under-expanded”. The description given here is for single under-expanded sonic jets. In this section let us see how the potential core region in twin under-expanded sonic jets get altered.

Figures 4.a, b, c and d show the pressure profiles for under-expanded sonic jets ($r = 2.04$) in the case of $\alpha = 0, 10$ and 15 deg and also for a single circular jet. In the case of under-expanded jets, as already seen, the core region is dominated by expansion and compression waves. The flow through the expansion waves becomes supersonic and that through compression waves gets decelerated. In highly under-expanded jets as in the present case, the flow immediately behind the Mach disc becomes subsonic. The strength of the shock cells decreases with increasing downstream distance. The first Mach disc normally occurs around $1 D$ from the exit (see photos). This is the strongest recompression of various profiles the relative strength of this first Mach disc is chosen. It may be observed that for the single jet at around $1 D$, there is a severe total pressure loss $\left(\frac{p_e - p_a}{p_o - p_a} \approx 0.4\right)$ indicating the presence of a strong Mach disc. In the case of parallel jets, at $1 D$, the pressure loss is comparatively less (≈ 0.7). In the case of $\alpha = 10^\circ$, it is around 0.6 . Hence it appears that in a twin jet flow field (in the case of under-expanded jets) the strength of Mach discs gets reduced as compared to a single jet. This may be explained as follows:

In the case of single jets the ambient pressure acts uniformly over the periphery of the jet. In the case of an individual jet in a twin jet configuration there is a subatmospheric region between the inner layers. This reduced pressure acting over nearly one half of the jet periphery weakens the recompression and hence the Mach disc strength decreases. From the results it is seen that for parallel jet and for the case of $\alpha = 10^\circ$, the Mach disc strengths are almost equal, whereas for $\alpha = 15^\circ$ the Mach disc appears to have become stronger resulting in greater total pressure loss. The possible reason could be that as the angle α is increased the subatmospheric decreases. Which should lead to stronger recompression but the mutually approaching inner layers intensify the recirculation in the enclosed zone thereby increasing the “activeness” of the subatmospheric zone. This perhaps, nullifies the previous effect and makes the situation similar to an equivalent parallel jet. In the case of $\alpha = 15^\circ$, the increased inclination results in further reduction of subatmospheric zone and early merging of inner layers close to the nozzle exit. This brings the situation in the flow field closer to that of a single jet and hence the increased strength of recompression zone.

The determination of potential core length may be made by comparing the profiles with that of the single jet. In the case of single jet it was observed that upto an axial location of around 7 D the alternating deceleration and acceleration of the flow occurred indicated by increase and decrease of total pressure and beyond that the total pressure started decreasing rapidly. Hence the length of potential core may be taken as around 7 D. By a similar observation, it is found that for all the cases the core length is around 7 D.

Hence, it may be inferred that for the nozzle spacing of the present study, the core length of the highly under-expanded jet is not altered in the twin jet configuration and is almost independent of the angle of intersection. But the strength of Mach disc gets reduced in the case of twin jets.

3.6 Merging and Combining points

3.6.1 Subsonic jets

The variation of merging point (nondimensional) location X_{mp} , the combining point location X_{cp} , and the peak centreline pressure (p_m/p_o) with Mach number and half angle of intersection are presented in tabular form in Table-A, for subsonic jets.

M	$\alpha = 0^\circ$		$\alpha = 5^\circ$			$\alpha = 10^\circ$			$\alpha = 15^\circ$		
	X_{mp}	p_m/p_o	X_{mp}	X_{cp}	p_m/p_o	X_{mp}	X_{cp}	p_m/p_o	X_{mp}	X_{cp}	p_m/p_o
	D		D	D		D	D		D	D	
0.2	6.0	0.974	3.4	11.6	0.979	3.2	9.2	0.986	2.5	8	0.992
0.4	6.0	0.91	3.4	12.0	0.926	3.2	9.2	0.95	2.5	9.35	0.965
0.6	6.0	0.807	3.4	12.5	0.849	3.2	9.5	0.89			
0.8	6.0	0.69	3.4	13.0	0.753						

Table-A

3.6.2 Sonic and Under-expanded sonic jets

The variation of merging point, the (non dimensional) peak centreline pressure (p_m/p_o) with degree of under-expansion (r) for different angles α are given in Table-B. X_l is the axial distance by which the combining point C.P is pushed upstream of geometric intersection point G.P.

α	r	X_{gp}	X_{mp}	X_{cp}	p_m/p_o	X_l
		D	D	D		D
$\alpha = 0^\circ$	1	∞	5.5	30.0	0.562	-
	1.4	∞	5.33	30.0	0.447	-
	1.7	∞	5.33	30.0	0.362	-
	1.83	∞	5.17	30.0	0.34	-
$\alpha = 5^\circ$	1	19.6	3.4	12.5	0.66	+7.1
	1.4	19.6	3.0	10.4	0.526	+9.2
	1.7	19.6	2.4	10.4	0.436	+9.2
	1.85	19.6	2.0	10.0	0.406	+9.6
$\alpha = 10^\circ$	1	9.2	3.23	9.83	0.723	-0.63
	1.47	9.2	3.06	10.65	0.575	-1.45
	1.79	9.2	2.74	12.1	0.542	-2.90
	1.98	9.2	2.42	13.06	0.515	-3.86
$\alpha = 15^\circ$	1	6.3	2.8	10.86	0.82	-4.56
	1.4	6.3	2.15	11.345	0.653	-5.05
	1.7	6.3	2.0	12.0	0.604	-5.70
	1.83	6.3	1.68	12.474	0.617	-6.174

Table-B . Comparison of C.P, M.P and Pressure loss with under-expansion ratio.

In general it may be seen that compared to subsonic jets non dimensional peak pressure p_m/p_o values are much lower in the case of under-expanded jets. This is because of the shock cell structures in the core region of under-expanded jets which results in total pressure loss. With increasing r this loss also increases due to higher strength of the shock.

As in the case of subsonic jets the value of p_m/p_o increases with increasing α where the inertial forces are predominant. An empirical relation between p_m and cross angle α has

been arrived at on the basis of the results as follows:

$$\frac{p_m}{p_o} = c_1 \alpha + c_2 \quad (3.9)$$

where c_1 and c_2 are constants for a particular value of r .

The sign of X_l indicates whether the combining of jet takes place upstream or downstream of intersection point (G.P). If X_l is positive, it means that C.P is upstream of G.P and vise versa.

In the case of subsonic jet may be it is seen that for $\alpha = 0^\circ$ and 5° X_l is positive and for $\alpha = 10^\circ$, $X_l \approx 0$ and for $\alpha = 15^\circ$, X_l is negative. In the case of under-expanded jets for $\alpha = 0^\circ$ and 5° same trend is seen but for $\alpha = 10^\circ$, X_l is negative and with increasing r , C.P is pushed further downstream of G.P. For $\alpha = 15^\circ$, X_l is negative and this downstream shifting tendency is more than for $\alpha = 10^\circ$.

3.7 Similarity profile

The combined jet propagates just like any single jet. Even though two axisymmetric jets have combined to form a single jet, the combined jet is not axisymmetric with different rates of spread in Y and Z directions. This combined flow region is found to be self preserving (self similar). In all single jet studies this self similar region is described by the similarity profile using the non dimensional parameters U/U_m and $Y_{0.5}$ or $Z/Z_{0.5}$. Here U/U_m is the non dimensional velocity scale, $Y/Y_{0.5}$ and $Z/Z_{0.5}$ are the non dimensional length scales in Y and Z direction. Self similar nature of the jet is proved by the collapse of the data into a single curve for all axial locations.

Figures 5.a1 and 5.a2 show the similarity profile for parallel jets for both Y and Z direction at $X/D = 30.0$ for various M_e and r . Figures 5.b1 and 5.b2 show the similarity profile at different X/D locations, for $M_e = 0.2$ and 0.6 respectively for $\alpha = 5^\circ$. Figures 5.c1 and 5.c2 show the similar profiles for $r=1.1$ and 1.7 . Figures 5.d1 and 5.d2 show

the profiles at $X/D = 30.0$ for different M_e and at $X/D = 40$ for different r respectively. Figures 5.e and 5.f show the profiles for $M_e = 0.2$ at different axial locations for $\alpha = 10^\circ$ and 15° respectively. Comparing all the profiles, it may be noticed that for all intersecting jets the profiles are same irrespective of α , M_e , r and X/D . Interestingly the profiles are the same for Y and Z directions. This shows the self preserving nature of the combined jet is independent of initial geometric and flow conditions and also that the jet is axisymmetric with respect to non dimensional velocity and length scales. This similarity profile can be represented by the following equations.

$$\begin{aligned}\frac{u}{u_m} &= \exp \left(-0.693 \eta_z^2 \right) \\ \frac{u}{u_m} &= \exp \left(-0.693 \eta_y^2 \right)\end{aligned}\tag{3.10}$$

The parallel jet appears to have a slightly flatter profile at the central region. This may be because of the higher combining distance X_{cp} of the parallel jets which leads to nearly zero velocity gradient around the centreline.

3.8 Iso Mach lines

The twin jet flow field structure is best visualized by the iso Mach lines shown in figures 6.a–c. In all the figures the boundary of the jet is represented by Mach lines for $M = 0.2 M_e$. Those Mach lines were generated using experimental points and smooth contours were obtained by interpolation. The merging and combining of the intersecting jets can be clearly seen in the figures. For a given jet exit Mach number M_e , the iso Mach lines represent the decay of jet kinetic energy as the flow propagates downstream. The kinetic energy of the jet decreases due to the addition of entrained ambient air. From these figures it may be seen that close to the nozzle exit, ie in the merging region, the iso Mach lines in the inner shear layer are more closely spaced as compared to the outer shear layer indicating velocity gradients are steeper in the inner layer than in the outer layer. The close spacing

of Mach lines increases with increasing angle α .

The Iso Mach lines for the under-expanded jet ($r=1.7$) in figure 6.a3 do not represent the flow field exactly. This is due to the following reasons:

- ⊕ The measured total pressures in the under-expanded jet are less than the actual values due to the normal shock in front of the total probe.
- ⊕ The static pressure in the flow field varies continuously and the measurement of local static pressure is very difficult.

The Mach numbers in the flow field were calculated assuming the static pressure to be atmospheric.

3.9 Spread rate

Figures 7.a, b show the variation of jet half widths (both Y and Z directions) with axial distance for different half angles. It can be seen clearly that the spread in Z (spanwise) direction increases with decreasing half angle and the spread in Y (transverse) direction increases with increasing half angle. The slope of the half width lines of intersecting jets are negative up to the combining point and then the slope becomes positive. This is visualized in figures of iso Mach lines also.

3.10 The Integral momentum equation

Integrating the equation of motion 3.8 from $y=-\infty$ to $y=\infty$, we have:

$$\rho \int_{-\infty}^{\infty} u \frac{\partial u}{\partial x} dy + \rho \int_{-\infty}^{\infty} v \frac{\partial u}{\partial y} dy = \int_{-\infty}^{\infty} \frac{\partial \tau_t}{\partial y} dy \quad (3.11)$$

consider the different terms of the above equation

$$\rho \int_{-\infty}^{\infty} u \frac{\partial u}{\partial x} dy = \frac{1}{2} \int_{-\infty}^{\infty} u \frac{\partial \rho u^2}{\partial x} dy = \frac{1}{2} \frac{d}{dx} \int_{-\infty}^{\infty} \rho u^2 dy \quad (\text{Liebnitz rule})$$

$$\rho \int_{-\infty}^{\infty} v \frac{\partial u}{\partial y} dy = \frac{1}{2} \frac{d}{dx} \int_{-\infty}^{\infty} \rho u^2 dy \quad (\text{from Rajaratnam})$$

$$\int_{-\infty}^{\infty} \frac{\partial \tau}{\partial y} dy = |\tau|_0^{\infty} = \tau(\infty) - \tau(0) = 0$$

This implies

$$\frac{d}{dx} \int_{-\infty}^{\infty} \rho u^2 dy = 0 \quad (3.12)$$

For the three dimensional flow the summation of square of velocities taken along the Z and Y direction is not enough and the velocities on the whole grid at that cross section is to be integrated. So the equation (3.12) can be written as

$$\frac{d}{dx} \int_{-\infty}^{\infty} \int_{-\infty}^{\infty} \rho u^2 dy dz = 0 \quad (3.13)$$

this implies that the momentum flux in the x-direction is constant. Since there is no external force involved, the momentum of the jet in the axial direction is preserved.

Figure 8 shows that the momentum is conserved for all cross angles at $M = 0.2$. There is some scatter in the momentum up to 10%. The reason why this scatter occurs may be due to

\Rightarrow the lesser sensitivity of the probe i.e. it is unable to measure the low velocities accurately at far field and in the outer region of jet.

\Rightarrow the vigorous growth of turbulence

\Rightarrow and due to some reverse flow in the combining region

3.11 Variation of entrainment with axial distance

If Q is the volume flow rate in the X direction at any section of the jet

$$Q = \int_{-\infty}^{\infty} \int_{-\infty}^{\infty} U dy dz \quad (3.14)$$

If Q_o is the exiting flow from the nozzle, due to the entrainment of ambient fluid $\frac{Q}{Q_o}$ is greater than unity at all downstream locations and increases with increasing downstream distance in a linear fashion. This may be represented by

$$\frac{Q}{Q_o} = kX \quad (3.15)$$

where k is known as entrainment constant. The amount of actual volume flow entrained can be calculated and normalized as $\left(\frac{Q-Q_o}{Q_o}\right)$. This normalized entrainment at any section, calculated using numerical integration, is found to increase almost linearly with downstream distance. It is clearly inferred from the figure 9 that as the half angle α decreases for a given exit Mach number M_e , entrainment increases. The maximum entrainment at any axial location is observed for parallel jets. This could be due to the fact that the early merging of the individual jets with increasing α , reduces the effective circumferential area of the jet, thereby reducing interaction with ambient air. The rate of change of entrainment with axial distance is lower upto the combining point and becomes higher in the combined flow for all the cases.

3.12 Constant velocity contours

The jet development along the X -direction is presented in the form of constant velocity contours of jet cross section at various downstream locations in figures 10.a-c for the intersecting jets. Figure 10.a gives the constant velocity contours at four X/D locations for $M_e = 0.2$ for $\alpha = 5^\circ$. It is seen from the figure that the combined jet cross section shape at $X/D = 8.0$ (just prior to combining) is approximately in the form of an ellipse. The jet

growth in the downstream direction shows a tendency to stretch the minor axis and shrink the major axis of the elliptical section seen at $X/D = 8.0$, as seen from the contours at $X/D = 10.0$ and 12.0 . At a further downstream station of $X/D = 15.0$, it is clearly seen that the major and minor axes of the elliptic shape at $X/D = 8.0$ have been reversed. This is similar to the well known “**Axis switching**” phenomenon associated with non circular jets (This phenomenon is explained in detail in Part-2 of the thesis).

The same type of phenomenon is observed for cases of $\alpha = 10^\circ$ and $\alpha = 15^\circ$ also as shown in figures 10.b and c respectively. It also may be seen that with increasing angle α , the aspect ratio (ratio of major to minor axis) of the elliptical shape of the contours increases as seen from the figure 10. It is interesting to note that the axis switching phenomenon which is considered to be a prime controlling mechanism of entrainment in the case of non circular jets can be achieved even with circular nozzles by the proper choice of geometrical configurations.

Chapter 4

SUMMARY AND CONCLUSIONS

A turbulent cross jet formed by two circular jets at 10° , 20° and 30° angles have been measured in detail to determine its structure. The results of this experimental study on a turbulent cross jet in relation with cross angle and Mach number for the nozzle spacing studied ($S/D = 3.1$) are summarized as follows:

1. **F**or all the cases studied the mean velocity / pressure along the centreline increases almost linearly in the combining region and attains a maximum. Then it decays exponentially.
2. **I**n all the cases the rate of decay of the combined jet is almost the same irrespective of the initial geometrical and flow condition beyond $X/D = 40.0$.
3. **I**n the case of parallel jet and jet with half angle $\alpha = 5^\circ$, the individual jets are attracted toward each other due to the subatmospheric zone between the merging jets. The jets merge and combine and the combined jet propagates as a single jet.
4. **I**n the case of jets with half angles $\alpha = 10^\circ$ and 15° , the subatmospheric zone is reduced and the merging and combining of the jets appear to be mainly guided by the half angle α .

5. **T**he merging of the inner layers of the individual jets is independent jet exit Mach number in the case of subsonic and correctly expanded sonic jets for all the cases studied.
6. **F**or a given intersecting angle, the merging occurs closer to the nozzle exit as the degree of under-expansion increases. At a particular degree of under-expansion the jets merge earlier as the half angle increases.
7. **I**n the case of parallel jet the combining of the jet is found to be independent of M_e and r . In all the cases the combining of the jet occur at around 30.0 D.
8. **I**n the case of intersecting jets the combining point of the jets is shifted downstream as M_e and r increases for a particular intersecting angle.
9. **I**n all the cases studied, it is found that the potential core length is found to be influenced only by M_e and r and is independent of α .
10. **T**he entrainment is strongly influenced by the half angle α for a particular M_e . The entrainment is maximum for parallel jet and with increasing *alpha*, entrainment decreases.
11. **S**pread of the combined jet in the Z (spanwise) direction increases with decreasing α and the spread in Y(transverse) direction increases with increasing half angle.
12. **T**he slope of the half width lines of intersecting jets are negative upto the combining point and then the slope becomes positive.
13. **F**or a particular M_e/r , the peak centreline velocity / pressure increases with increasing α .
14. **I**n the case of inter secting jets, the similarity profiles of the combined jet are the same irrespective of α , M_e , r , X/D and also for Y or Z direction. Thus it seems

the self preserving nature of the combined jet is independent of initial geometric and flow conditions and also that the jet is axisymmetric with respect to non dimensional velocity and length scales.

15. The axis switching phenomenon which is considered to be a prime controlling mechanism of entrainment in the case of non circular jets may be achieved even with circular nozzles by the proper choice of geometric configurations.

4.1 Suggestions for future work

Further studies which may be of interest in this area are the following:

- # The static pressure variation along the nozzle centreline may be studied in detail especially for higher angles of intersection and for high subsonic, sonic and under-expanded sonic jets.
- # The static pressure distribution in the subatmospheric zone between the inner layers will be a valuable information.
- # The reverse flow in the subatmospheric zone may be studied in detail.
- # The wall static pressure variation at the nozzle exit plane may be studied.
- # Similar studies can be carried out for supersonic jets also for different Mach numbers and levels of expansion.
- # The present study has been made for only one nozzle spacing. Further studies can be made for different spacing.
- # The flow field of diverging jets and their interaction may be studied.

Bibliography

- [1] Becker, H.A. and Booth, B.D. *“Mixing in the interaction zone of two Free Jets”*, AIChE J, 1975, 21, pp 949–958.
- [2] Elbanna, H. and Gahins, S. *“Investigation of two plane parallel jets”*, AIAA J, 1983, 21, pp 186–991.
- [3] Elbanna, H., Sabbagh, J.A. and Rashed, M.I.I. *“Interception of two equal Turbulent Jets”*, AIAA J, 1985, 23, pp 985–986.
- [4] Murai, K., Taga, M. and Akagawa, K. *“An Experimental study on Confluence of two two-dimensional Jets”*, Bull JSME, 1976, 19, pp 958–964.
- [5] Okamoto, T., Yagita, M., Watanabe, A., and Kawamura, k. *“Interaction of twin turbulent circular jet”*, Bull JSME, 1985, 28, pp 617–622.
- [6] Bidyasagar pani and Raghunath Dash. *“Three-Dimensional Single and Multiple free jets”*, J Hydraulic Engineering, 1983, 109 (2).
- [7] Rajaratnam, N. and Khan, A.A. *“Intersecting Circular turbulent Jets”*, J Hyd Res, 1992, 30, pp 373–387.
- [8] Rho, B.J., Kim, J.K. and Dwyer, H.A. *“Experimental study of a Turbulent Cross Jet”*, AIAA J, 1990, 28, pp 784–789.

- [9] Rho, B.J., Choi, J.C. "*On the structure of a turbulent cross jet corresponding to cross angle variation*", Fluids Engineering, edited by Kim, J.H., Hynn, J.M., Lee, C.O., pp 269–280, Hemisphere Publishing corporation, N.Y, 1989.
- [10] Tanaka, E. "*The interference of two dimensional parallel jets (Ist report)*", Bull JSME, 1970, 13, pp 272–280.
- [11] Tanaka, E. "*The interference of two dimensional parallel jets (IInd report)*", Bull JSME, 1974, 17, pp 920–927.
- [12] Rathakrishnan, E., Vijayabhaskara Reddy, P. and Padmanabhan, K. "*Some studies on twin jet propagation*", Mech Res Comm, 1989, 16, pp 279–287.
- [13] Donaldson, C.D. and Snedeker, R.S. "*A study of free jet impingement. Part 1. Mean properties of free and impinging jets*", J Fluid Mech, 1971, 45 (2), pp 281–319.
- [14] Wlezien, R.W. "*Nozzle geometry effects on supersonic jet interaction*", AIAA J, 1989, 27, pp 1361–1367.
- [15] Sherrieb, H. E. "*Ground effects testing of two, three and four jet configuration*", J. Aircraft, 1979, 16, pp 393–397.
- [16] Wang, C.S., Lin, Y.F. and Shen, M.J "*Measurements of turbulent inclined plane dual jets*", Expts in Fluids, 1993, 16, pp 27–35.
- [17] Abramovich, G. N. "*The theory of Turbulent Jets*", Massachusetts Institute of Technology Press, Cambridge, 1963.
- [18] Rajaratnam, N. "*Turbulent Jets*", Elsevier Scientific Publishing Co., New York, 1976.
- [19] Hermann Schlichting, "*Boundary Layer Theory*", McGRAW-HILL BOOK COMPANY, INC, New York, 1960.

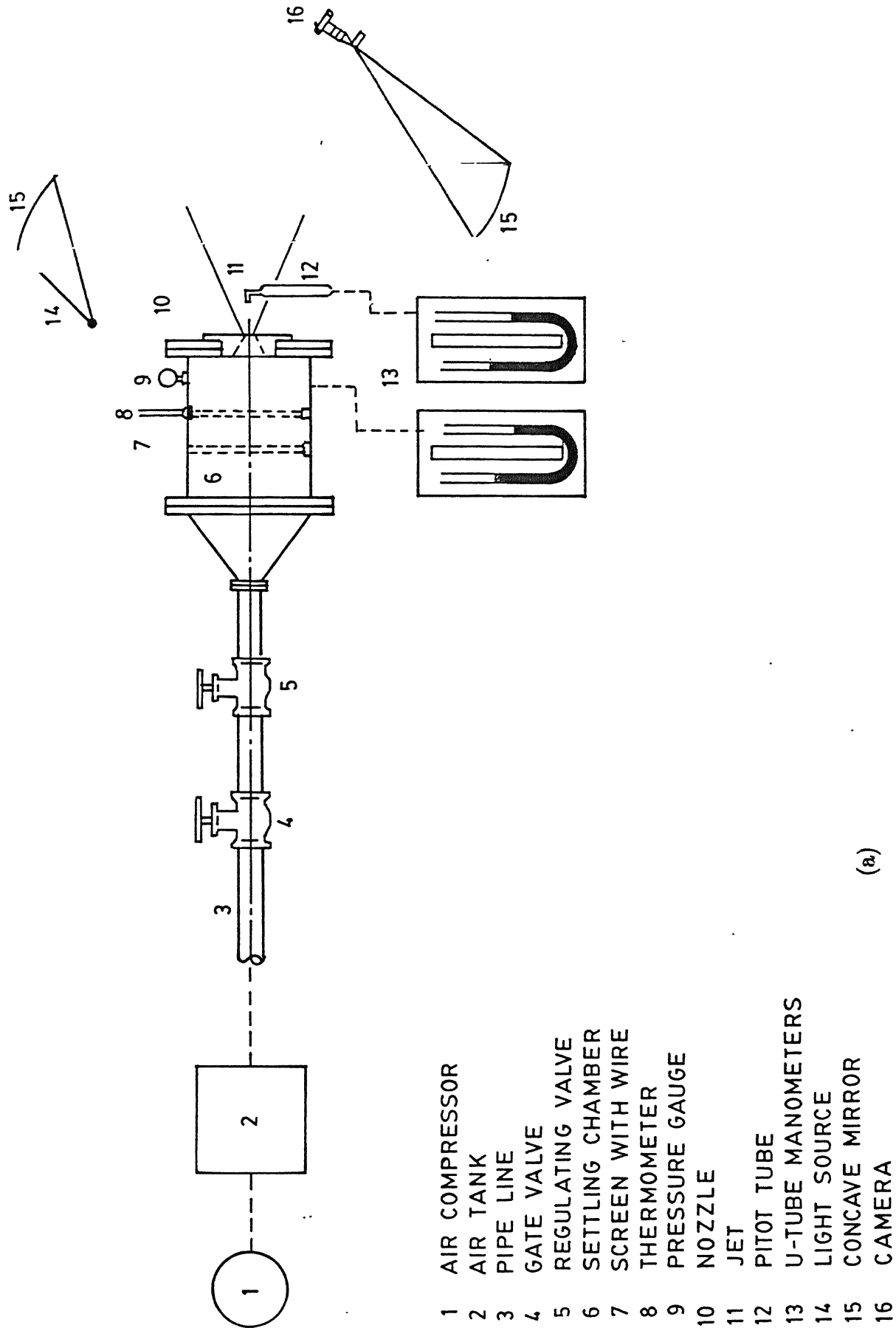


FIG.1 EXPERIMENTAL APPARATUS

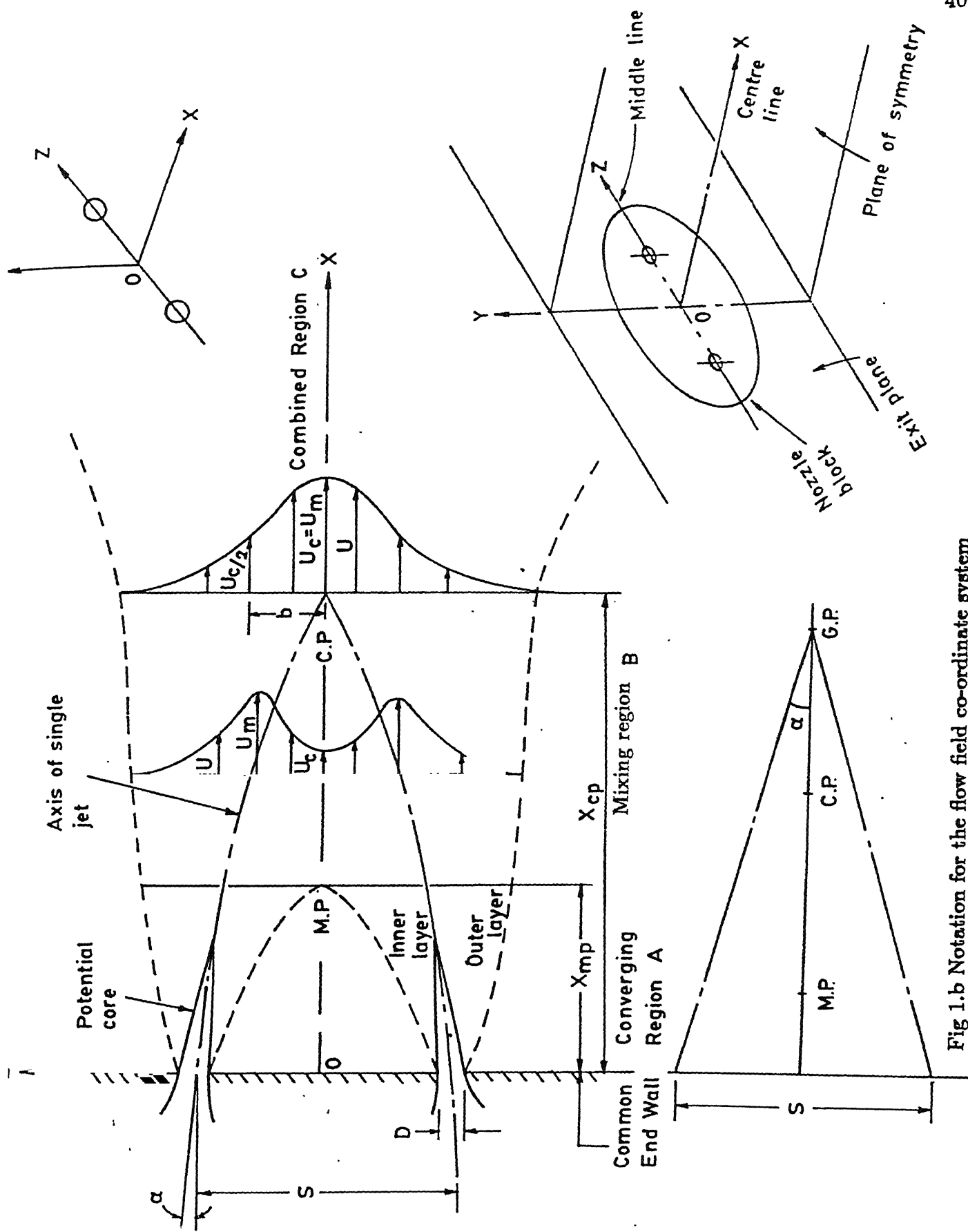


Fig 1.b Notation for the flow field coordinate system

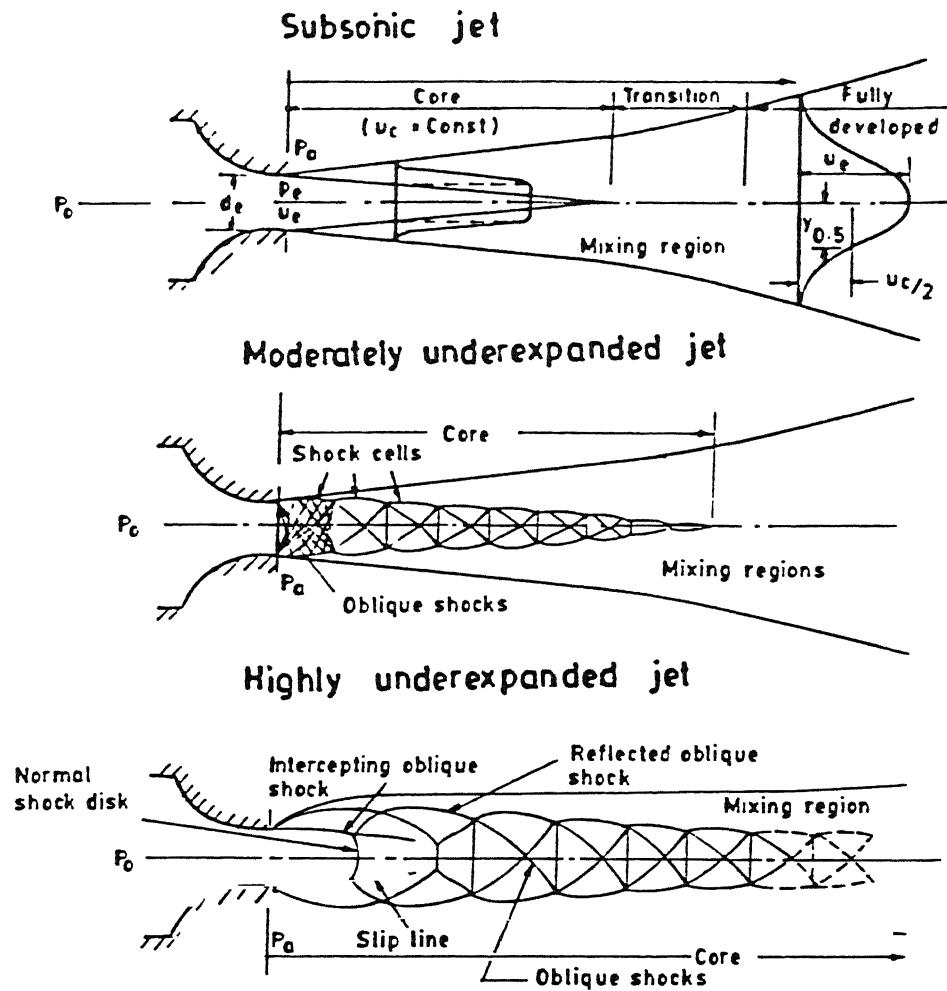
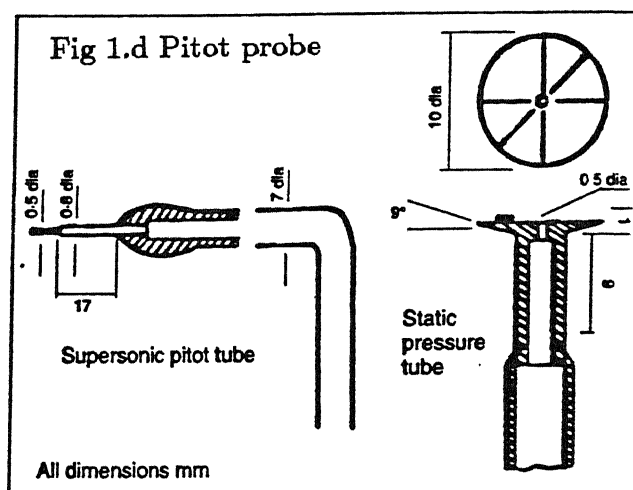
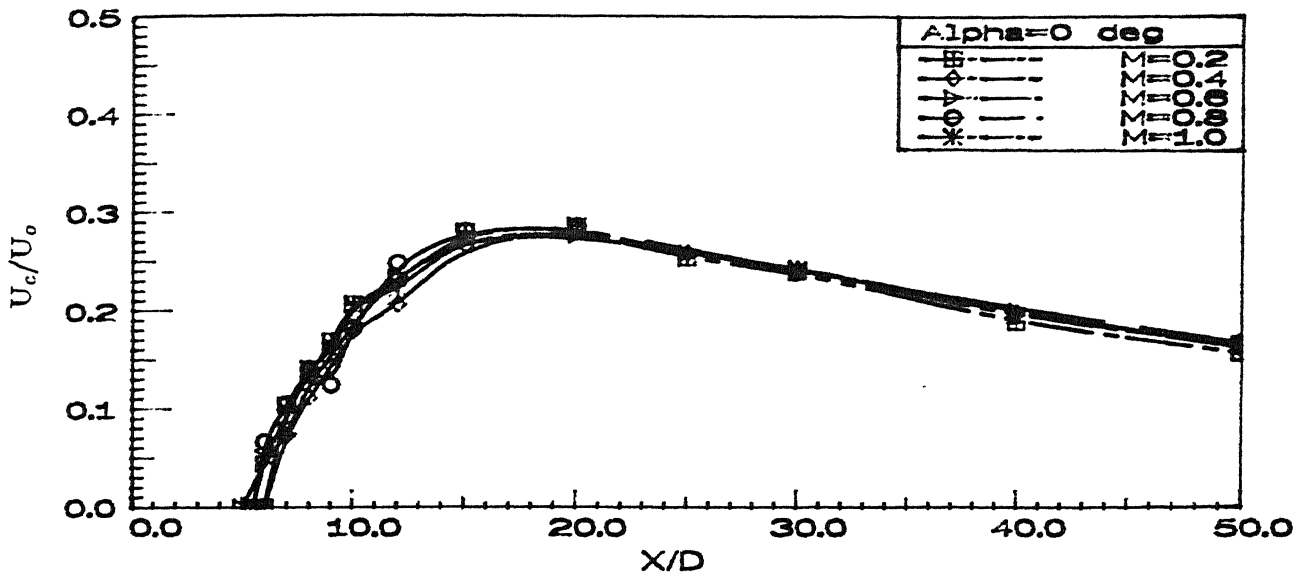
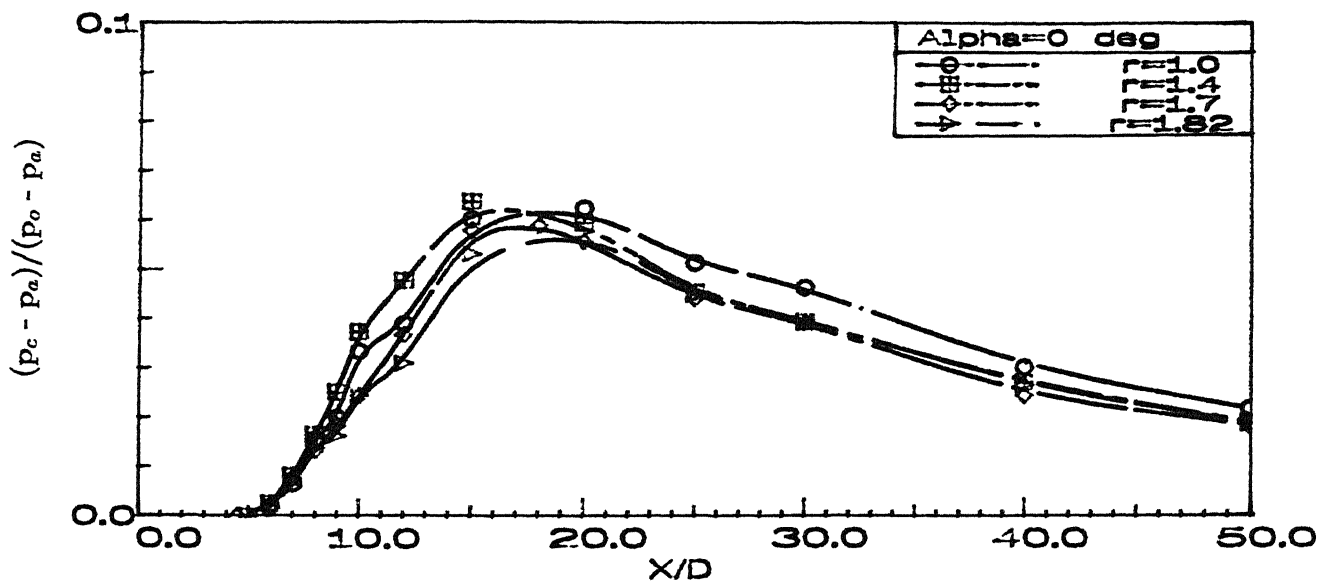
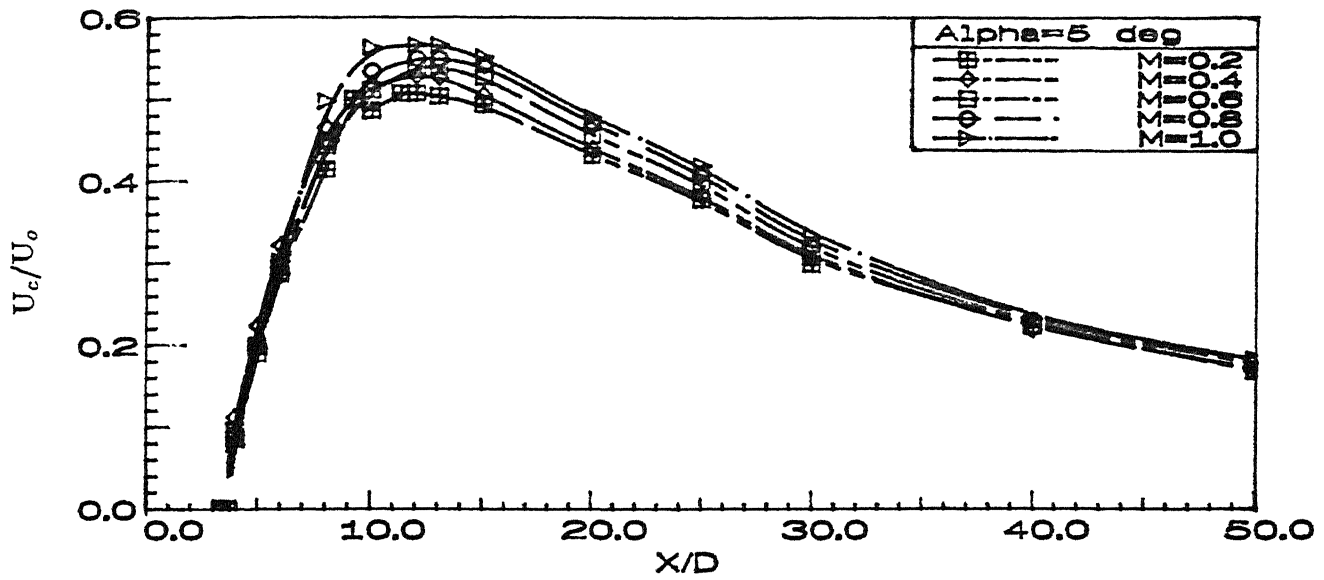
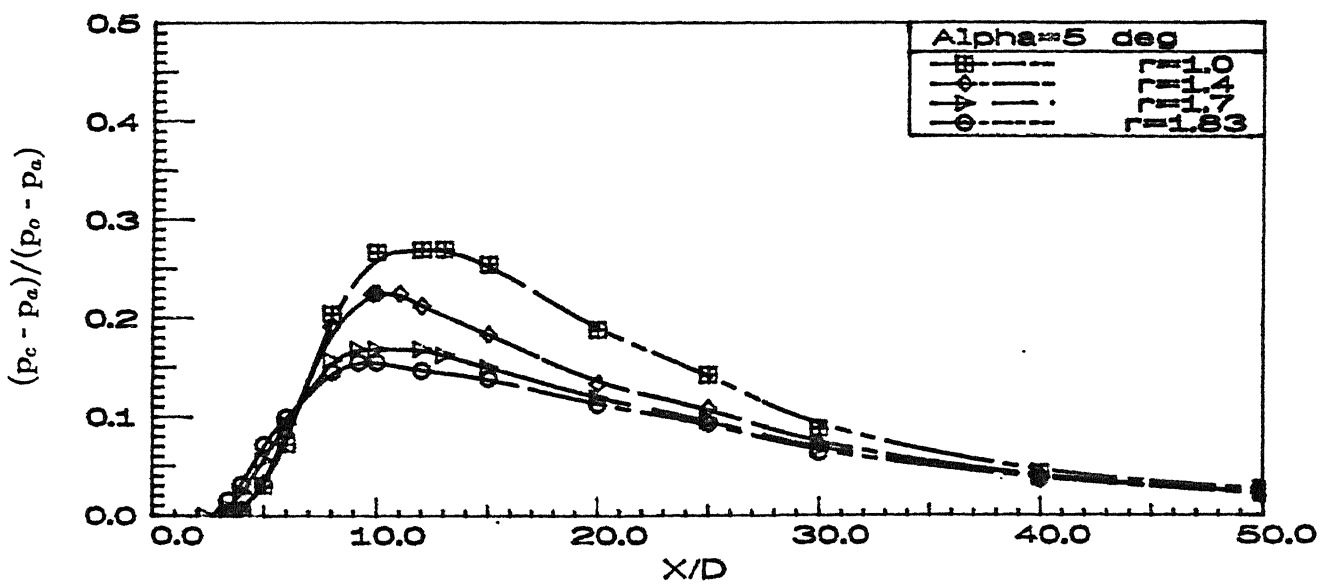


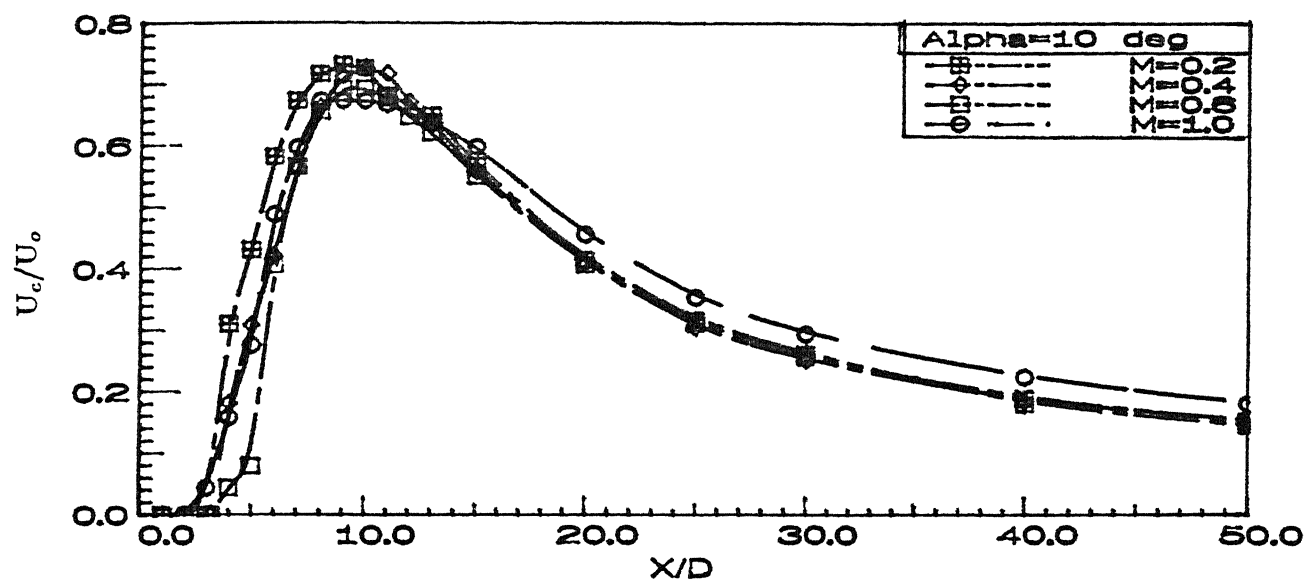
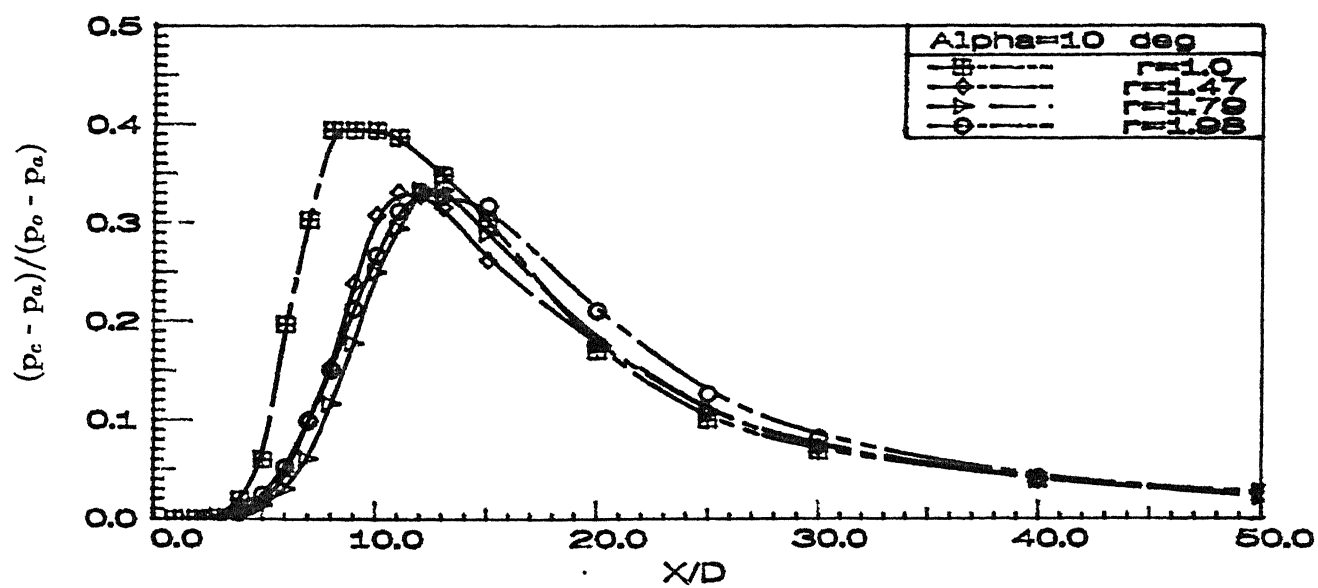
Fig 1.c Under-expanded jets

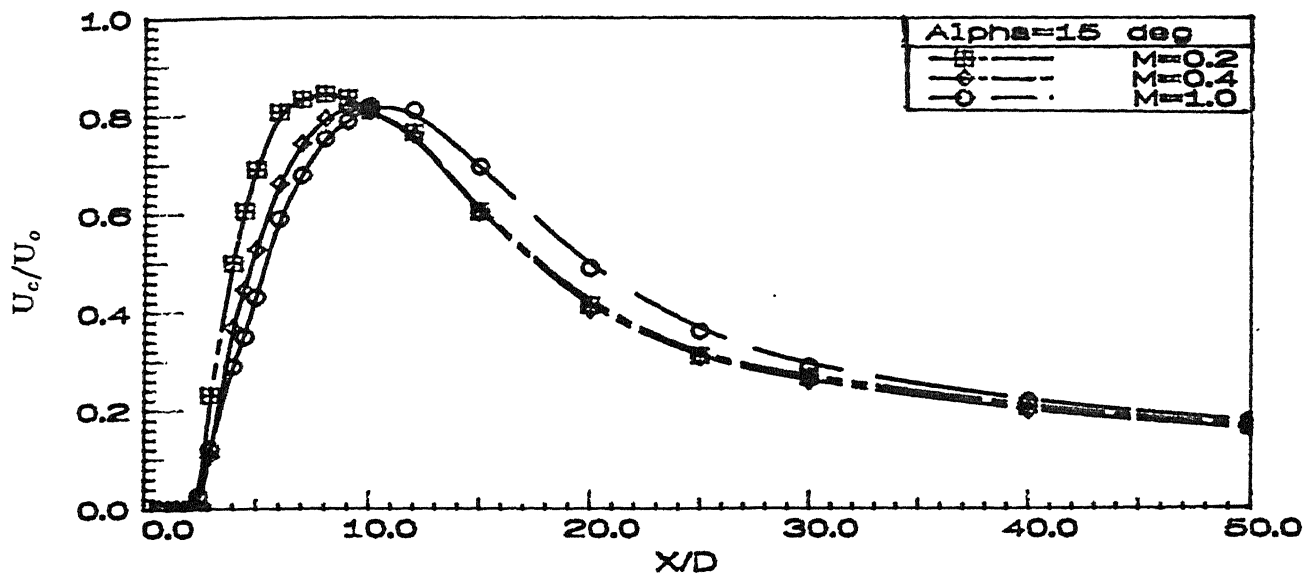
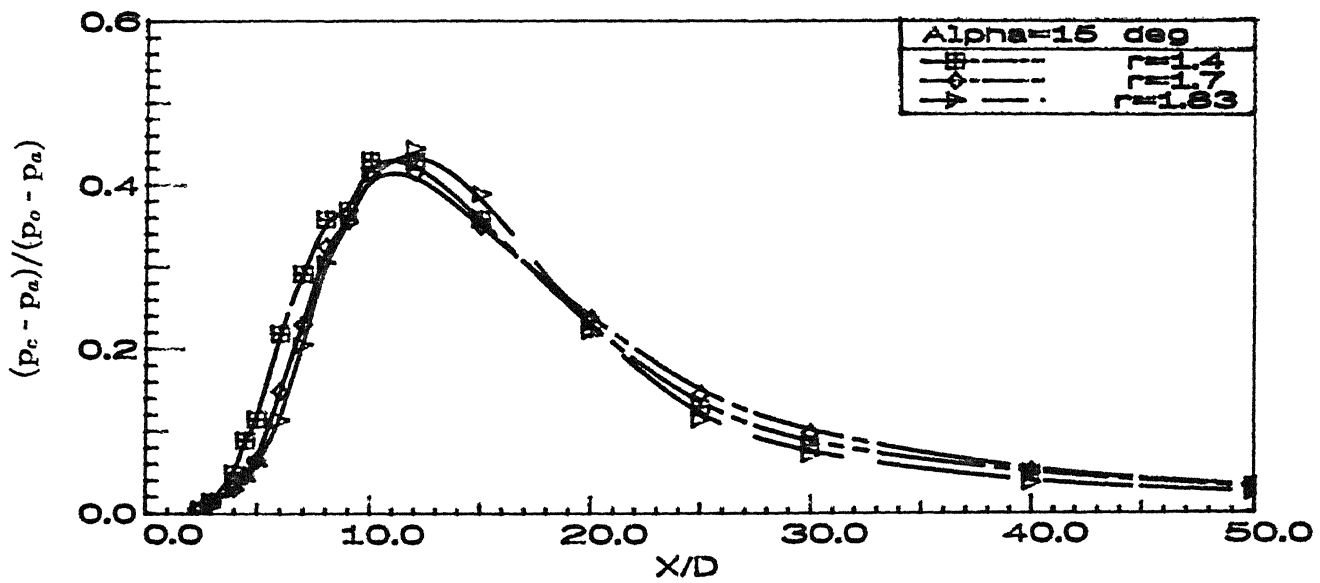


Pressure probes.

Fig 2.a1 Centerline velocity decay ($\alpha = 0^\circ$)Fig 2.a2 Centerline pressure decay ($\alpha = 0^\circ$)

Fig 2.b1 Centerline velocity decay ($\alpha = 5^\circ$)Fig 2.b2 Centerline pressure decay ($\alpha = 5^\circ$)

Fig 2.c1 Centerline velocity decay ($\alpha = 10^\circ$)Fig 2.c2 Centerline pressure decay ($\alpha = 10^\circ$)

Fig 2.d1 Centerline velocity decay ($\alpha = 15^\circ$)Fig 2.d2 Centerline pressure decay ($\alpha = 15^\circ$)

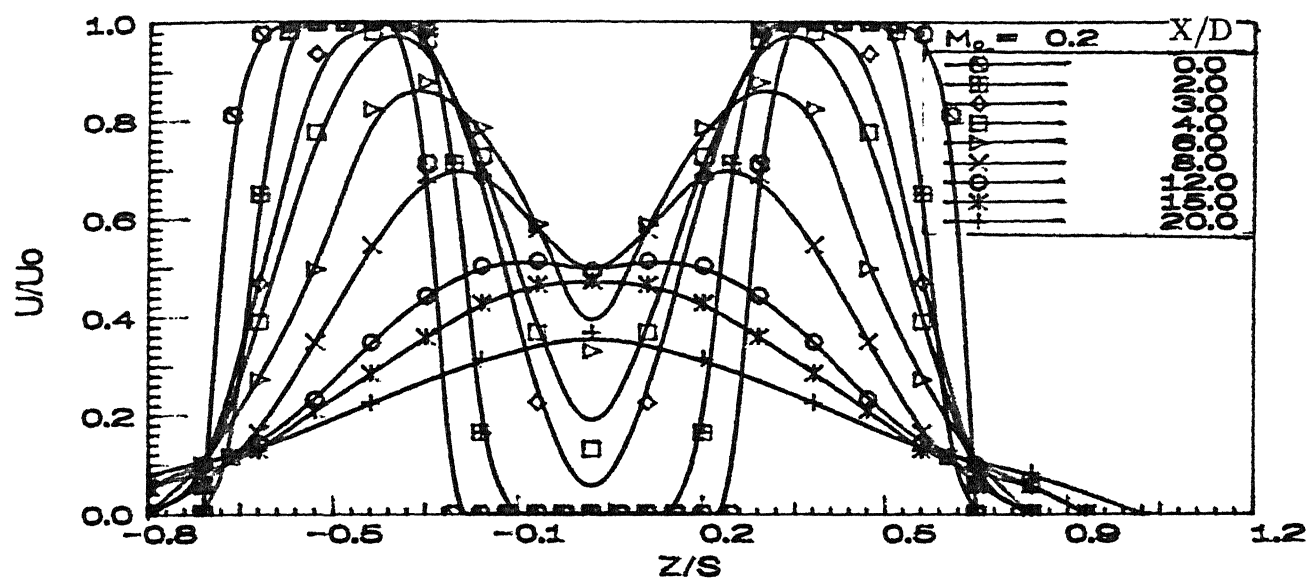


Fig 3.a1 Mean velocity profiles at various X/D ($\alpha = 5^\circ$) in X-Z plane

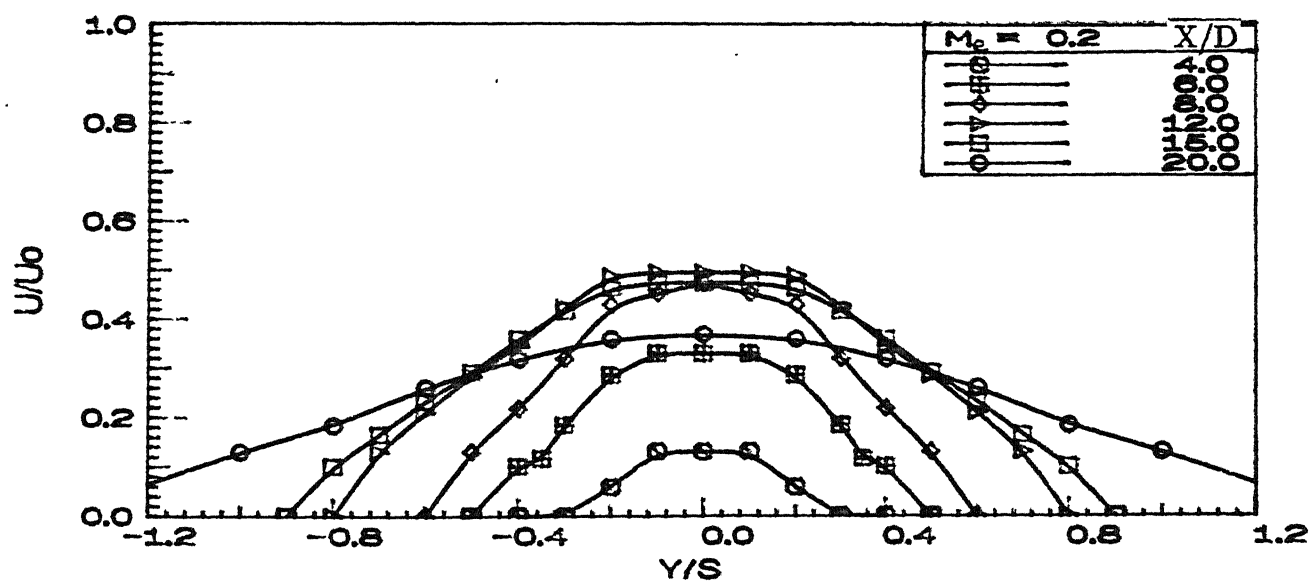


Fig 3.a2 Mean velocity profiles at various X/D ($\alpha = 5^\circ$) in X-Y plane

Fig 3.b1 Isometric view of mean velocity profiles for twin cross jets in X-Z plane

$[M_e = 0.2, \alpha = 10^\circ]$

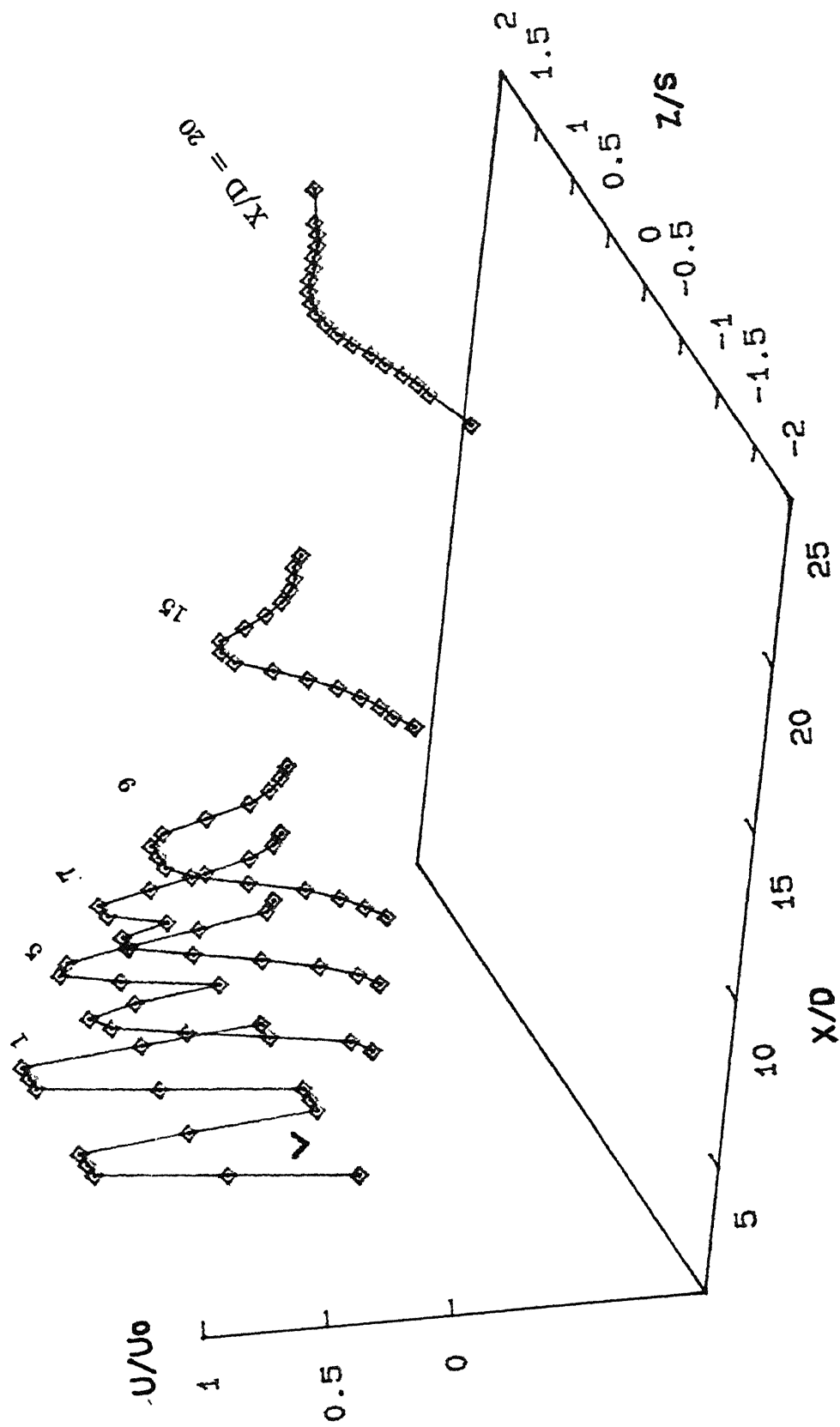
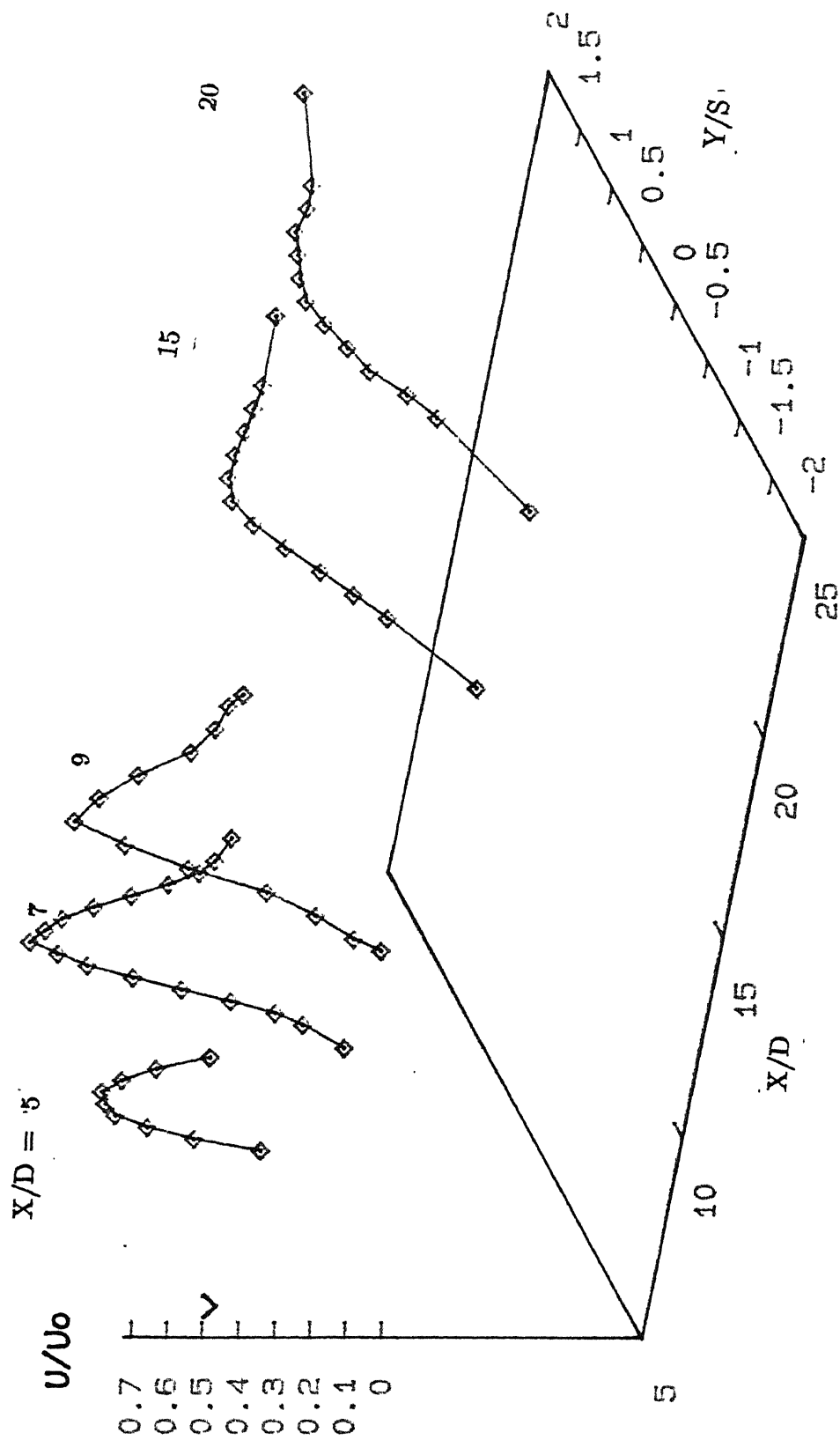


Fig 3.b2 Isometric view of mean velocity profiles for twin cross jets in X-Y plane

$[M_e = 0.2, \alpha = 10^\circ]$



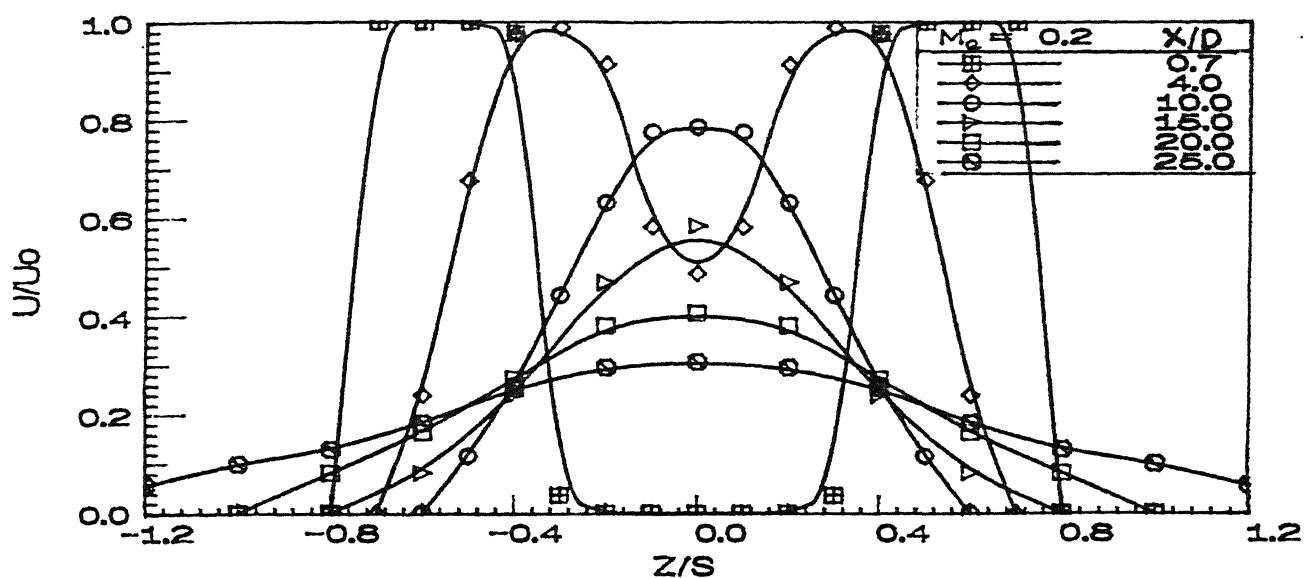
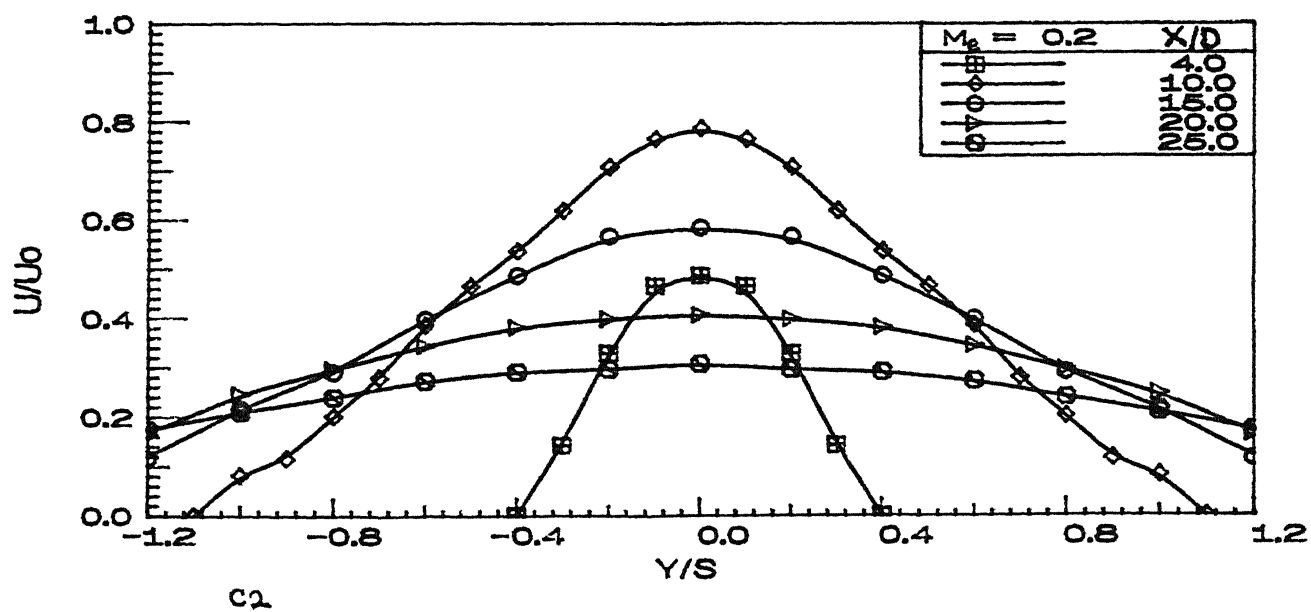


Fig 3.c1 Mean velocity profiles at various X/D ($\alpha = 15^\circ$)



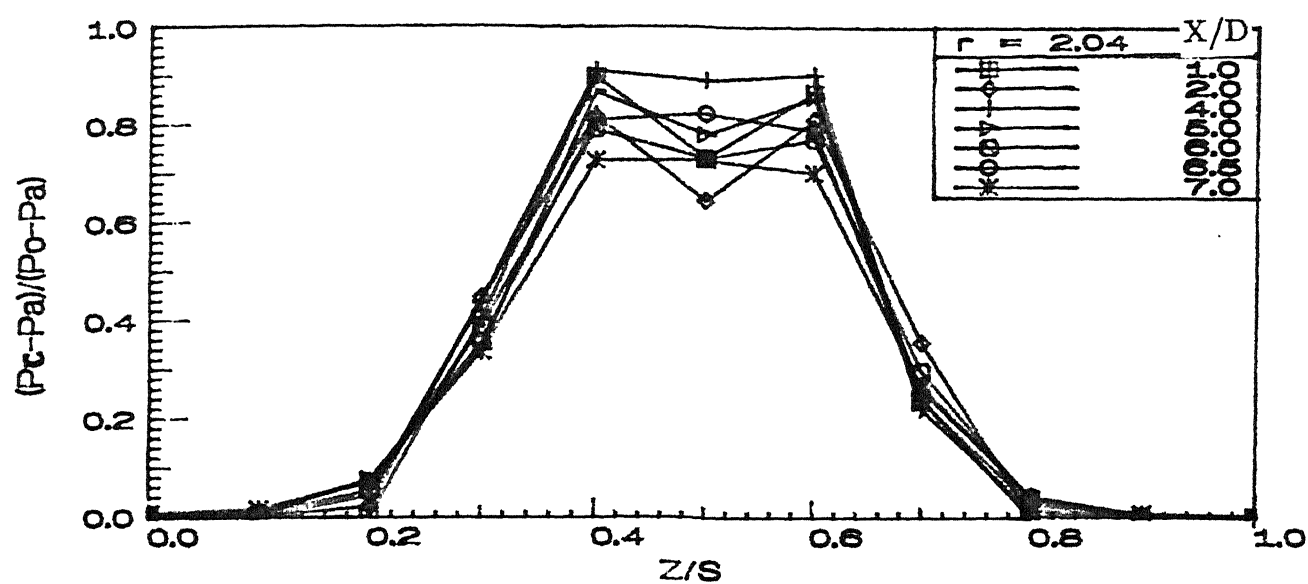


Fig 4.a Velocity profiles in the potential core region ($\alpha = 0^\circ$)

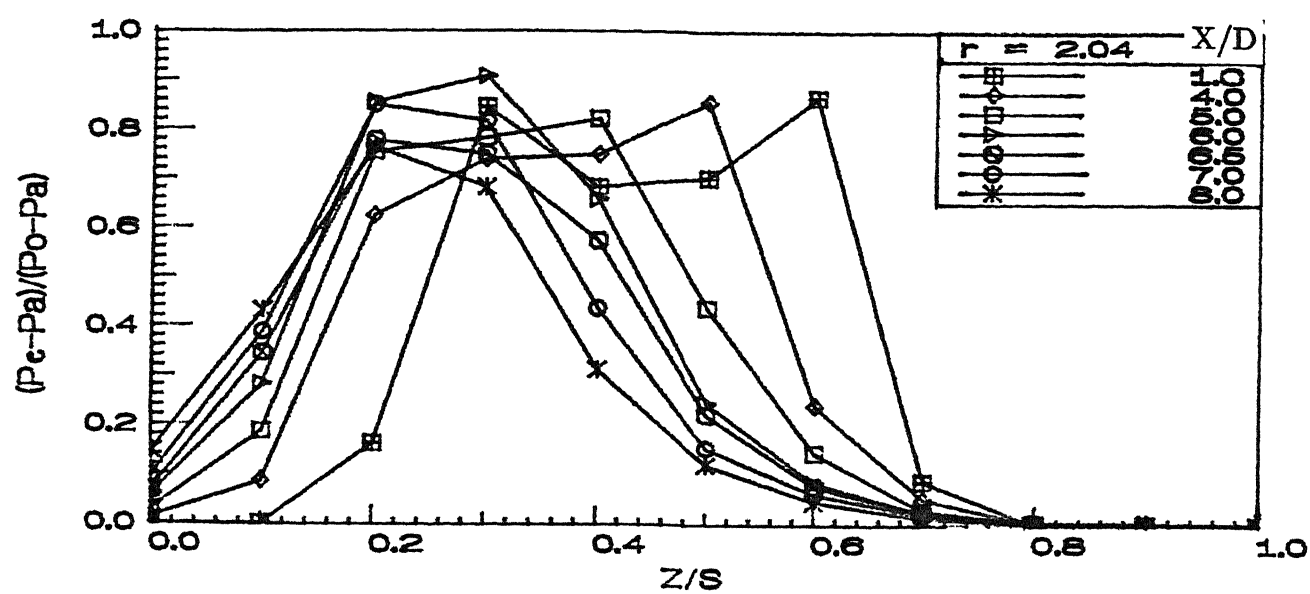


Fig 4.b Velocity profiles in the potential core region ($\alpha = 10^\circ$)

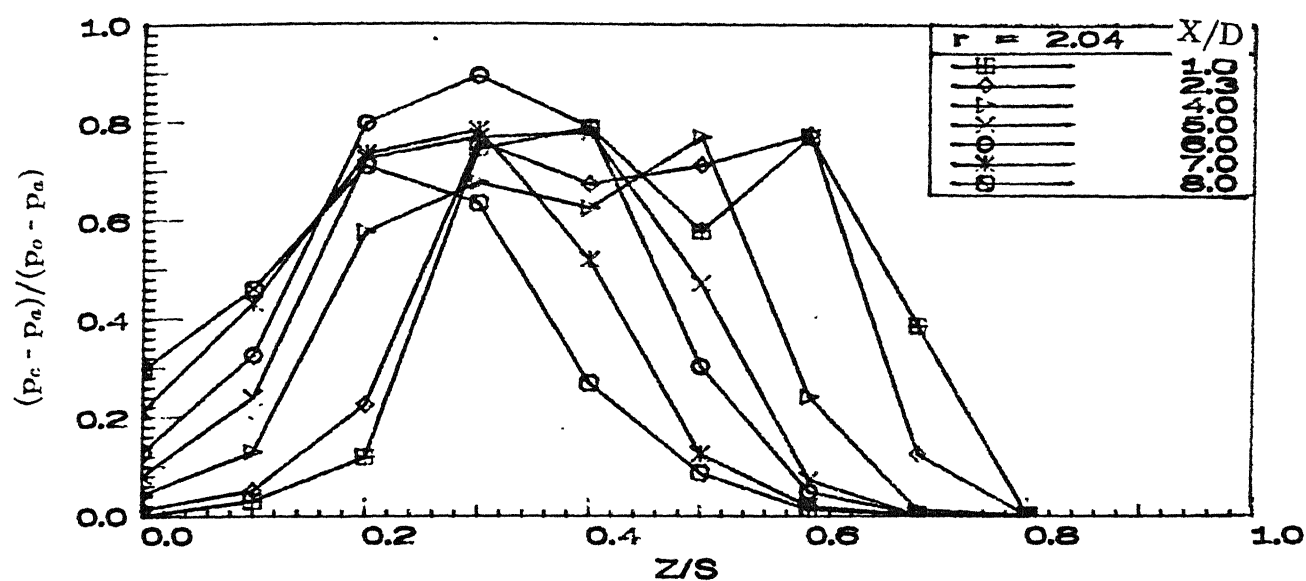


Fig 4.c Velocity profiles in the potential core region ($\alpha = 15^\circ$)

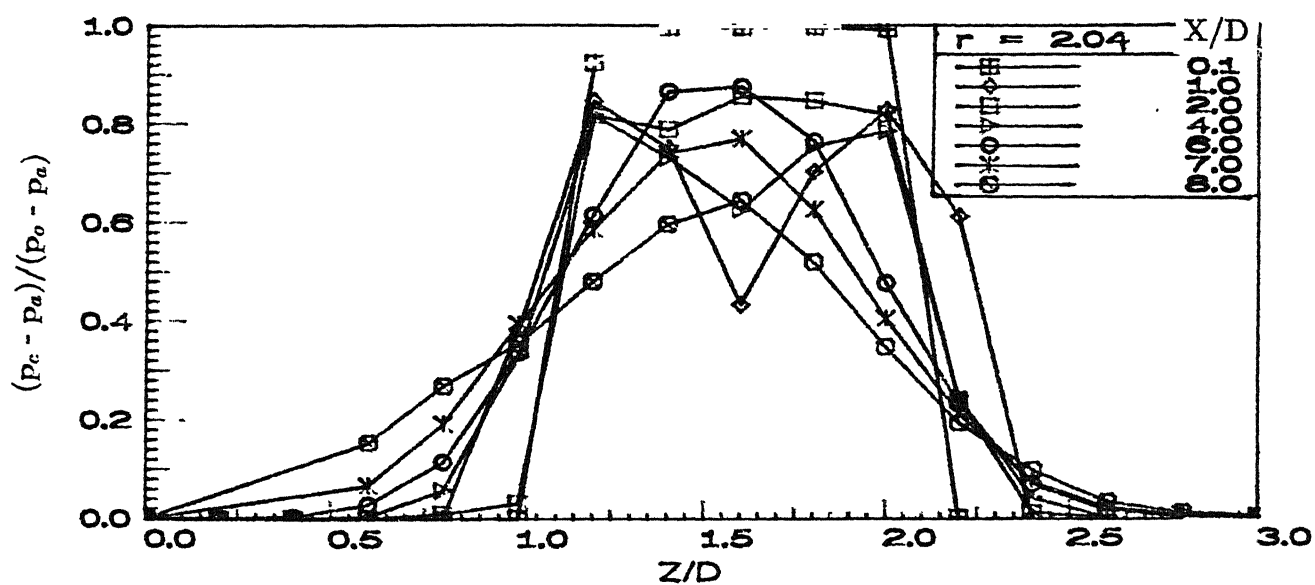


Fig 4.d Velocity profiles in the potential core region (Single jet)

CENTRAL LIBRARY
I. I. T., KANPUR
Ser. No. A. 117799

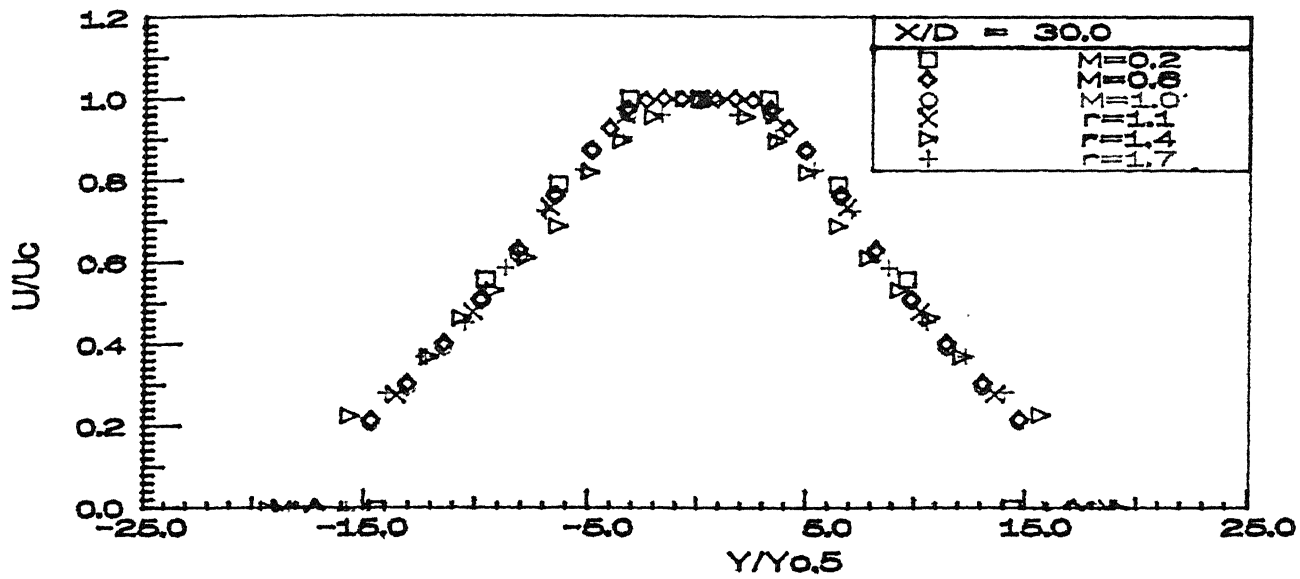


Fig 5.a1 Similarity profiles (Parallel jet) in X-Y plane ($X/D = 30$)

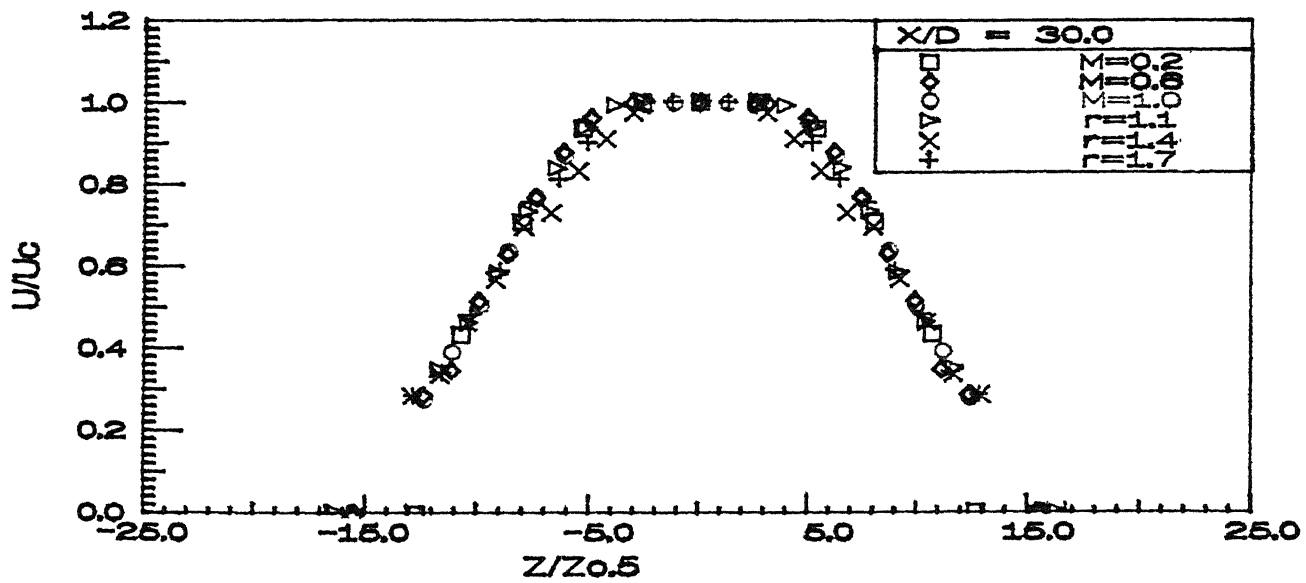


Fig 5.a2 Similarity profiles (Parallel jet) in X-Z plane ($X/D = 30$)

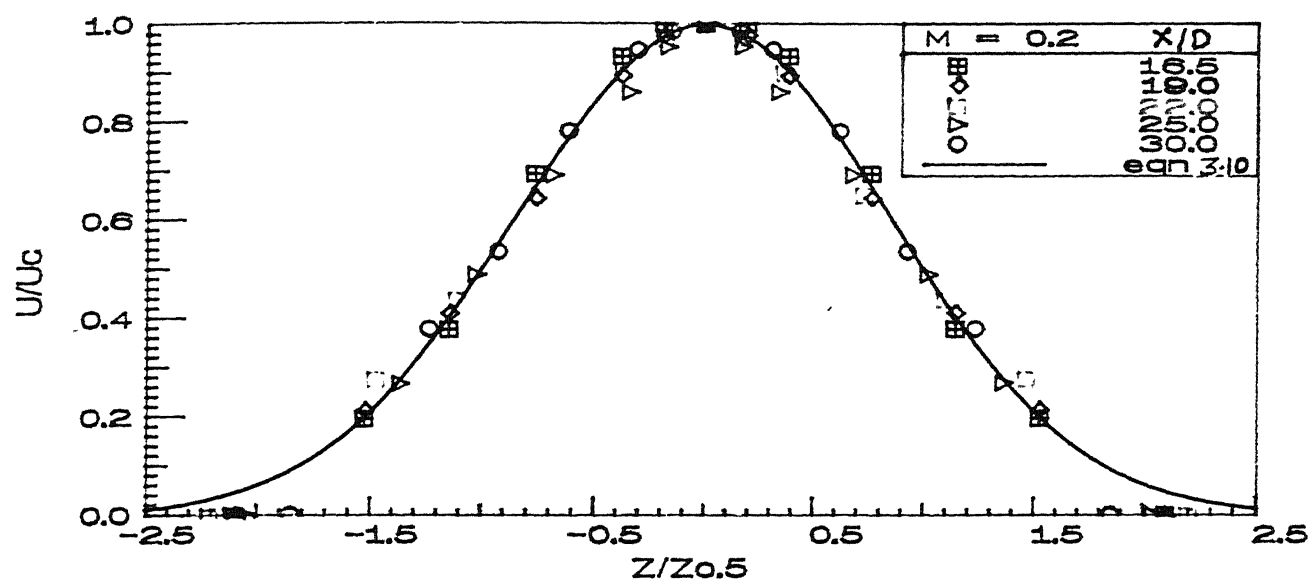


Fig 5.b1 Similarity profiles ($\alpha = 5^\circ$) in X-Z plane ($M_e = 0.2$)

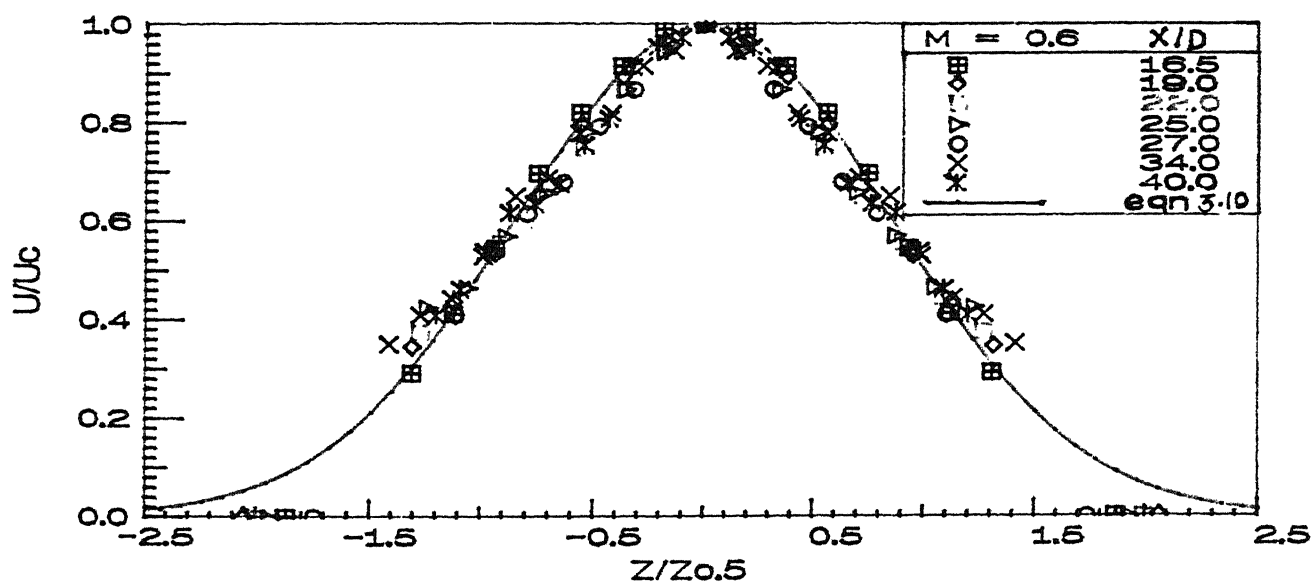


Fig 5.b2 Similarity profiles ($\alpha = 5^\circ$) in X-Z plane ($M_e = 0.6$)

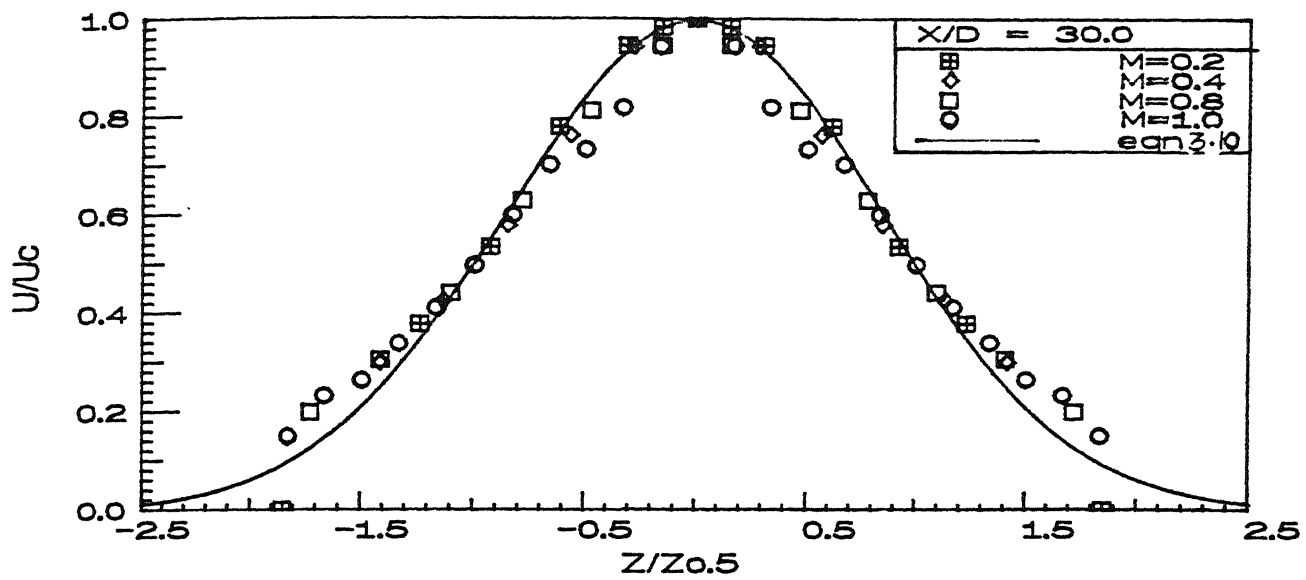


Fig 5.d1 Similarity profiles ($\alpha = 5^\circ$) in X-Z plane ($X/D = 30$)

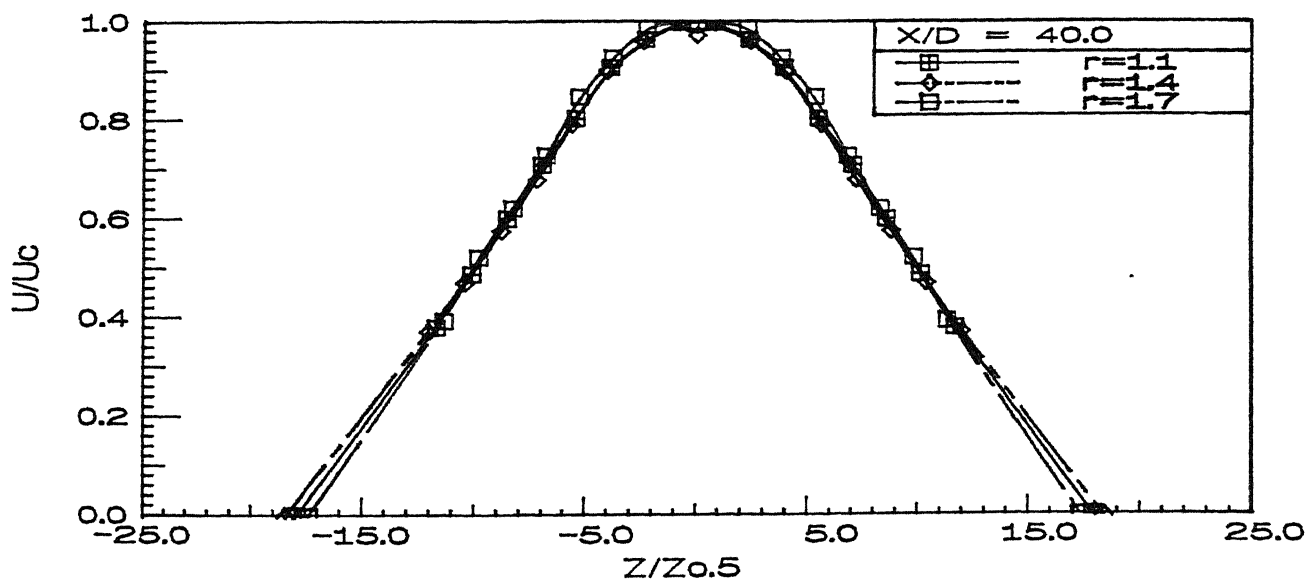


Fig 5.d2 Similarity profiles ($\alpha = 5^\circ$) in X-Z plane ($X/D = 40$)

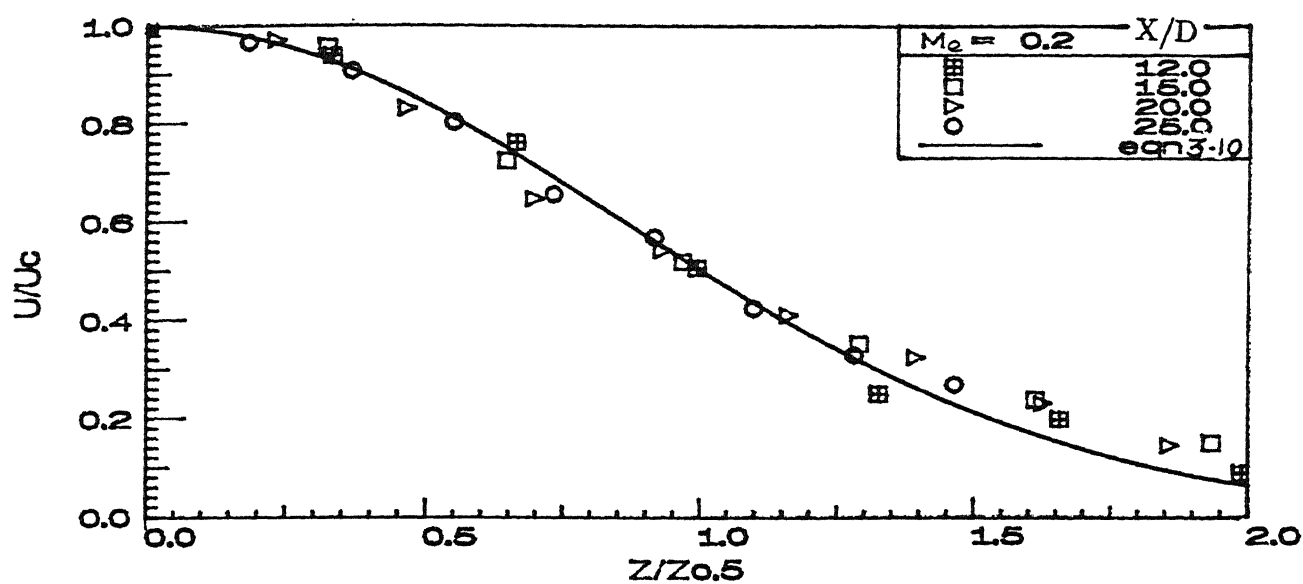


Fig 5.e Similarity profiles ($\alpha = 10^\circ$) in X-Z plane ($M_e = 0.2$)

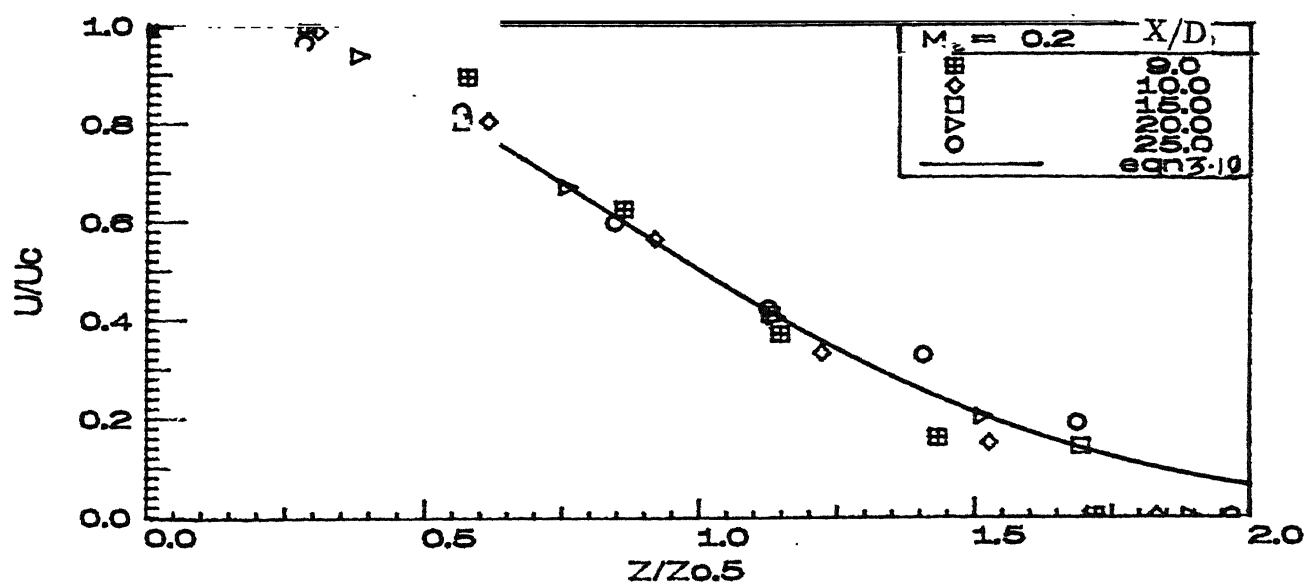


Fig 5.f Similarity profiles ($\alpha = 15^\circ$) in X-Z plane ($M_e = 0.2$)

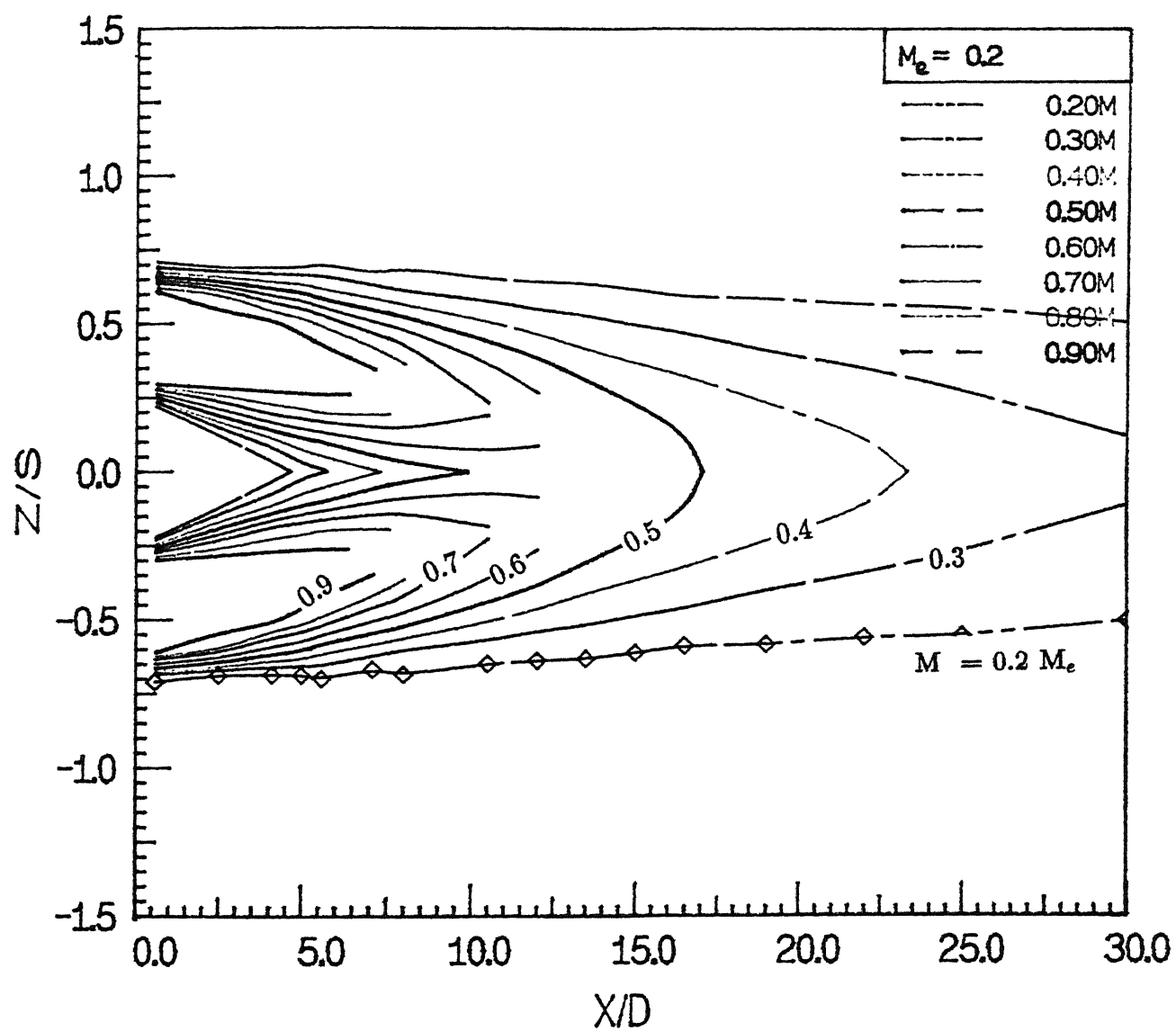


Fig 6.a1 Iso Mach number profiles ($\alpha = 5^\circ$, $M_e = 0.2$)

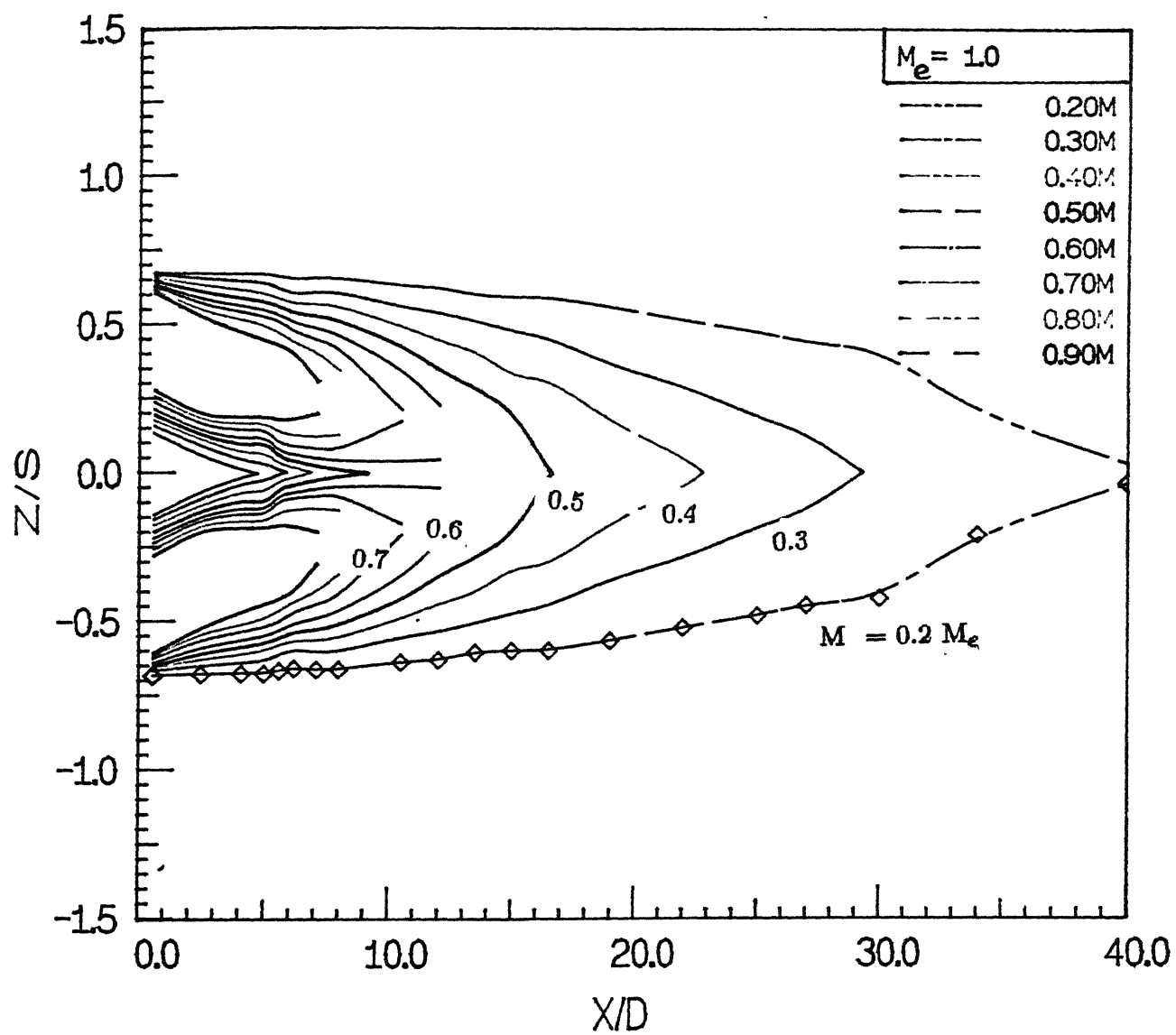


Fig 6.a2 Iso Mach number profiles ($\alpha = 50$, $M_e = 1.0$)

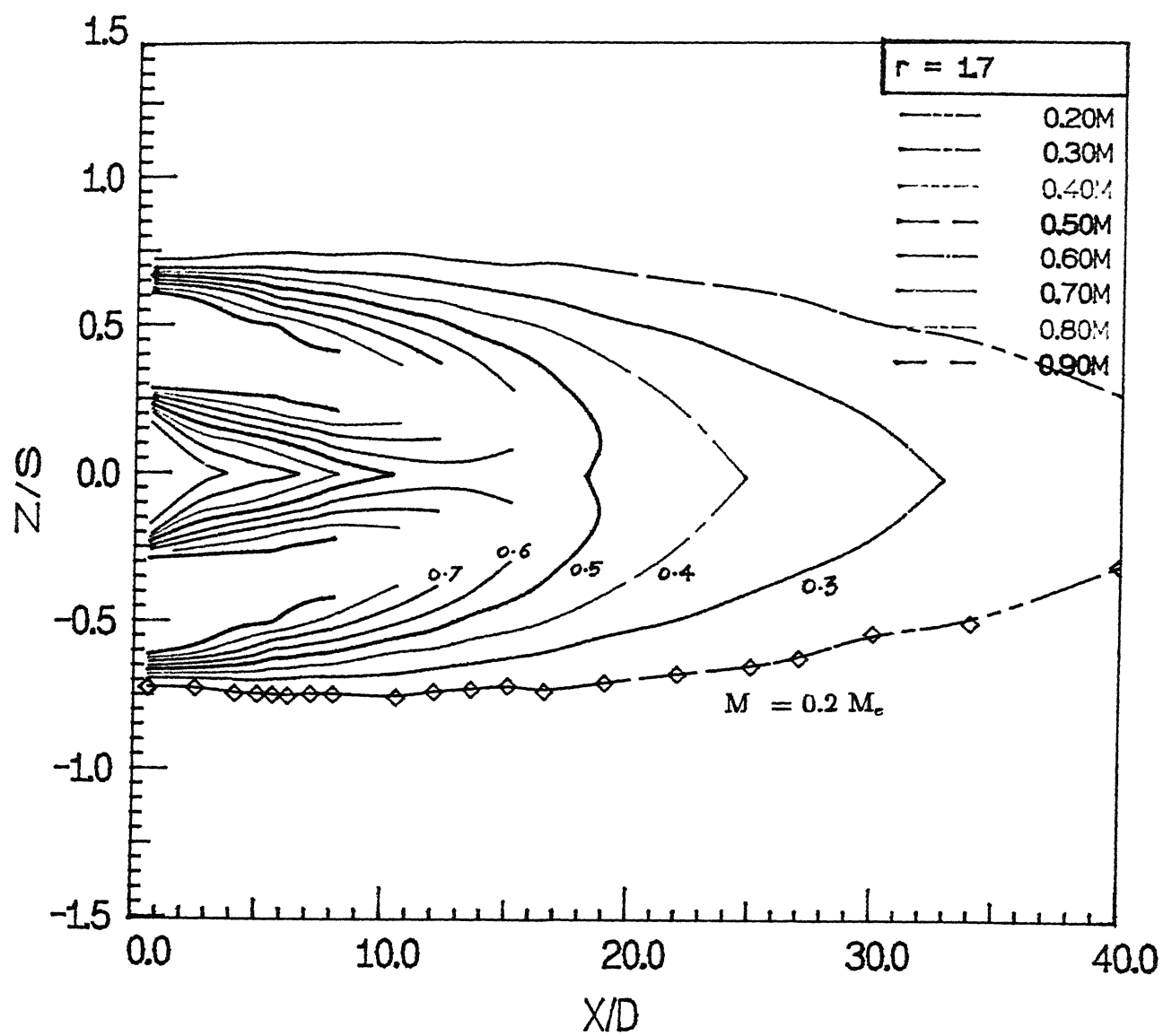


Fig 6.a3 Iso Mach number profiles ($\alpha = 50$, $r = 1.7$)

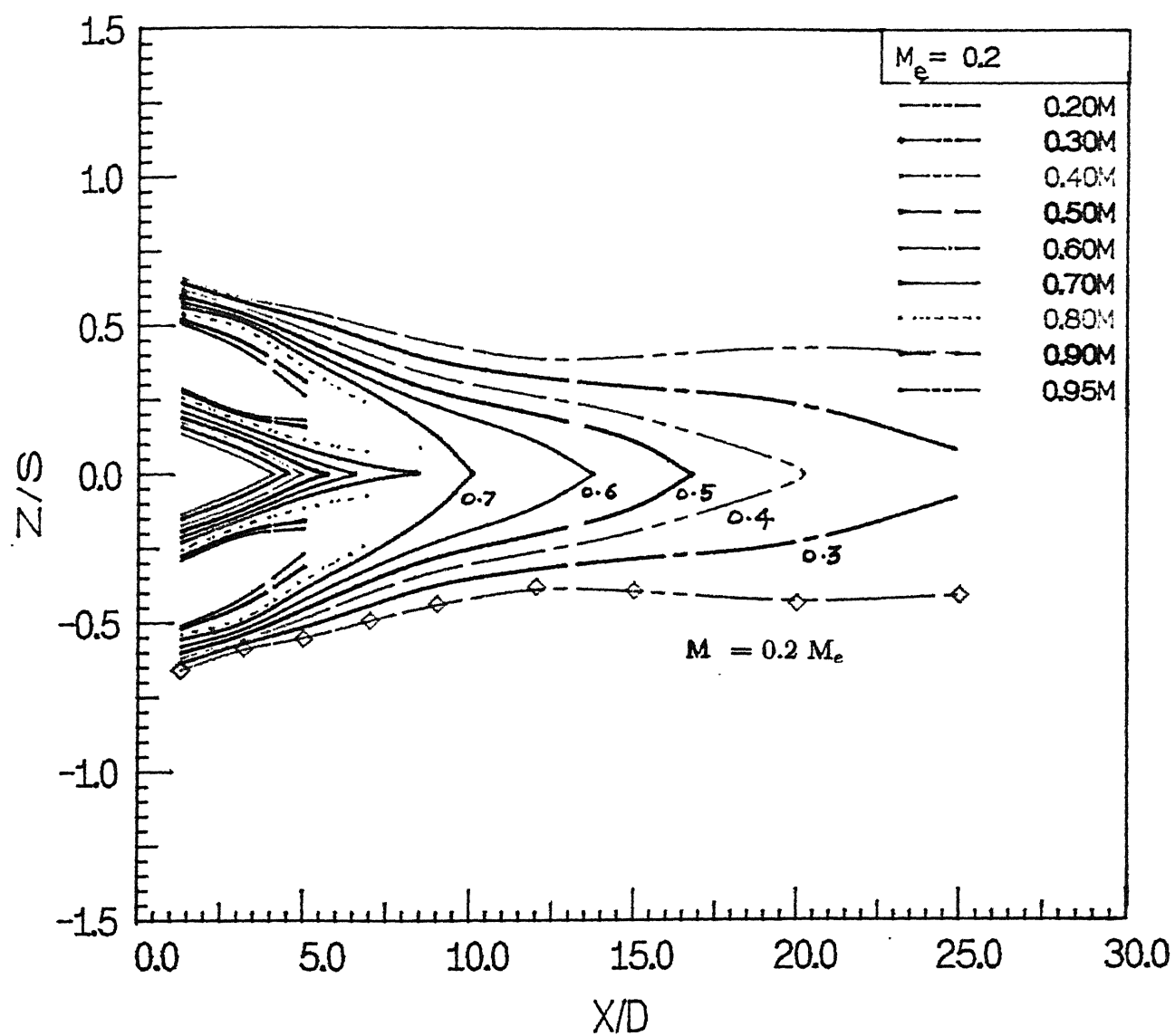


Fig 6.b Iso Mach number profiles ($\alpha = 10^\circ$, $M_e = 0.2$)

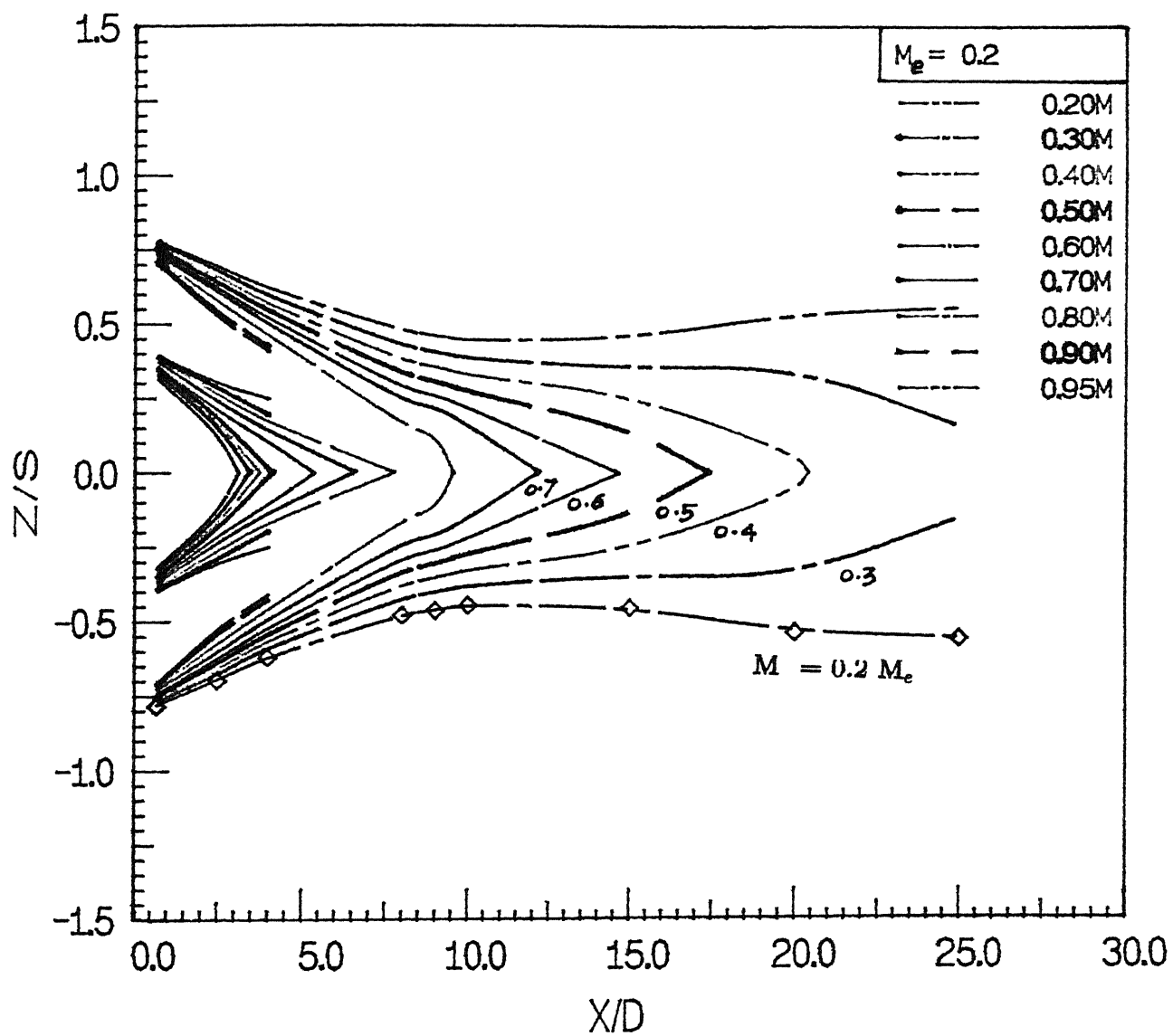


Fig 6.c Iso Mach number profiles ($\alpha = 15^\circ$, $M_e = 0.2$)

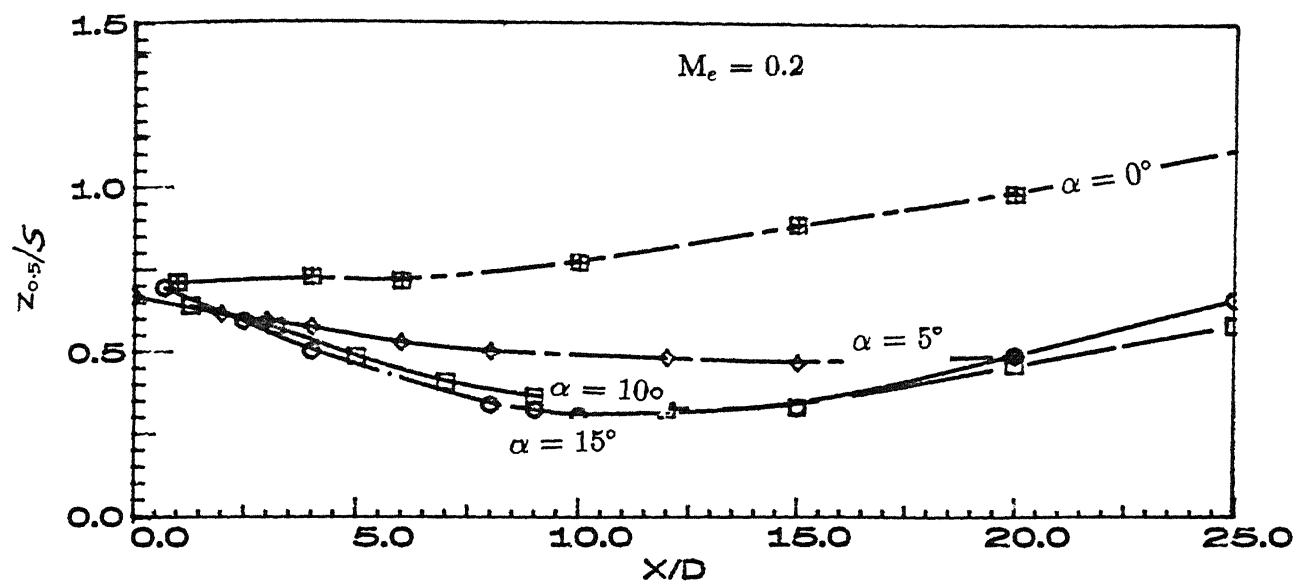


Fig 7.a Variation of half width with X/D for $M_e = 0.2$ in X-Z plane

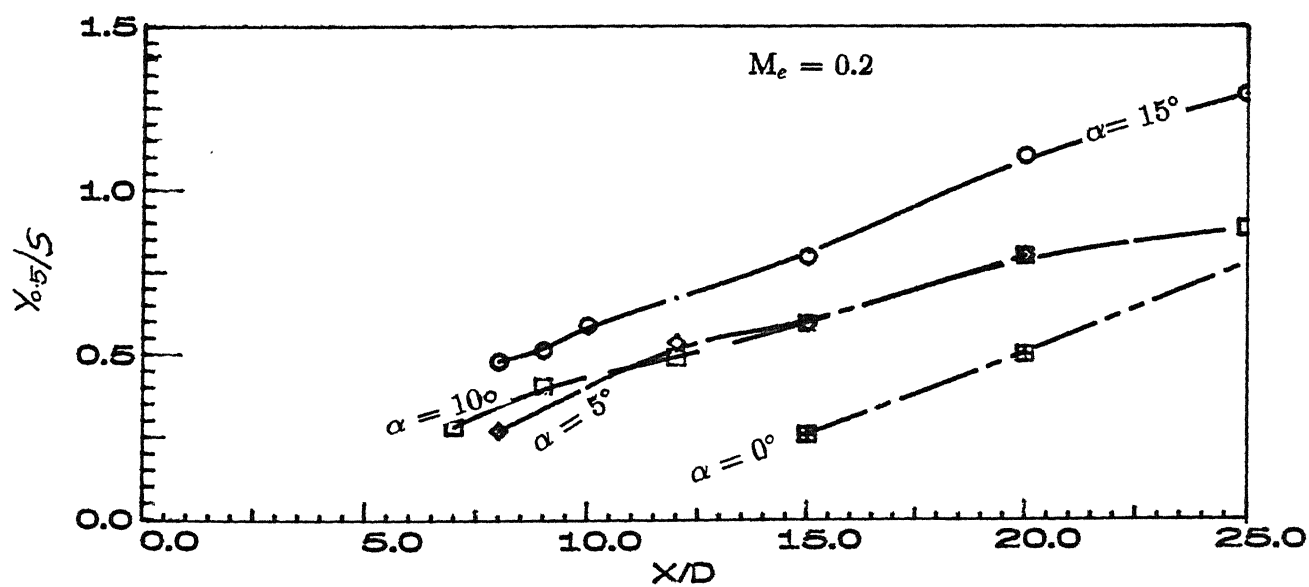


Fig 7.b Variation of half width with X/D for $M_e = 0.2$ in X-Y plane

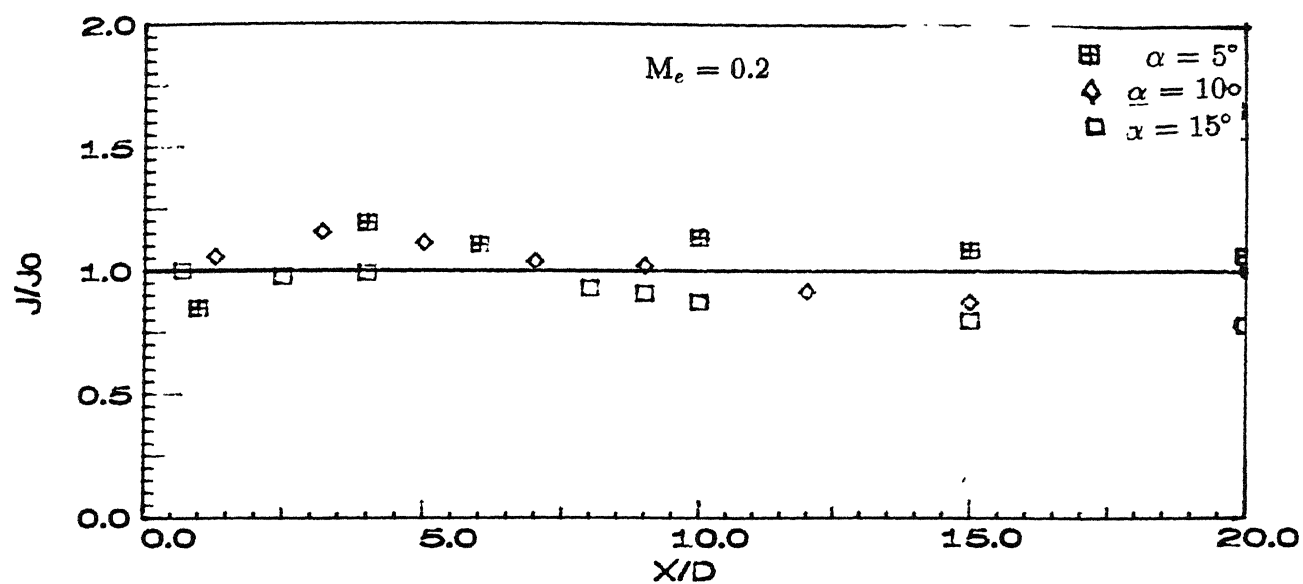


Fig 8 Momentum flux along axial direction ($M_e = 0.2$)

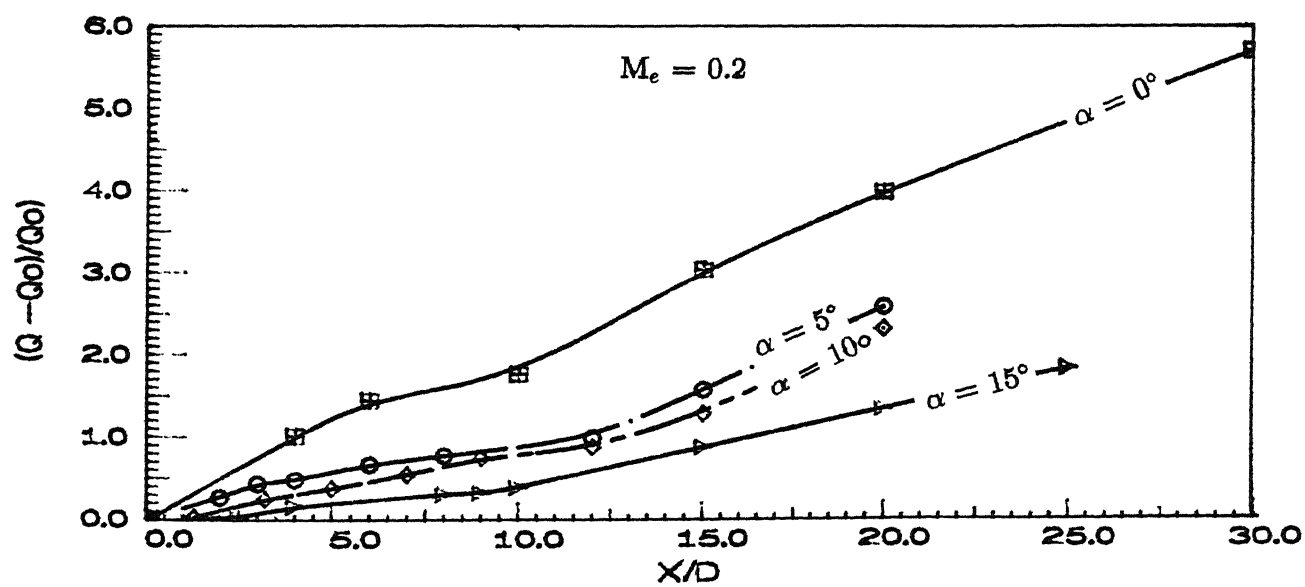


Fig 9 Variation of entrainment with axial distance ($M_e = 0.2$)

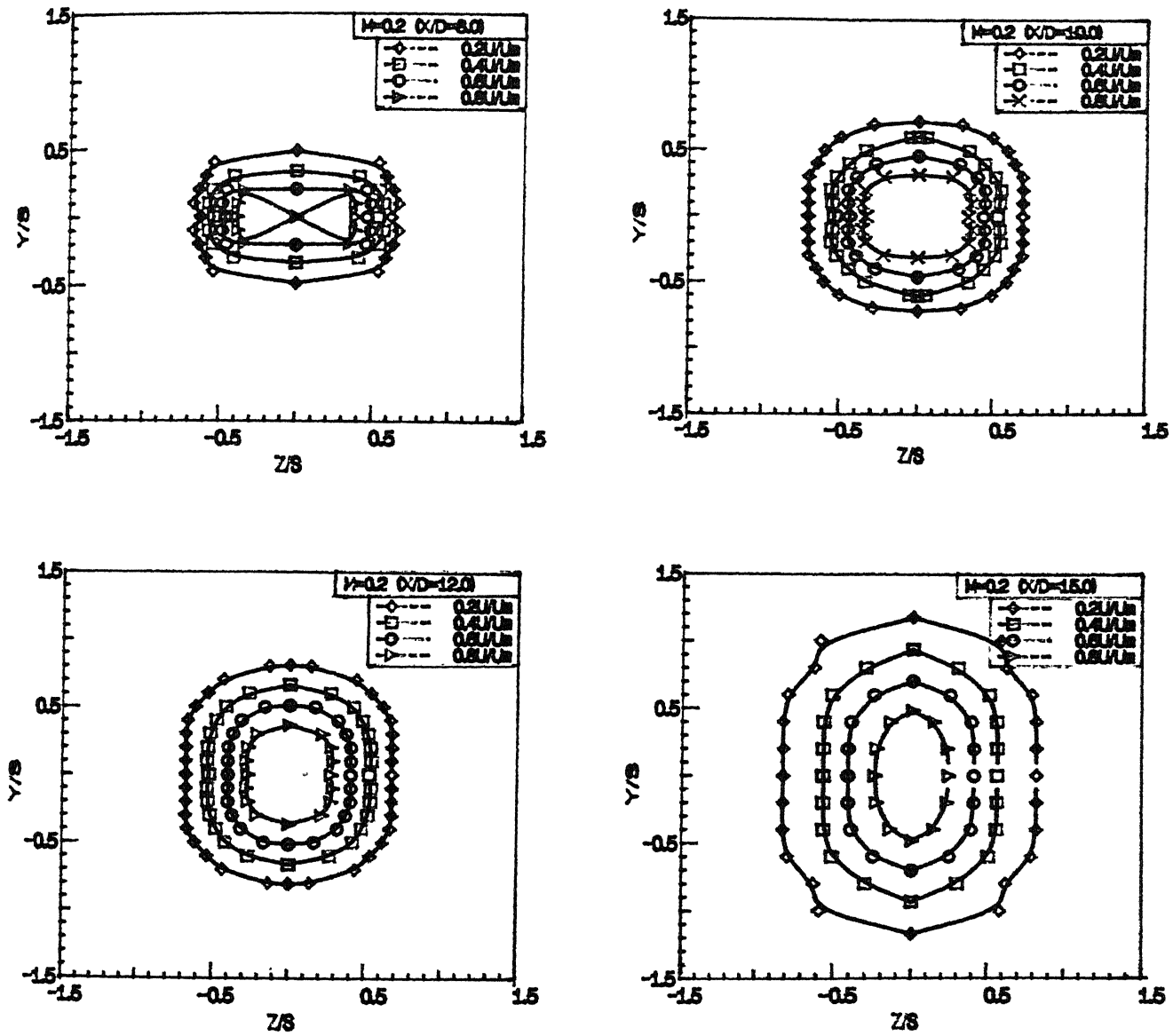


Fig 10.a Constant velocity contours ($\alpha = 5^\circ$)

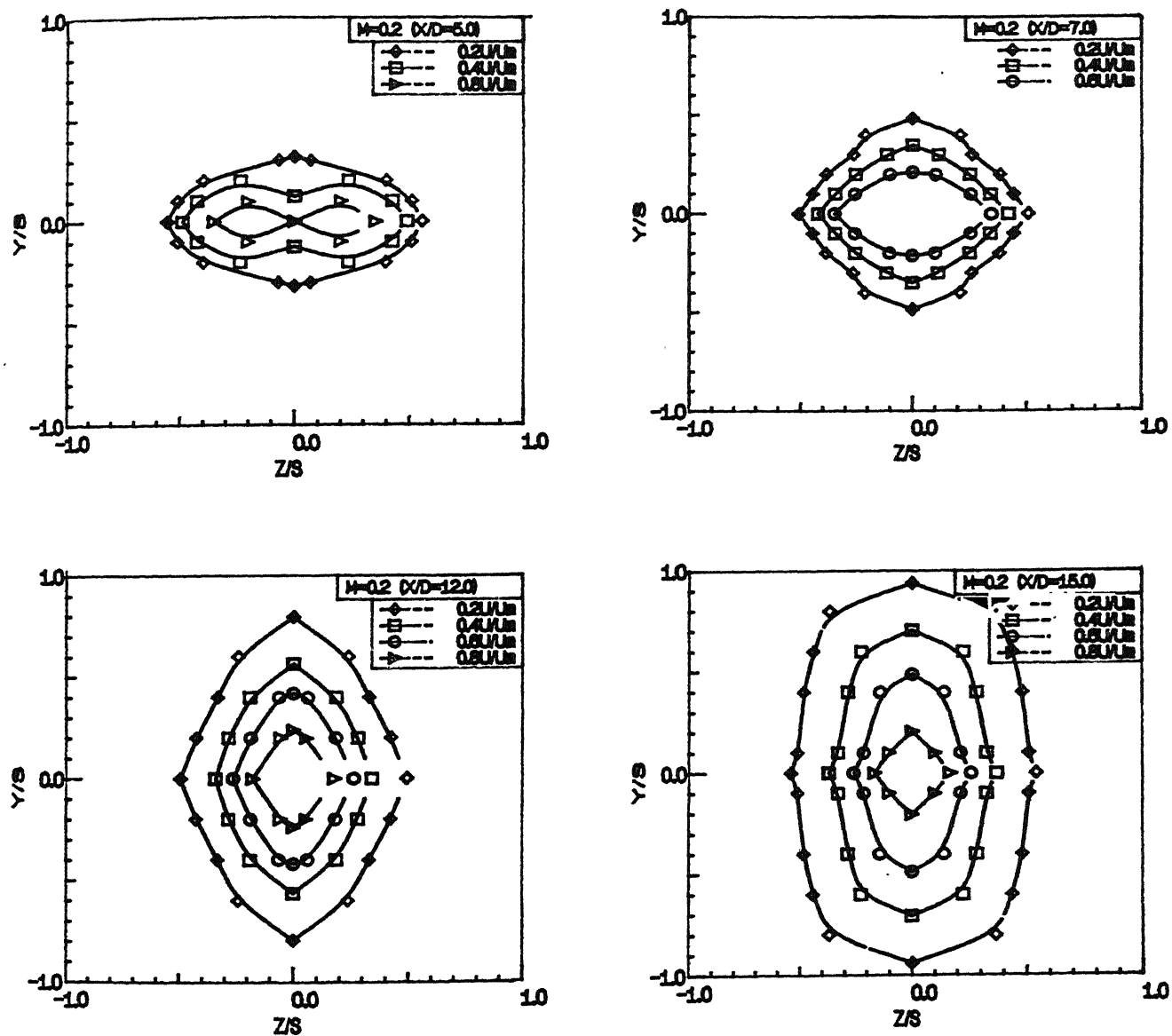


Fig 10.b Constant velocity contours ($\alpha = 10^\circ$)

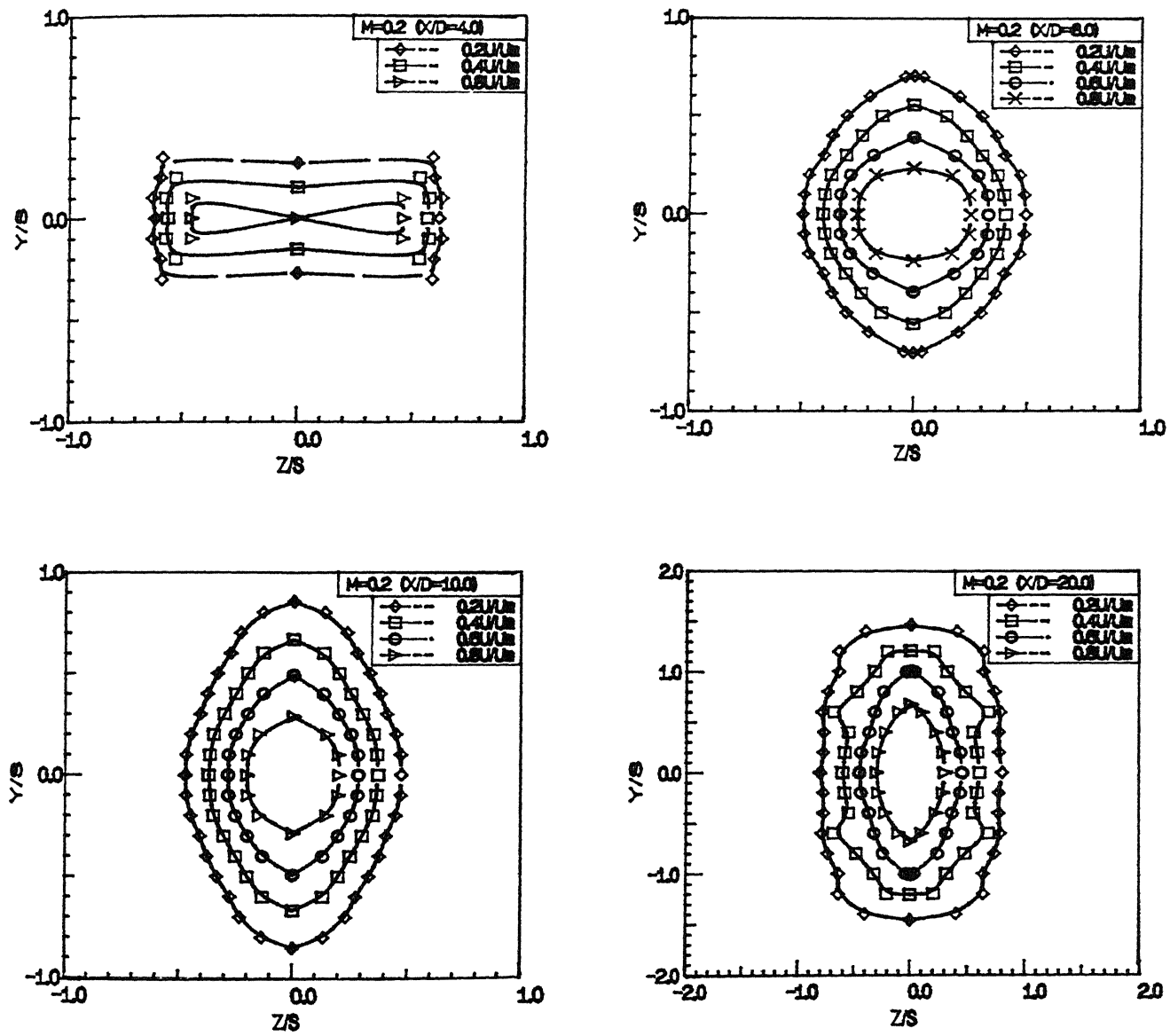
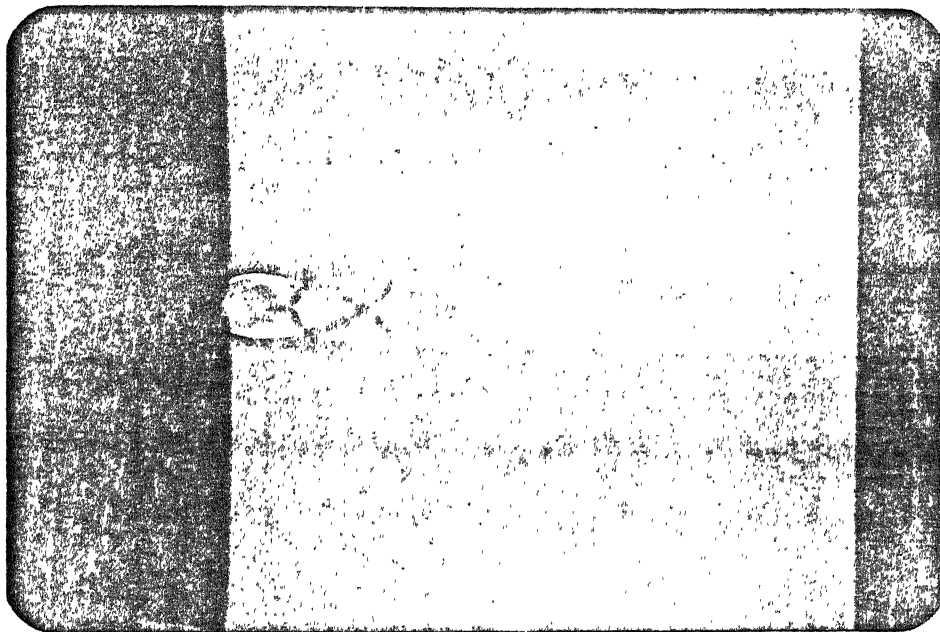
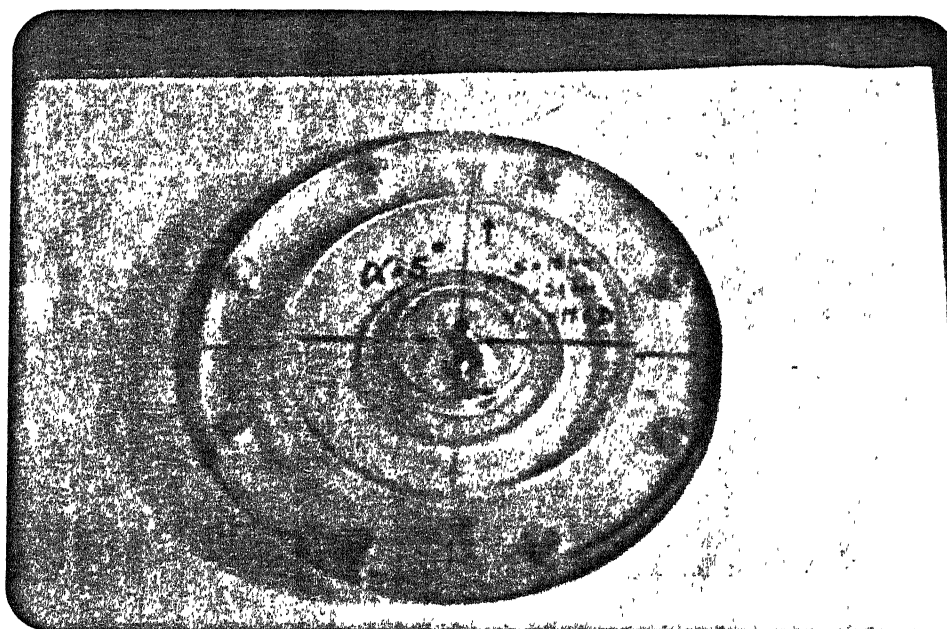


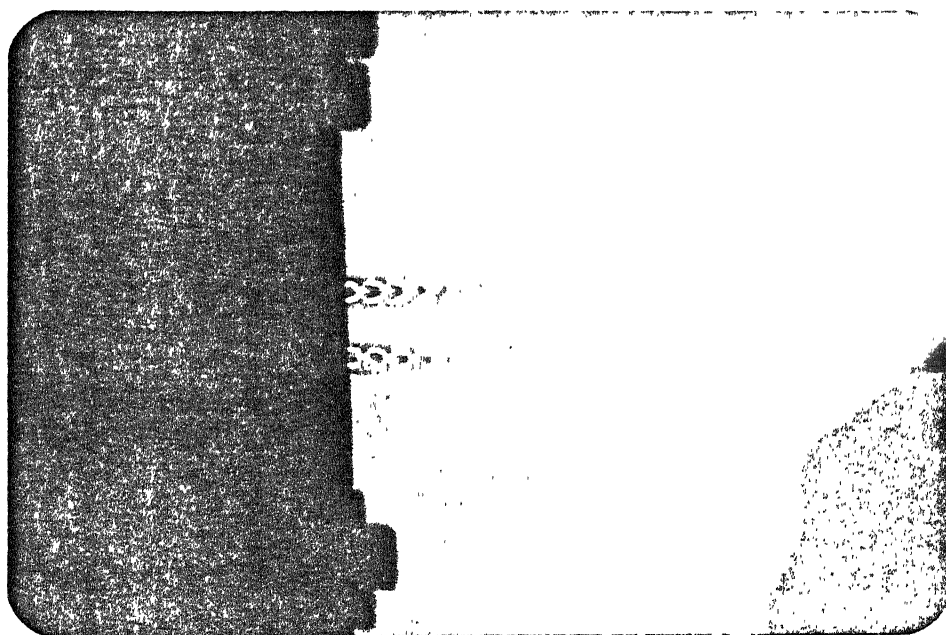
Fig 10.c Constant velocity contours ($\alpha = 15^\circ$)



Single set.



$\alpha = 5^\circ$ - Nonglare



$\alpha = 0^\circ$

Part II

STUDIES ON PARALLEL TWIN ELLIPTIC JETS

NOMENCLATURE

a	Semi major axis of elliptic orifice
AR	Aspect ratio of elliptic orifice (a/b)
b	Semi minor axis of elliptic orifice
D_e	Equivalent diameter of single circular jet
J_o	Momentum flux at the exit plane
J	Momentum flux at jet cross section
M_e	Exit Mach number
M	Mach number in the flow field
Q_o	Volume flow rate at the exit plane
Q	Volume flow rate in the X-direction
p_a	Ambient pressure
p_e	Static pressure at the exit plane
p_t	Total pressure in the flow field
p_o	Stagnation pressure
S	Orifice centre to centre spacing
U	Mean velocity
U_c	Velocity along centreline
U_m	Maximum velocity along centreline at any cross section
U_o	Velocity at the exit plane
X	Coordinate perpendicular to exit plane
Y	Transverse coordinate parallel to plane of symmetry (major axis plane)
$Y_{0.5}$	Half width of jet in Y direction
Z	Spanwise coordinate perpendicular to plane of symmetry (minor axis plane)
$Z_{0.5}$	Half width of jet in Z direction
γ	Specific heat ratio of fluid
ν	Kinematic viscosity of fluid
ρ	Mass density of fluid

Chapter 5

INTRODUCTION

Each planet describes an elliptic path with Sun at one of the foci.

—Kepler's law of planetary motion

Non circular jets are emerging as a new class of passive control mechanism of jet flow. Jet issuing out of non circular nozzles like rectangular, square, triangular, elliptic *etc.*, are found to entrain ambient fluid several times more than equivalent axisymmetric nozzles. Non circular jets are generally referred to as non axisymmetric or three dimensional jets. The increased entrainment of these asymmetric jets has attracted the attention of many researchers.

In the present investigation on non circular jets, jets issuing from elliptic slots have been chosen. The study of elliptic jets is interesting for two major reasons.

⇒ First, it is an intermediate configuration between the two simple and extensively studied geometries — circular and plane jets. Although, the existence of two geometric length scales (*ie* major and minor axes) makes the problem more complicated, a detailed study of elliptic jets with these length scales might facilitate better understanding.

⇒ Second, studies have revealed that the rectangular structures become elliptic-like soon after their roll up in rectangular jets. Thus a systematic study of elliptic jets is also highly relevant to an understanding of the dynamics of rectangular jets which have important practical applications.

The ratio of the major to minor axis of elliptic jet is referred to as the aspect ratio of the jet. The aspect ratio is the obvious major parameter in determining the enhancement of the jet spreading, because large entrainment was not reported in previous three dimensional jet studies [1] in which the aspect ratios were larger than 5:1. Schadow *et al* [9] made measurements in jets with several aspect ratios and suggested that the optimum value is between 2:1 and 3:1. Hence three dimensional jets of low aspect ratio are beneficial from entrainment point of view.

One of the distinguishing features of asymmetric or three dimensional jets is the axis switching phenomenon. Earlier work done on these jets showed that the spread in the minor axis plane is more than that in the major axis plane, resulting in a cross over point at which the jet becomes locally quasi axisymmetric. Downstream of the point the major axis became the minor axis and vice versa. The axial location of this cross over point was found to be proportional to the aspect ratio of the jet nozzle. The possible reason for this different entrainment characteristics in major and minor axis planes could be that the velocity gradients are steeper in the minor axis plane than in the major axis plane and the attainment of equilibrium conditions require more entrainment of ambient fluid in the minor axis plane to equalise the velocity gradients in both the planes.

5.1 Literature review

Previous work on elliptic turbulent free jets [3–6] has been based on low aspect ratio nozzles with contoured contraction. The jets had a smooth transition from the contraction to the nozzle exit plane in all the studies, which have established that elliptic turbulent free

jets entrain significantly more ambient fluid than their circular counterparts in the initial region. Ho and Gutmark [5] observed three axis switchings within the axial distance of 40 equivalent diameters. The first switching occurred at $X/D_e \approx 5$.

Hussain and Husain [6], [7] investigated extensively, the vortex structure development and interaction in elliptic jet flow fields. They observed (flow visualization) that elliptic jets of very low aspect ratio ($AR < 3:1$) had a different vortex interaction mechanism compared to elliptic jets of $AR\ 4:1$. But in either case the entrainment was found to be almost the same.

Quinn [8] investigated the mixing characteristics of an elliptic turbulent free jet from a sharp edged elliptical slot of $AR\ 5:1$. Two switches of the major and minor axes were observed and it was found that the jet attained an axisymmetry at about 30 equivalent slot diameters downstream of the exit plane. He concluded that compared to the round slot jet of the same exit area as that of the elliptic slot, the elliptic jet entrained ambient fluid faster both in near and far fields.

Passive control of jet flow can be achieved either by asymmetric jets or by multiple jets. Non circular jets are gaining lot of importance now. Multiple asymmetric jets are expected to emerge as an effective method of passively controlling the jets. Many researchers have studied the flow field of three dimensional and multiple jets. But study of multiple jets are invariably restricted to multiple circular or plane (rectangular jets of very high aspect ratio) jets. Similarly three dimensional jet studies have been carried out only on single jet flow field. This lack of information on multiple three dimensional jets provided the motivation for the present study.

In multijet studies the mutual influence of neighbouring jets on one another requires clear understanding and hence twin jet flow studies assume importance. Therefore, the present experimental study presents detailed mean flow data for the flow of turbulent free air jet issuing from sharp edged twin elliptic slots. Elliptic slots, instead of contoured elliptic nozzles have been chosen for this study because of three reasons.

- ⊙ In many practical applications, expeditious manufacturing and ease of installation may necessitate the use of sharp edged slots in preference to nozzles with contoured upstream shaping.
- ⊙ Previous studies show that sharp edged slots have higher mean axial (streamwise) velocity decay rates than contoured nozzle jets implying higher entrainment rates of ambient fluid and consequently better mixing.
- ⊙ One more consideration prompted the choice of slots instead of nozzles for the present study. As already seen, the axis switching associated with this type of jets is very much dependent upon the aspect ratio of the slot or nozzle. The growth of shear layer in the initial region close to the nozzle exit depends very much upon the boundary layer within the nozzle. In order to study the effect of aspect ratio alone on the jet growth, it becomes necessary that nozzles of different aspect ratios must be fabricated for comparison, in such a way that identical development of boundary layer upto the nozzle exit is ensured. This practical difficulty can be overcome if slots are used instead of nozzles.

The plates on which the elliptic slots are made are very thin, thereby ensuring negligible growth of boundary layer at the exit.

5.2 Applications

In many practical applications like combustion systems, thrust augmenting ejectors in V/STOL aircrafts *etc.*, a large mass entrainment, especially near the nozzle, is desired. Low aspect ratio elliptic jets are found to entrain ambient fluid several times more than a circular or a plane jet. Most importantly, it is a passive device which is more desirable in technical usage.

5.3 Aim of the present investigation

So, our aim in the study would be

- ◇ to study the effect of jet exit Mach number on the twin elliptic jet flow field,
- ◇ to study the effect of aspect ratio on the flow field,
- ◇ to observe the axis switching phenomenon in a twin jet flow field,
- ◇ to compare the twin elliptic jet flow field with an equivalent twin circular jet flow field.

5.4 Experimental set-up and procedure

The experimental studies on twin elliptic jets were carried out using the same experimental set up, which is described in the first part. Sharp edged elliptic slots were made on thin (1.5 mm) aluminium sheets and were fixed at the end of settling chamber. The twin identical elliptic slots of aspect ratios 1:1, 2:1, 2.5:1, and 4 are shown in the photograph (1.a). In the case of twin circular jets, since keeping a spacing of 10 mm would mean joining the two slots, for ease of fabrication a spacing of 11 mm was kept. The readings were taken in exactly the same manner as explained earlier in part one.

The exit plane Reynolds number, based on the equivalent diameter D_e of the elliptical slot (same as the diameter of a round slot with the same exit area) was varied from 2.3×10^4 to 1.4×10^5 . Experiments were carried out at various stagnation to ambient pressure ratios. The jet exit Mach numbers were varied as 0.1, 0.2, 0.4 and 0.6. Each slot of the twin slot configuration had an equivalent diameter D_e of 10 mm and centre to centre spacing S of 10 mm, *ie* the major axes of the slots were parallel to each other and 10 mm apart as shown in figure 1.a. This spacing is the limiting case for twin slot jet studied; *ie* it is the lowest possible spacing.

Chapter 6

RESULTS AND ANALYSIS

*my tears glitter in moonlit night
my tears glitter in the darkest of dark night
my tears glitter even in the hot midday Sun
my tears glitter in the success and failure
my children be brave, tears will make you great*

– the agni man Dr A. Kalam

6.1 Length scale and Velocity scale

A length scale D_e , which is the equivalent diameter of a circular jet with a momentum flux equal to that of an elliptical jet has been defined. So by equating the area of an ellipse with the equivalent area of a circle of diameter D_e ,

$$\begin{aligned}\frac{\pi(D_e)^2}{4} &\equiv \pi ab \\ D_e &= 2\sqrt{ab}\end{aligned}\tag{6.1}$$

where a and b are semi major and semi minor axes of an elliptic jet respectively. D_e also represented sometimes as D for simplicity.

The results are presented after normalizing the half local velocity U in the flow field by the jet exit velocity U_o . The axial distance X along the twin jet centreline is normalized

by the equivalent diameter D_e . The lateral (Z) and transverse (Y) locations of the probe have been normalized by the centre to centre spacing S of the slots. This centre spacing S has been chosen as the normalizing parameter for presenting the lateral and transverse spread of the jet because for a given equivalent diameter D_e , the spacing between the slots greatly affects the jet spread.

The local major and minor axes of the elliptic jet often change at different cross sections, because of axis switching. Thus for better understanding, a major plane, the plane passing through the exit major axis and a minor plane, the plane passing through the exit minor axis, both planes perpendicular to the jet exit plane have been defined.

6.2 Centreline jet decay

As mentioned in Part-I, the overall characteristics of a jet flow field are best described by the variation of the mean centreline velocity of the jet along the jet axis. The centreline between the two jets is taken as the axis of the twin jet flow field. Figure 1.b shows the variation of centreline velocity with axial distance for elliptic twin slots of AR 2.5:1 for jet exit Mach numbers of 0.1, 0.2 and 0.6. Many interesting observations can be made as follows:

- ★ For all Mach numbers, the centreline velocity is zero close to the nozzle exit. After merging the velocity starts increasing steeply, reaches a maximum value and starts decreasing monotonically.
- ★ It can be seen that with increasing Mach numbers, the maximum value of the centreline velocity also increases.
- ★ The rate of decrease of centreline velocity beyond the point of maximum velocity increases with decreasing Mach number.

- ★ At higher axial distance ($X/D_e > 30.0$) for all the Mach numbers studied, all the plots approach each other indicating that the jet field characteristics tend to be independent of Mach number in the far field.

Figure 1.c shows the centreline velocity decay for a jet Mach number of 0.2 for elliptic AR 2:1, 2.5:1 and 4:1. The observations may be listed as follows:

- ⊗ It can be seen that for a given Mach number the aspect ratio of the slots has a strong influence on the jet flow field in the initial region close to the exit (near field). The centreline velocity increases steeply with decreasing aspect ratio and the maximum value of the centreline velocity decreases with increasing aspect ratio.
- ⊗ The axial location at which the velocity maximum occurs, increases marginally with aspect ratio. This axial location varies from around $3.5 D_e$ for AR, 2:1 to around $4.3 D_e$ for AR, 2.5:1. For AR 4:1, it is around $5.0 D_e$.
- ⊗ It is interesting to note that the monotonic decrease of the centreline velocity with axial distance is almost same for all the aspect ratios studied. Particularly beyond $X/D_e = 20.0$, all the plots merge indicating that the flow field characteristics are similar and almost independent of AR, in the far field.

6.3 Mean axial velocity profiles

Figures 2.a1 & a2 show the axial velocity profiles in the Y and Z directions for Mach number of 0.2 and AR = 2:1. The potential core of the individual jets is clearly seen from the flat profile close to the exit. For AR 2:1, the length of the potential core is found to be around $3.5 D_e$. The velocity profiles in the transverse (Y) direction show that the centreline velocity increases from an initial value of almost zero to about $U/U_o = 0.9$ at an axial location of $X/D_e = 3.5$. Then it starts decreasing as the flow propagates downstream. The velocity profiles in Z direction show that, in the region close to the exit the individual

jets approach each other as indicated by the shifting of the maximum velocity location towards the centreline. At the point of complete combining of the two jets the peak value of velocity shifts to the centreline. For AR 2:1, this shifting of peak to the centreline occurs around $5.0 D_e$. Beyond this axial location, the combined twin jet propagates as a single jet with the twin jet centreline as the axis. The increasing spread of the combined jet in both Z and Y direction with increasing downstream distance X/D_e can be clearly seen from both the profiles.

Figures 2.b1–b4 show similar profile for AR = 2.5:1 for $M_e = 0.1$ and 0.6. The general features are same as that for AR = 2:1. A close observation of the profiles show that the potential core length of the individual jets is almost $3.0 D_e$. The complete combining of the jet, indicated by the single peak of the velocity profile at the centreline, occurs at around $5.0 D_e$ as in the case of AR 2:1. The maximum centreline velocity also occurs at this location. It can also be noticed that Mach number does not alter the velocity profile significantly.

Figures 2.c1–c2 show the velocity profiles for AR = 4:1. The potential core length of the individual jets is remarkably reduced in this case. As compared to a core length of around $3 D_e$ in the case of AR = 2:1 and 2.5:1, for AR = 4:1, it is found to be around $2 D_e$. The maximum centreline velocity occurs around $5.5 D_e$ but this location does not coincide with the shifting of peak velocity to the centreline, instead it is observed at around $7.0 D_e$.

A comparison of the velocity profiles for different aspect ratios indicate that the profiles are almost independent of aspect ratio in the far field ($X/D_e > 20.0$).

6.3.1 Potential core

As seen, the length of the potential core decreases with increasing aspect ratio, and this variation is given in Table–C.

M	AR	X/D_e
0.2	1.1	3.5
0.2	2:1	3.5
0.2	2.5:1	3.0
0.2	4:1	2.0

Table-C. Potential core length

6.4 Shear layers

Figures 3.a1 & a2 show the growth of iso spread lines *ie.*, lines of the same velocity ratio $\frac{U}{U_m}$, for $M_e = 0.2$ and $AR = 2:1$ (note that the $U/U_m = 0.5$ line represents the half width). The spread lines in the Z direction are shown only for the outer layer of an individual jet in the combining region. It may be seen that the lines of velocity ratio $0.9 U/U_m$ is straight along X direction indicating the extent of potential core, *ie.*, upto $X/D_e = 3.5$. Beyond this region because of the merging of the shear layers steeper velocity gradients exist around the centreline. The intense mixing in the central region of the combined jet leads to smooth velocity gradients as the flow propagates downstream. This is indicated by the gradual diverging of the spread lines.

A comparison of iso spread lines in Y and Z directions shows that the velocity gradients are steeper in the initial merging region ($X/D_e < 2.0$) in the Z direction as compared to that in the Y direction. Whereas in the far field the velocity gradients are steeper in Y direction compared to Z direction. The rate of spread with axial distance is more in the Y direction than in Z direction in the initial region. The reverse trend is seen in the far field. In general, figures 3, which show the iso spread lines for all the jets, show that the same trend continues for all aspect ratios.

6.5 Three dimensional half width spread

Figure 4 show the isometric view of the cross sectional development of the elliptic jets for $M_e = 0.2$ and for all aspect ratios and $M_e = 0.4$ and 0.6 for $AR = 2.5$. The boundary of the jet cross section is based on half width. It may be seen that the combined jet cross section transforms gradually into an elliptic shape from an initial diamond like shape for all the cases. It can be clearly seen that the combined jet does not attain axisymmetry within the axial distance $X/D_e = 25.0$ and the phenomenon of axis switching associated with single elliptic jets is not observed.

6.6 Conservation of momentum

Figures 5.a & b show that the momentum is conserved in all the cases (for all Mach number and for all aspect ratio) of jets studied.

6.7 Entrainment

The entrainment of ambient fluid into the twin jet is represented by $\frac{Q-Q_o}{Q_o}$, where Q_o = mass flux at the exit and Q = mass flux at any axial location. Figure 6.a shows the variation of entrainment with axial location for AR 2.5:1, for Mach numbers 0.1, 0.2, 0.4, and 0.6. It can be seen clearly that the parameter $\frac{Q-Q_o}{Q_o}$ increases almost linearly with X/D_e , the entrained mass is nearly three times the mass issuing out of the slot. The entrainment is not affected by the jet exit Mach number as can be seen from these plots.

Figure 6.b shows the variation of entrainment for $M_e = 0.2$, for different aspect ratios and twin circular jets. Here again it is seen that the aspect ratio does not affect the entrainment significantly. The marginal variation of entrainment with aspect ratio may be explained as follows: the entrainment of the ambient fluid is significant in the near field of a single elliptic jet. The close spacing of two neighbouring elliptic jets results in reduction

of effective circumferential area of the twin jets and consequently reduced entrainment of ambient fluid. Hence it appears that sufficient spacing of the slots is required for increase in entrainment.

6.8 Mixing flow cross sectional Contours

Figure 7 show the constant velocity contours of the developing jet at various axial locations for different Mach numbers and aspect ratios. In all the cases it is interesting to note that from an initial diamond like shape, the jet develops into an elliptic shape as the flow propagates downstream. The increasing cross sectional area with axial distance is an indication of entrainment.

6.9 Jet width

At any cross section the velocity does not become zero abruptly but decreases gradually, asymptotically reaching zero. This may arouse an ambiguity about where the jet ends. So, to eliminate such ambiguity, the point where the velocity reaches half the value of that at the centreline, is taken as the reference point. The distance from the centreline to this reference point is called **half-width**. The locus of such reference points (half velocity points), may be extrapolated to cut the centreline some where near the jet exit and this is point is called the virtual origin. For twin jets the half width is taken only after the combining point, *i.e.*, when it becomes single jet.

The spread of the combined jet (beyond $X/D_e = 5.0$) in both Y and Z directions (half width) at various axial location is illustrated in figures 8.a1 & a2 for Mach 0.2 and different aspect ratios, and is compared with circular slot ($AR = 1:1$) jet of an equivalent area. It can be seen that the spread of the jets in the Y direction is highest for the circular jet and the lowest for the AR 4:1. The spread in Y direction decreases with increasing AR. The

reverse trend is observed in the case of spread in the Z direction.

From figure 8.d it can be seen that elliptic jets have not attained axisymmetry within an axial distance of $X/D_e = 25.0$ as seen from the different spreads of the jet in Y and Z direction. The twin circular jet shows two axis switchings after the first cross over point at around $7 D_e$ and after that at around $22 D_e$. By extrapolation it is found that all the twin jets including circular jets do not become axisymmetric till $45 D_e$. The jet of AR 4:1 is found to attain axisymmetry at around $50 D_e$ (by actual measurement).

6.10 Iso Mach lines

Figure 9 show the iso Mach lines -lines of constant Mach numbers in the flow field - give a clear picture of the jet flow field structure in XZ plane. The close spacing of the lines indicate steeper velocity gradients and vice versa.

6.11 Similarity profiles

Figures 10.a, b show the similarity profiles for all the cases for $M_e = 0.2$. In all the cases this self similar region is described by the similarity profile using the non dimensional parameters U/U_m (velocity scale) and $Z/Z_{0.5}$ (length scale). It can be seen clearly that the profiles are the same for all the cases, indicating that the self preserving nature of the combined jet is independent of the initial geometry and flow conditions. The solid lines in figures 10 represent the equation (3.10) in part-I.

Chapter 7

CONCLUSIONS

On the basis of the above discussions, for the range of aspect ratios (1:1, 2:1, 2.5:1 and 4:1) and slot centre to centre spacing studied, it can be summarized that:

1. The initial growth of the twin jet is affected by both Mach number and aspect ratio of the slots.
2. For a given aspect ratio the centreline velocity decays faster as the jet Mach number decreases. The maximum value of the centreline velocity increases with Mach number.
3. At a given Mach number the centreline velocity decay of the combined jet is independent of the aspect ratio.
4. The potential core length of the individual jets decreases with increasing aspect ratio.
5. The axial location at which the maximum centreline velocity occurs is affected marginally by the aspect ratio, but for a given aspect ratio, it is almost independent of Mach number.
6. The combining of the individual jets is delayed marginally as the aspect ratio increases.

7. The spread rate of the combined jet increases in the Y direction as the aspect ratio decreases and the reverse trend is observed in the case of spread in the Z direction.
8. The entrainment of the twin jet increases linearly with axial location and is found to be almost independent of Mach number and aspect ratio.
9. In all the cases the cross section of the combined jet just downstream of the combining point has a diamond like shape. Whereas the combined jet of twin circular jets exhibits axis switching, the same is not observed in the case of elliptic jets.
10. The similarity profile of the combined jet is the same for all the cases which implies the self preserving nature of the jets is independent of the initial geometric and flow condition.
11. The combined jet does not attain axisymmetry even upto an axial distance of 45 equivalent diameter.

7.1 Suggestions for future work

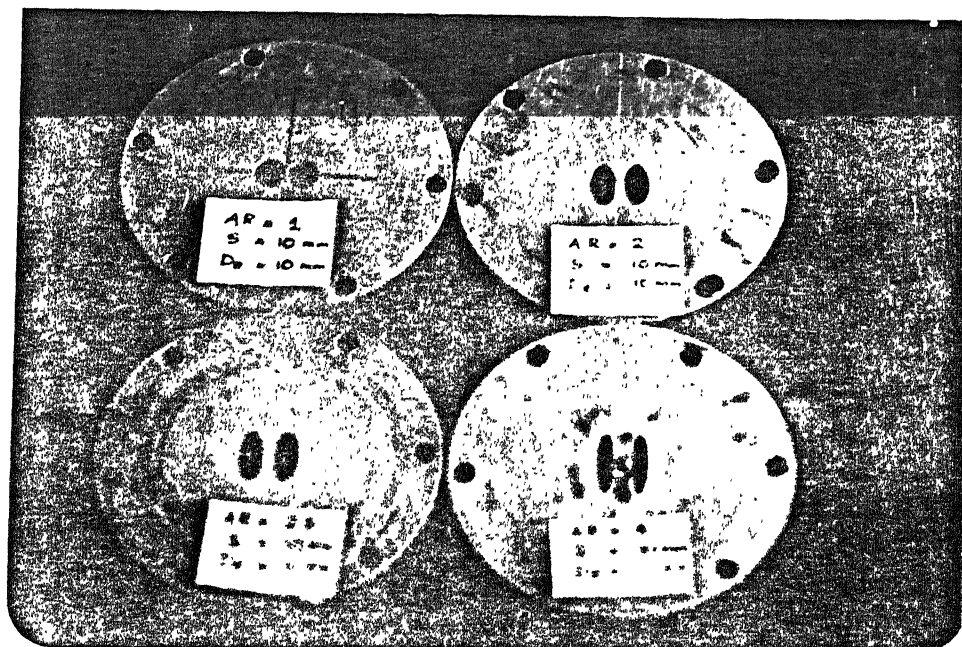
- The present investigation was carried out for only one centre to centre spacing (S) of the slots. It is suggested that further work for different spacings will be of value.
- Only three aspect ratios were studied. More studies can be done with aspect ratio 3:1 and intermediate aspect ratios like 5:1, 6:1 etc.
- It is felt that flow visualization studies using water table facility might yield interesting qualitative information.
- Multi jet studies can be carried out for different spacings and aspect ratios.
- The present study has been made only for low subsonic jets. it is suggested that the behaviour of the jet flow field at different higher Mach numbers and degree of

under-expansion can be investigated in detail.

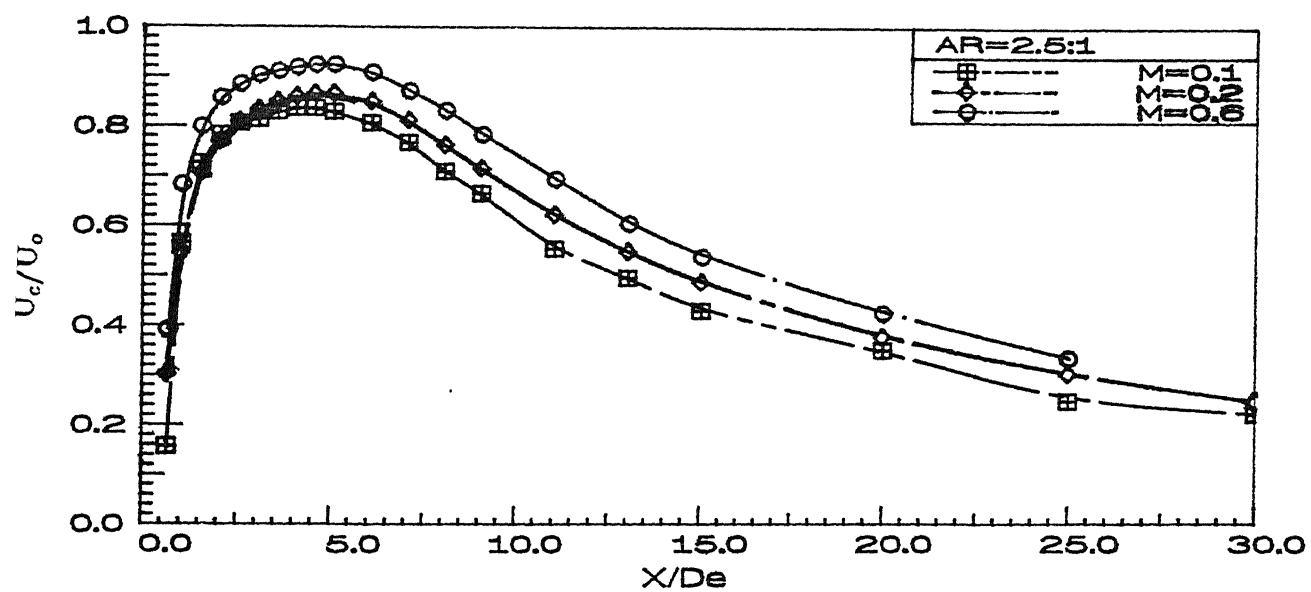
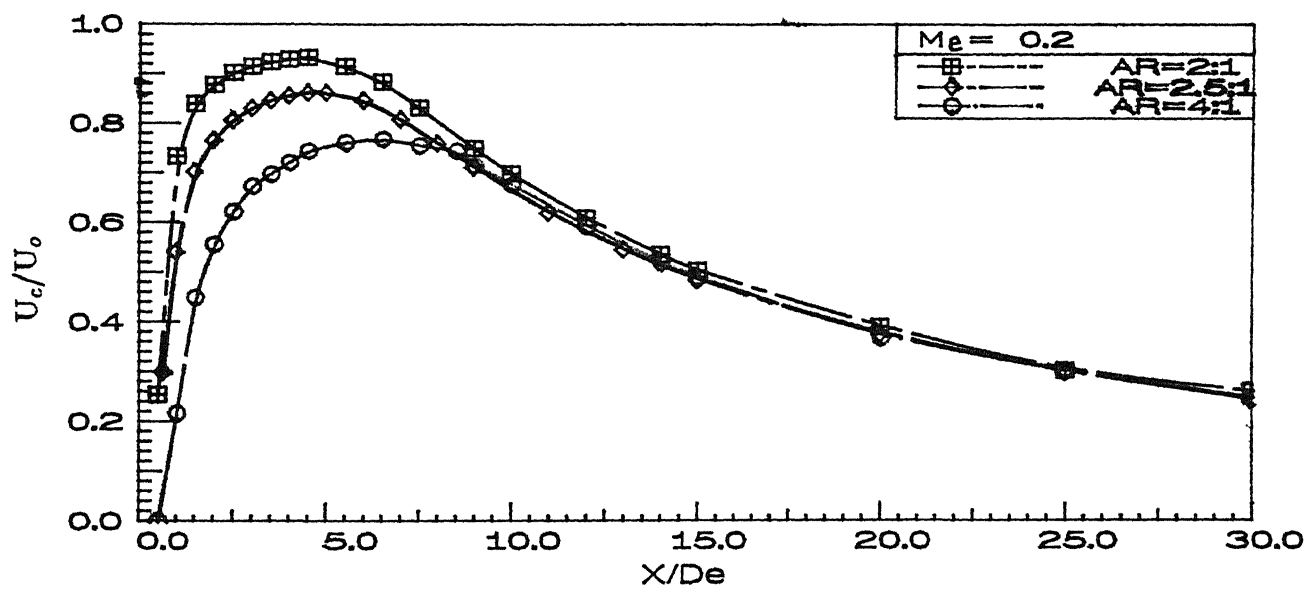
Bibliography

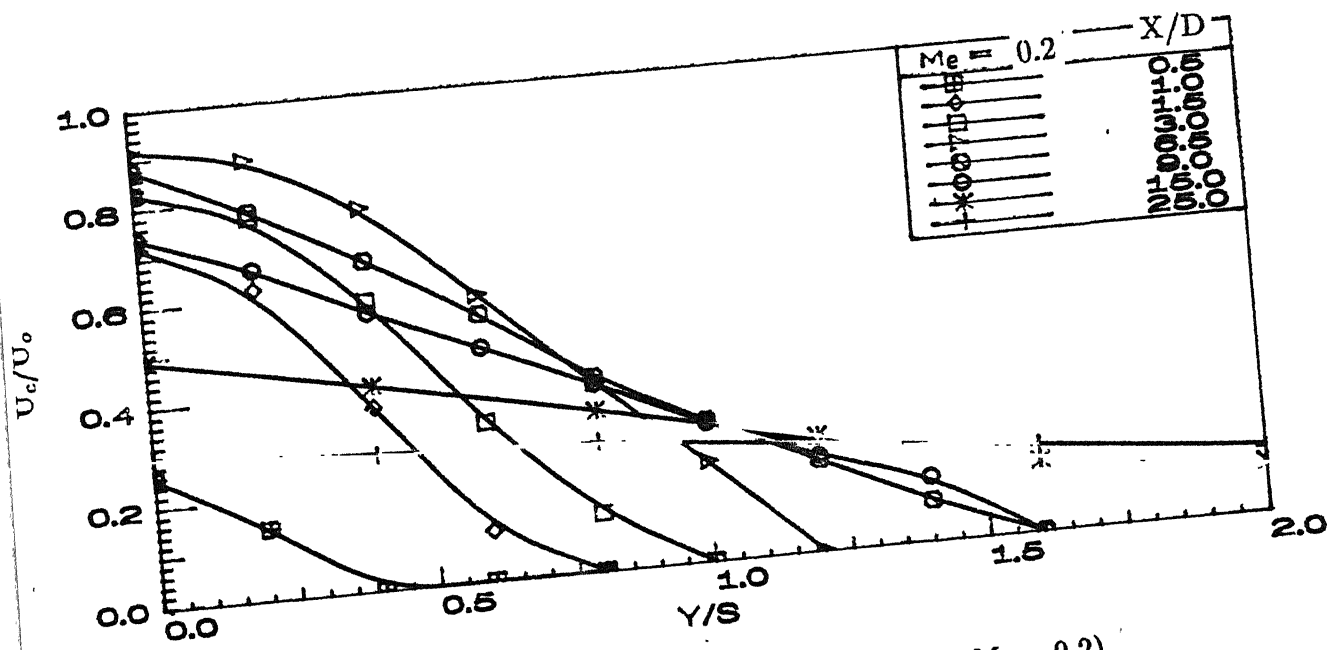
- [1] Trentacoste, N. and Sforza, P. "*Further experimental results for three dimensional free jets*", AIAA J, 1967, 5, pp 885–891.
- [2] Schadow, K.C., Wilson, K. J., Lee. M. J. and Gutmark, E. "*Enhancement of mixing in ducted rockets with elliptic gas-generator nozzles*", AIAA paper, 1984, 84-1260.
- [3] Husain, H. S and Hussain, A. K. M. F "*Controlled excitation of elliptic jet*", Phys.Fluids, 1983, 26, pp 2763–2765.
- [4] Gutmark, E. and Ho, C. M. "*Near field pressure fluctuations of an elliptical jet*", AIAA J, 1985, 23, pp 354–358.
- [5] Chih-Ming Ho and Ephraim Gutmark, "*Vortex induction and mass entrainment in a small-aspect-ratio elliptic jet*", JFM, 1987, 179, pp 383–405.
- [6] Hussain, F. and Husain, H. S. "*Elliptic jets. Part 1: Characteristics of unexcited and excited jets*", JFM, 1989, 208, pp 257–320.
- [7] Husain, H. S. and Husain, F. "*Elliptic jets. Part 2: Dynamics of coherent structures: pairing*", JFM, 1991, 233, pp 439–482.
- [8] Quinn, W. R. "*On mixing in an elliptic turbulent free jet*", Phys. Fluids, 1989, 1, pp 1716–1722.

- [9] Schadow, K. C., Gutmark, E., Koshigoe, S., and Wilson, K. J. "*Combustion related shear flow dynamics in elliptic supersonic jets*", AIAA J, 1989, 27, pp 1347–1353.
- [10] Crighton, D. G. "*Instability of an elliptic jet*", JFM, 1973, 59, pp 665–672.

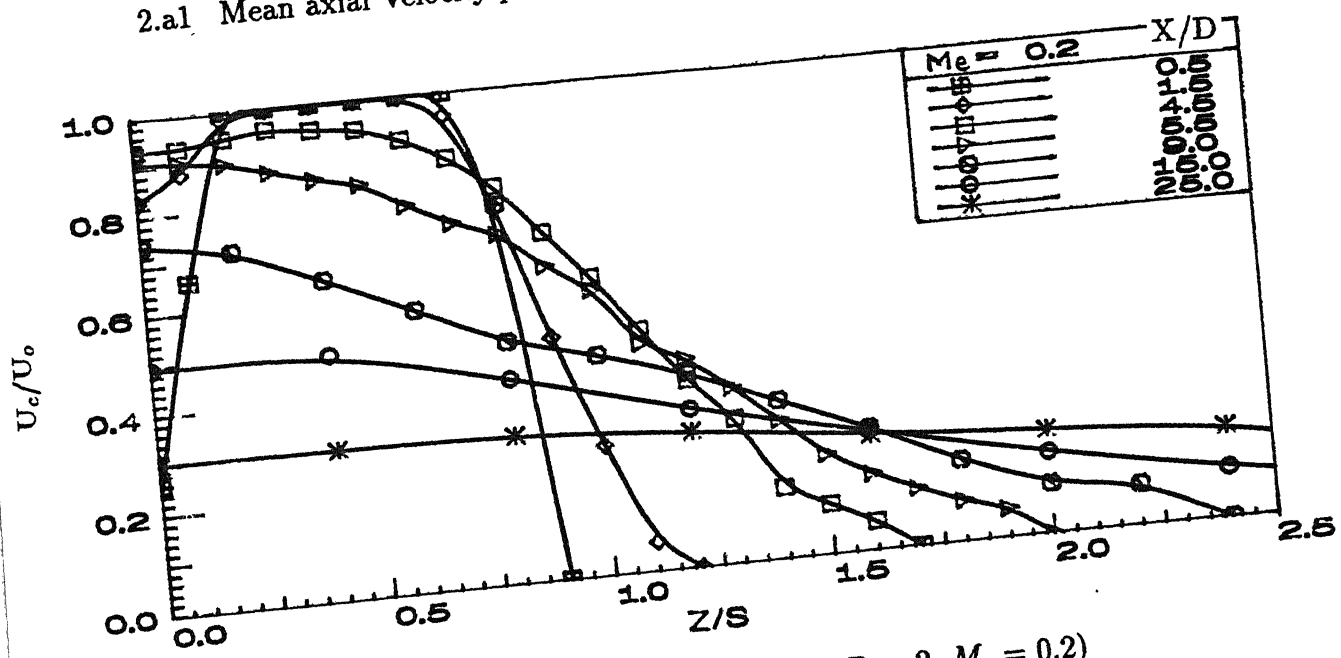


1.a Twin Elliptic Orifice - Photograph

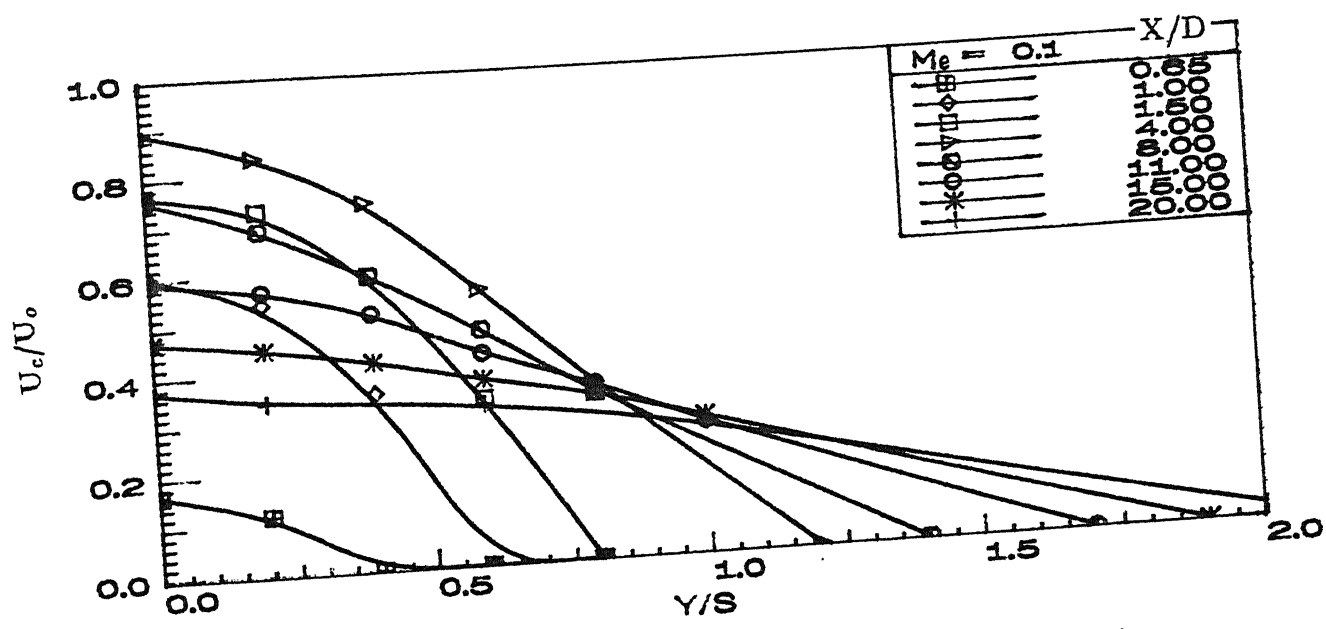
1.b Centreline Velocity variation ($AR = 2.5$)1.c Centreline Velocity variation ($M_e = 0.2$)



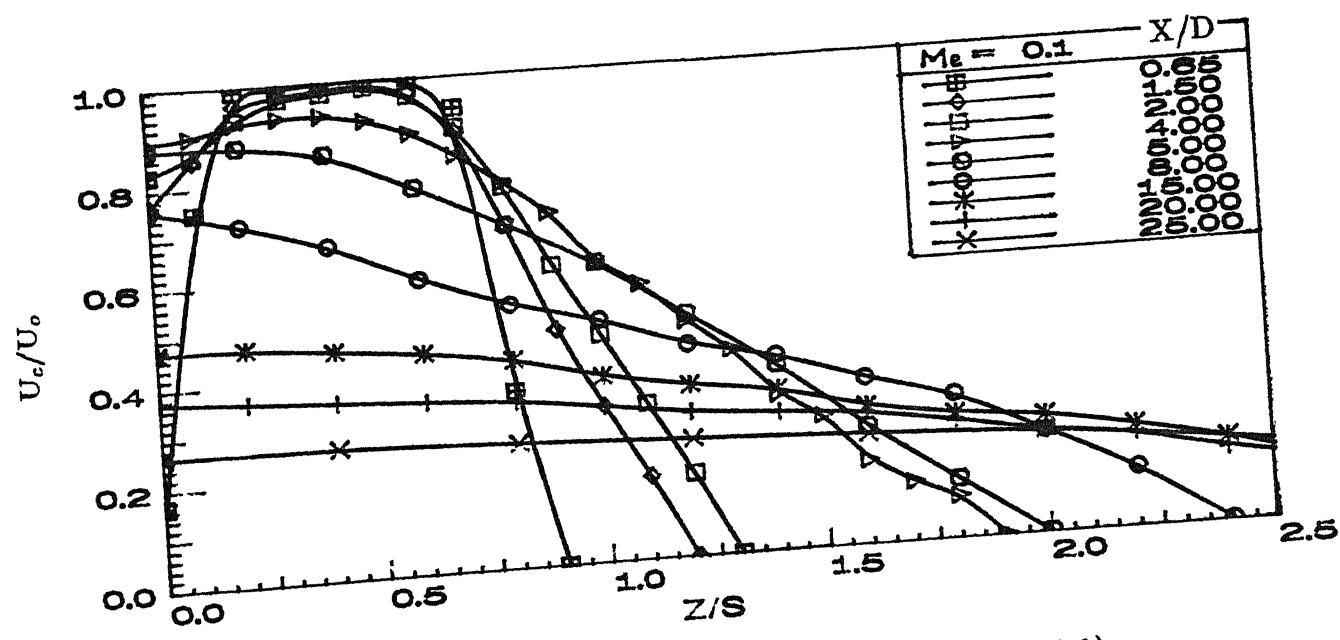
2.a1 Mean axial Velocity profiles in XY plane ($AR = 2$, $Me = 0.2$)



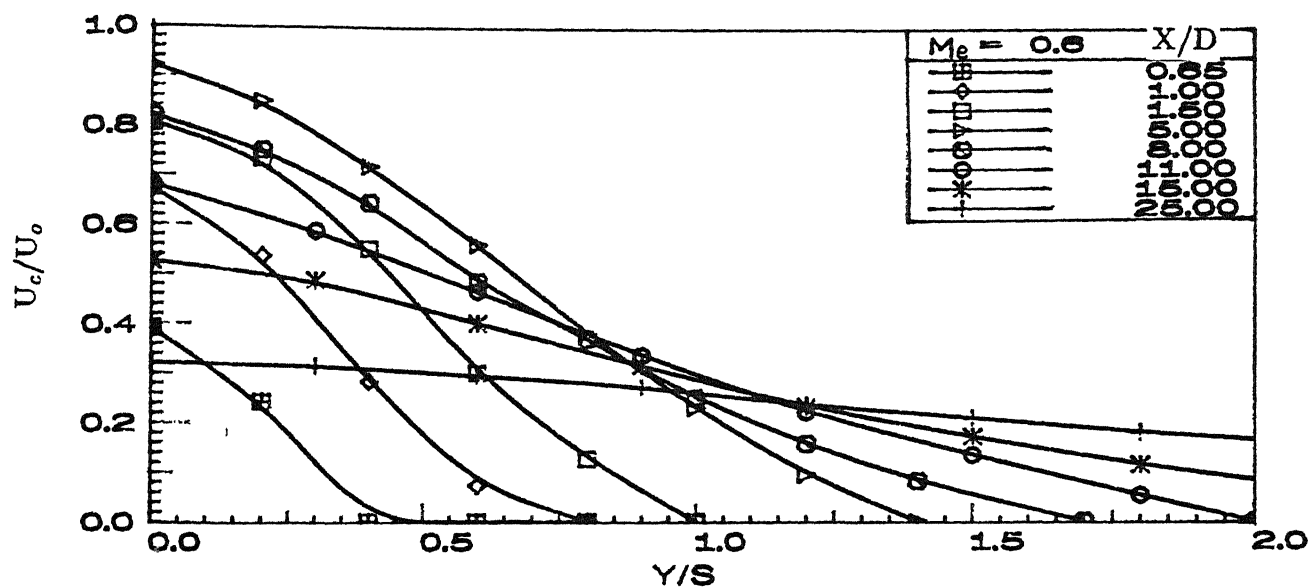
2.a2 Mean axial Velocity profiles in XZ plane ($AR = 2$, $Me = 0.2$)



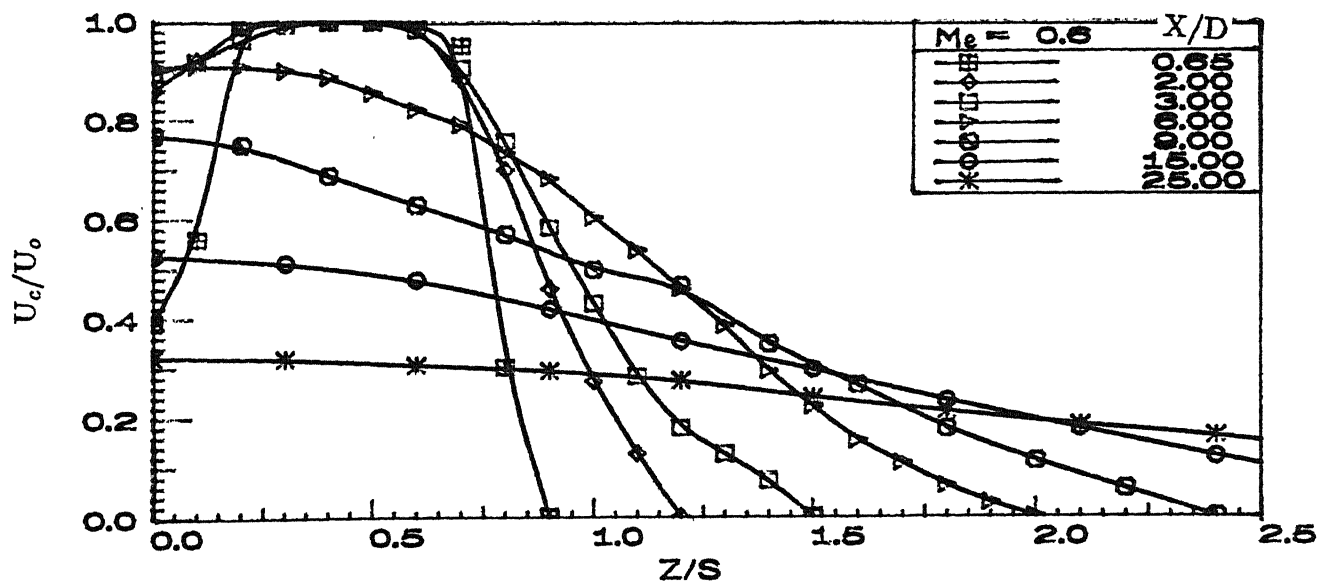
2.b1 Mean axial Velocity profiles in XY plane ($AR = 2.5, M_e = 0.1$)



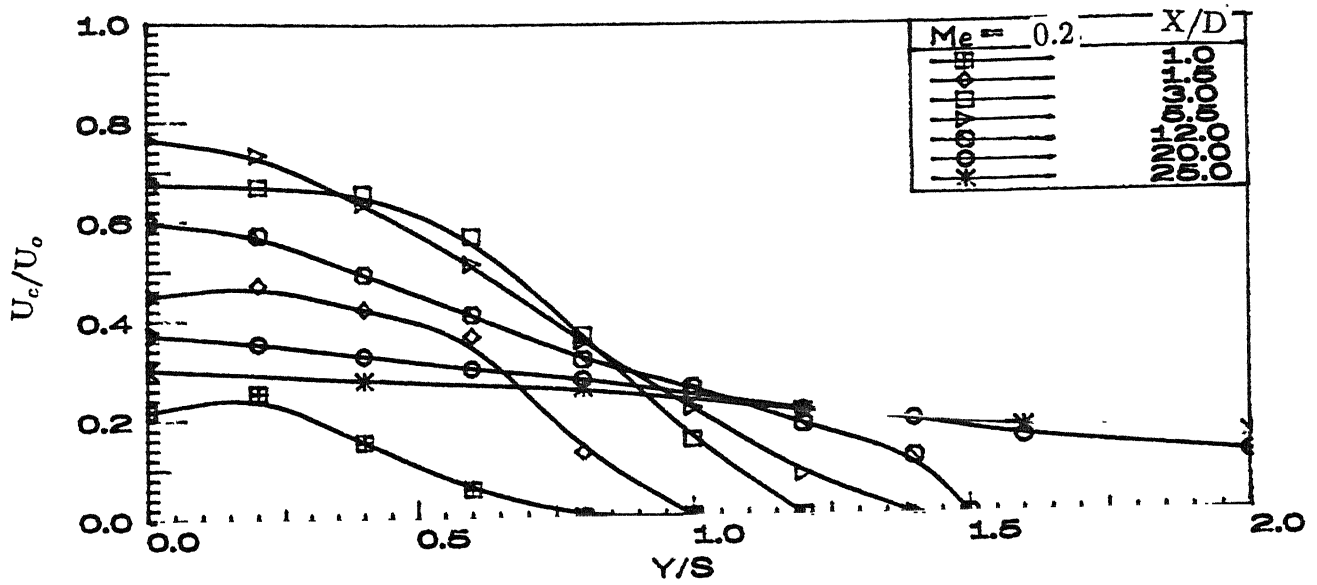
2.b2 Mean axial Velocity profiles in XZ plane ($AR = 2.5, M_e = 0.1$)



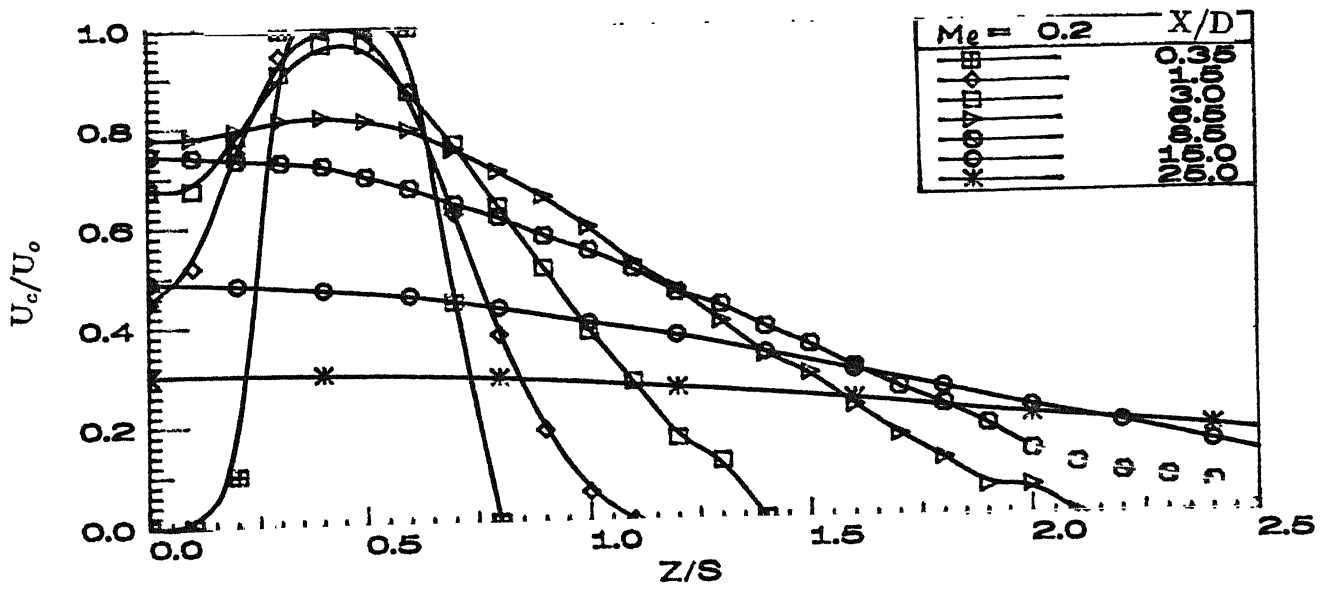
2.b3 Mean axial Velocity profiles in XY plane ($AR = 2.5$, $Me = 0.6$)



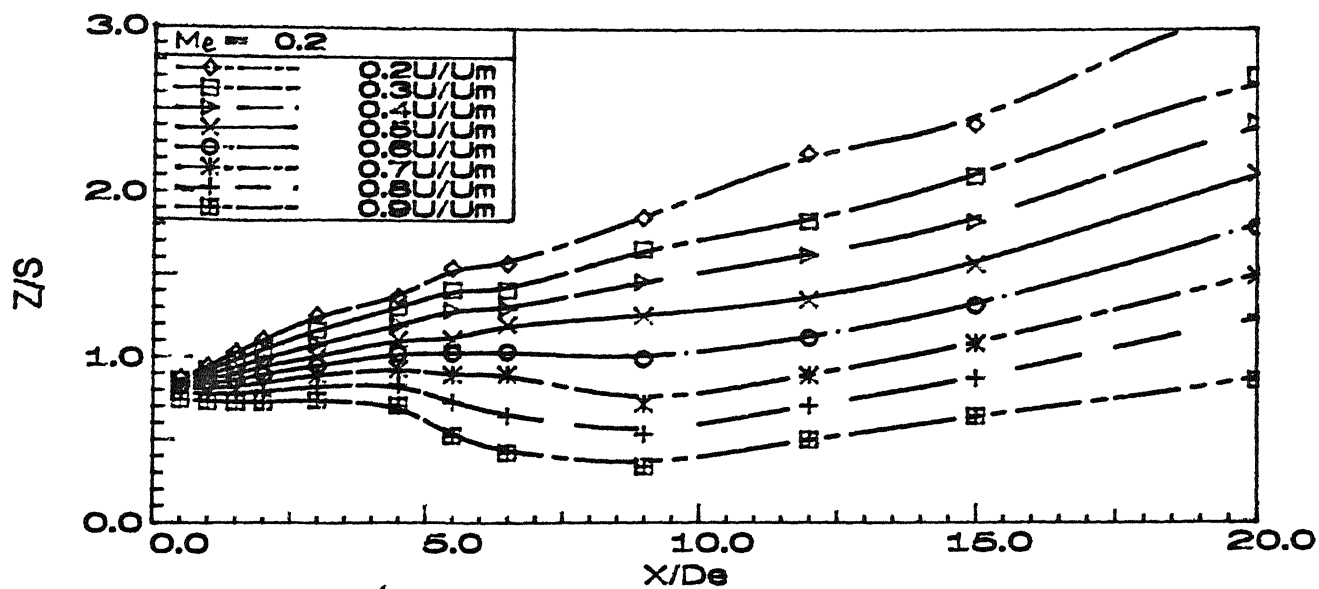
2.b4 Mean axial Velocity profiles in XZ plane ($AR = 2.5$, $Me = 0.6$)



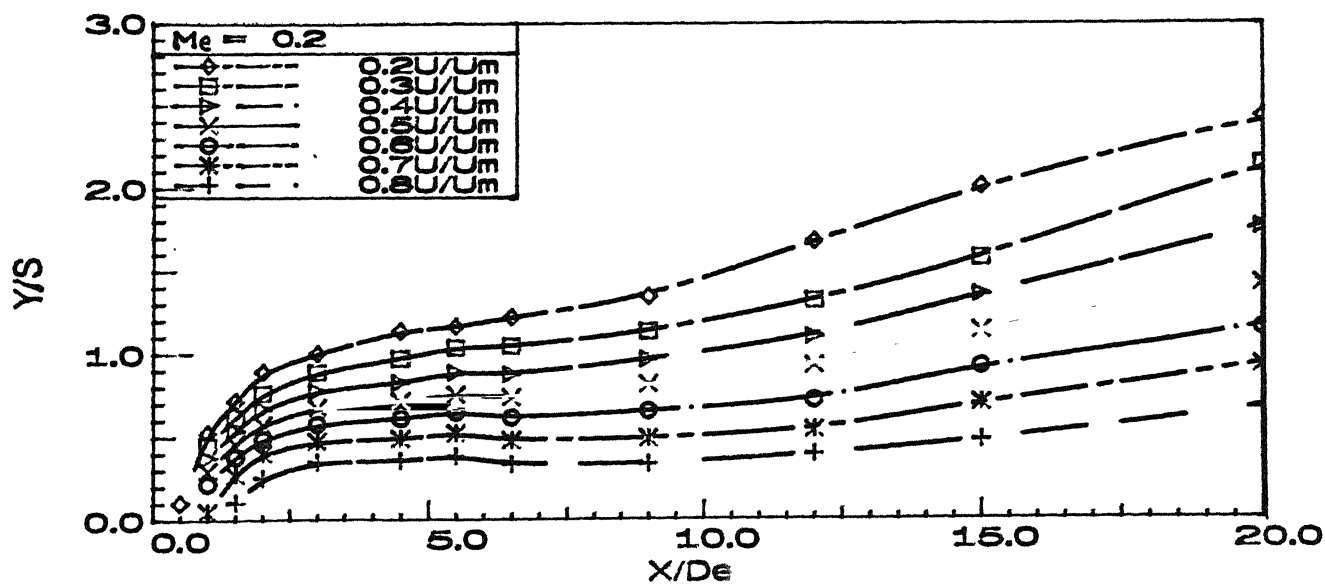
2.c1 Mean axial Velocity profiles in XY plane ($AR = 4$, $Me = 0.2$)



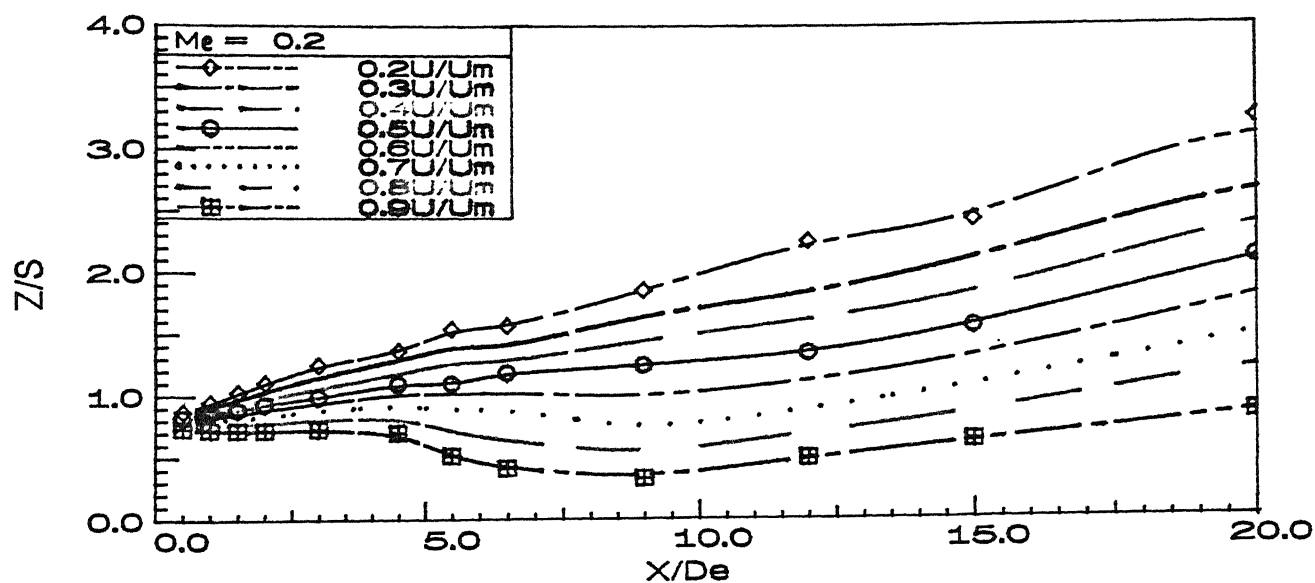
2.c2 Mean axial Velocity profiles in XZ plane ($AR = 4$, $Me = 0.2$)



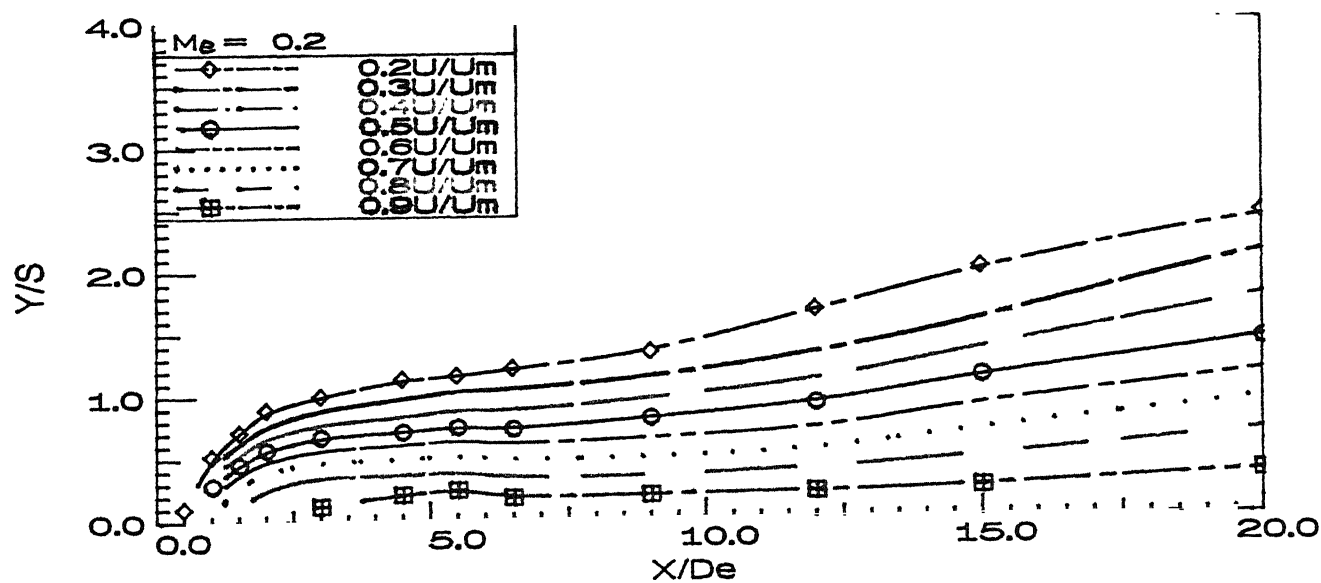
3.a1 Growth of Iso spread lines in XZ plane ($AR = 2$, $M_e = 0.2$)



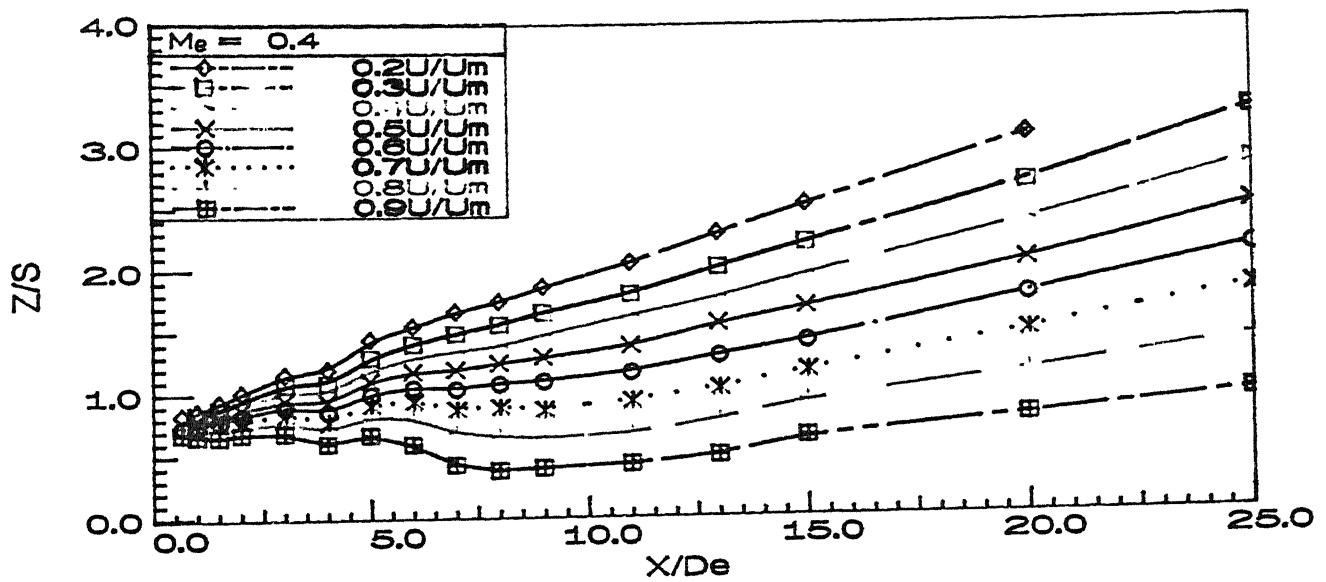
3.a2 Growth of Iso spread lines in XY plane ($AR = 2$, $M_e = 0.2$)



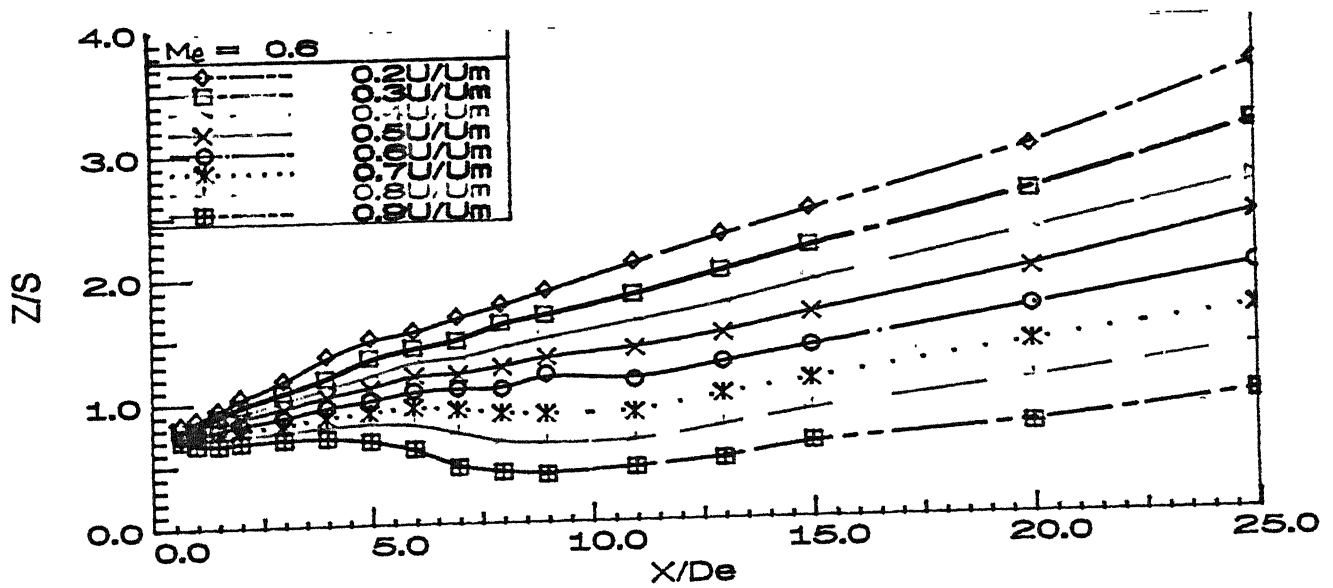
3.b1 Growth of Iso spread lines in XZ plane ($AR = 2.5$, $Me = 0.2$)



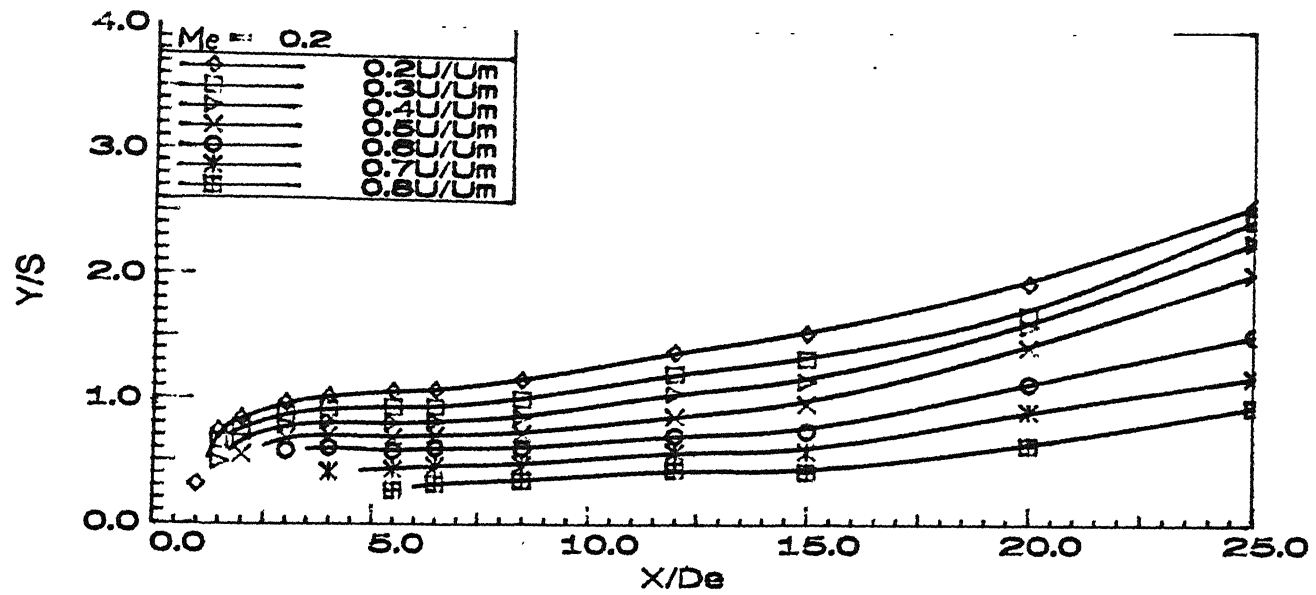
3.b2 Growth of Iso spread lines in XY plane ($AR = 2.5$, $Me = 0.2$)



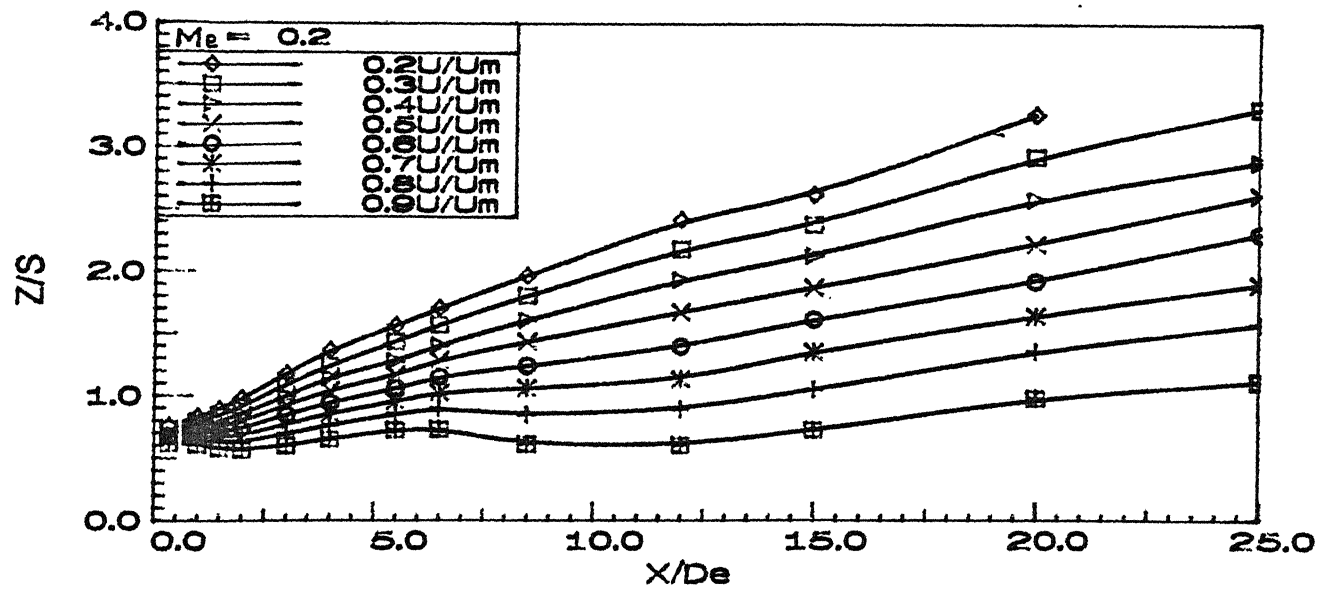
3.b3 Growth of Iso spread lines in XZ plane ($AR = 2.5$, $Me = 0.4$)



3.b4 Growth of Iso spread lines in XY plane ($AR = 2.5$, $Me = 0.6$)



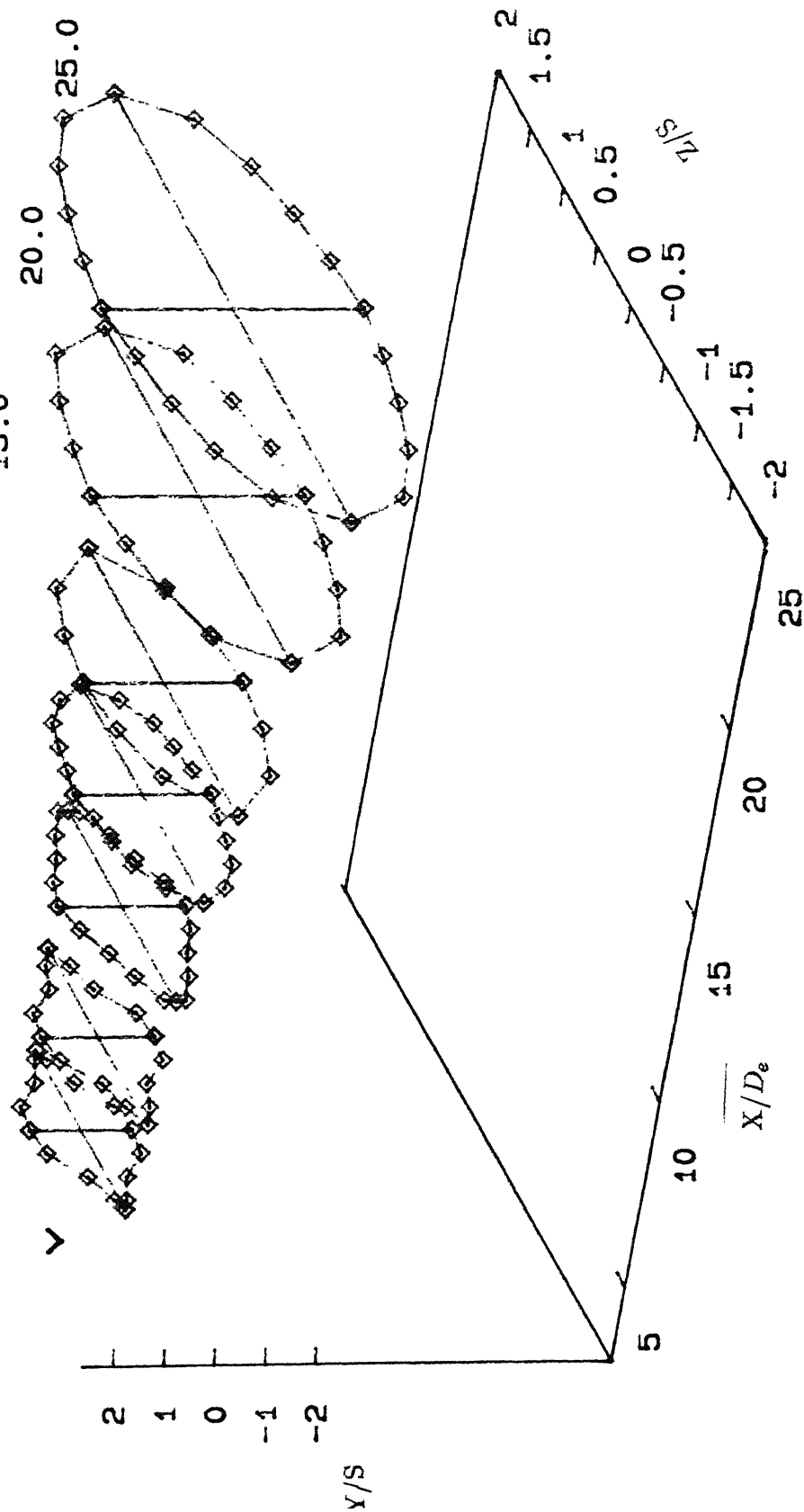
3.c1 Growth of Iso spread lines in XZ plane ($AR = 4$, $M_e = 0.2$)



3.c2 Growth of Iso spread lines in XY plane ($AR = 4$, $M_e = 0.2$)

3-d half width spread

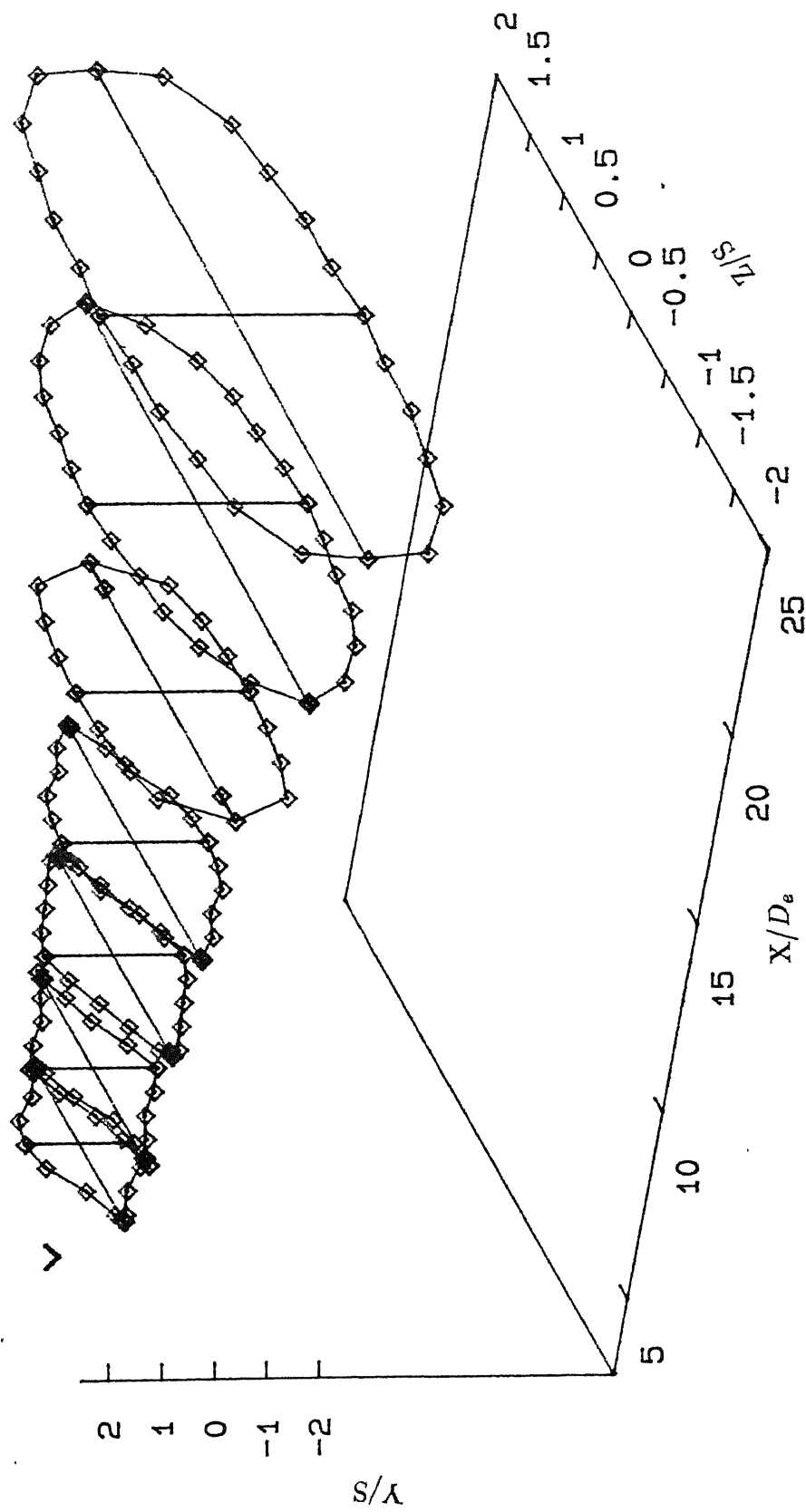
Twin elliptic jets, $M=0.2$, $AR=2:1$
 $X/D_e=3$ 5.5



4.a Three Dimensional half width spread ($AR = 2, M_e = 0.2$)

3-d half width spread

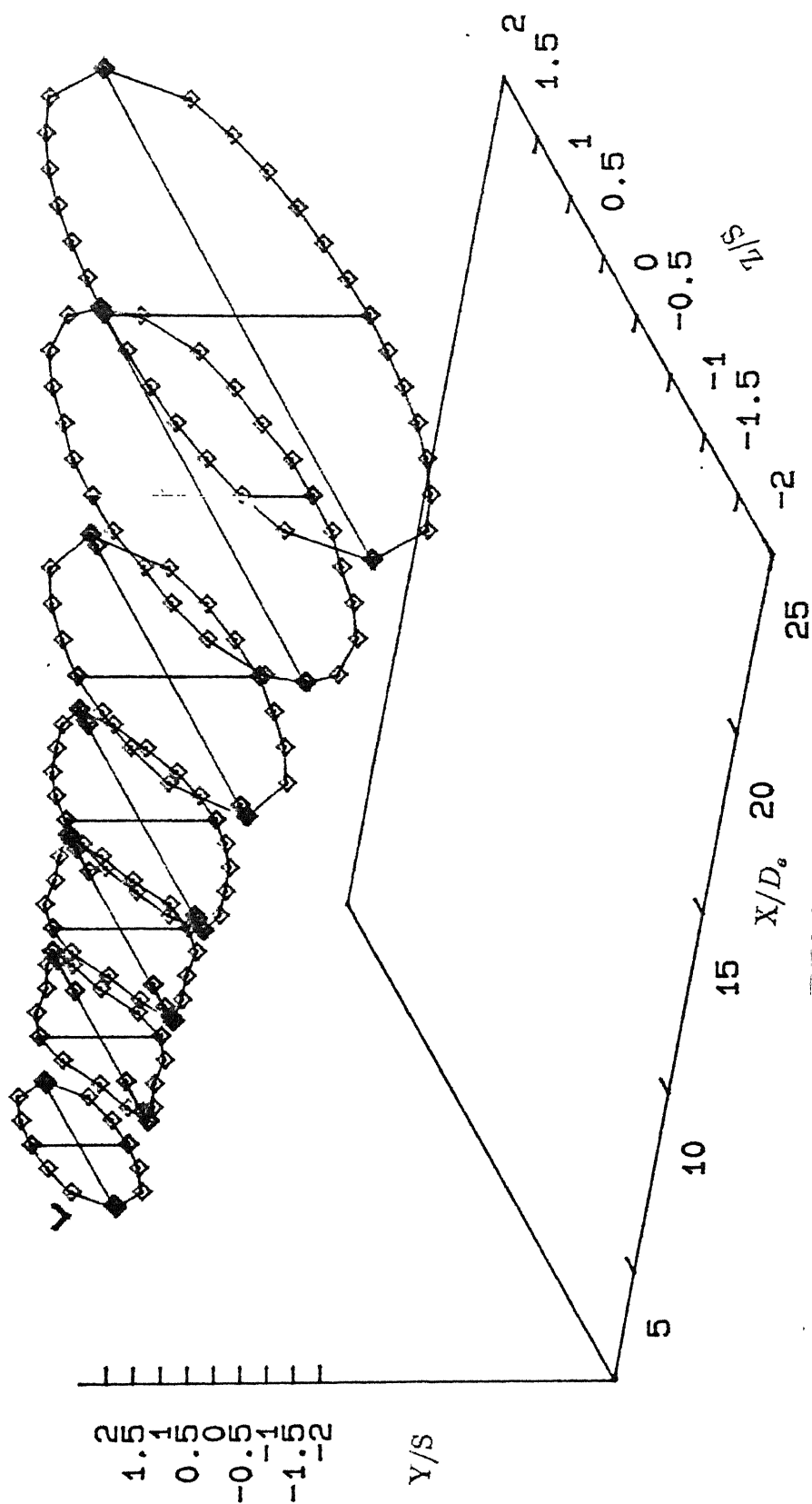
Twin elliptic jets

 $M_0 = 0.2$ (AR=2.5:1)4.b1 Three Dimensional half width spread (AR = 2.5 $M_c = 0.2$)

3-d half width spread

Twin elliptic jets

$M_e = 0.4$ (AR=2.5:1)

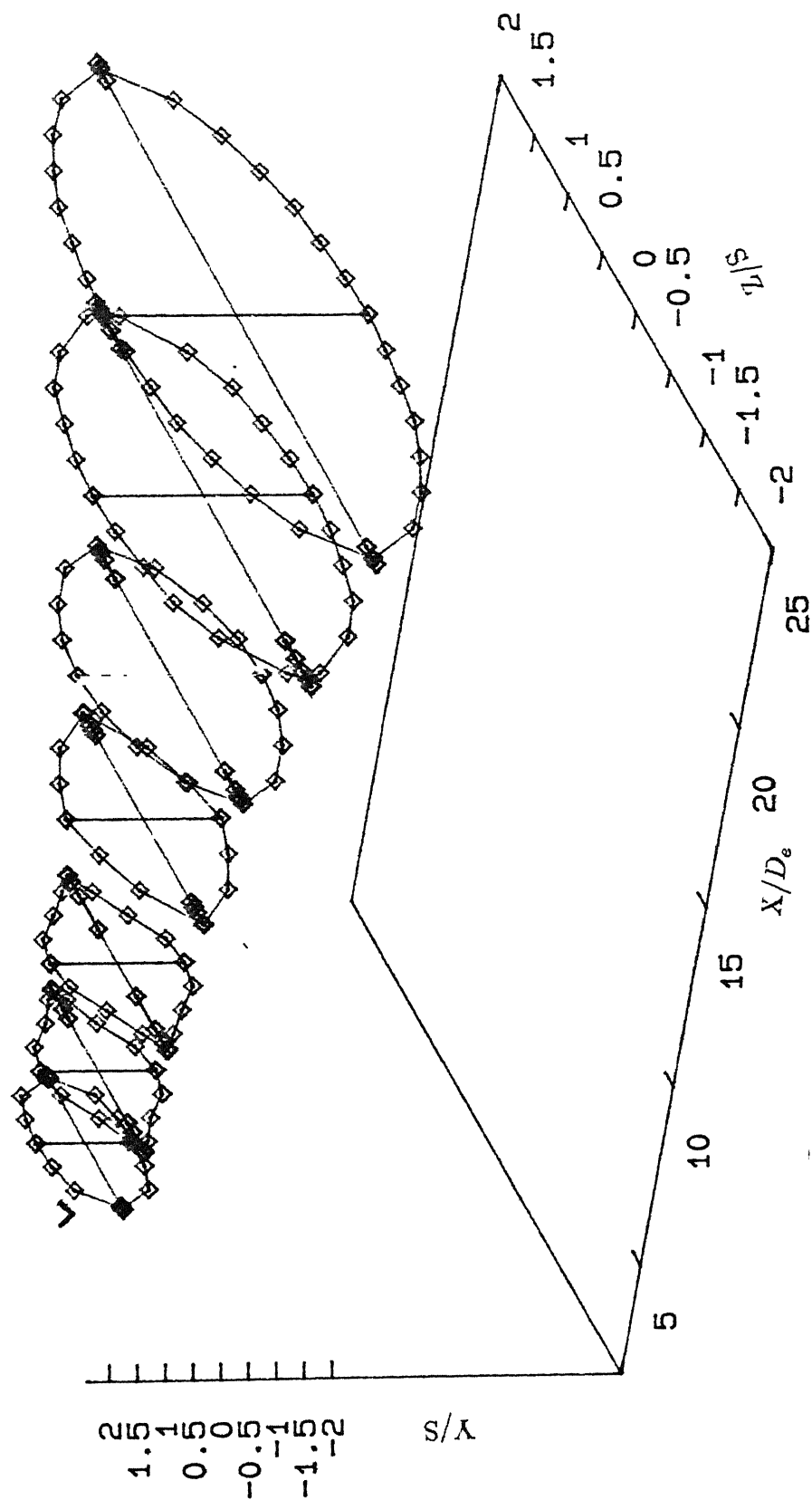


4.b2 Three Dimensional half width spread (AR = 2.5 M_e = 0.4)

3-d half width spread

Twin elliptic jets

$M_e = 0.6$ (AR=2.5: 1)



4.b3 Three Dimensional half width spread (AR = 2.5 M_e = 0.6)

3-d half width spread

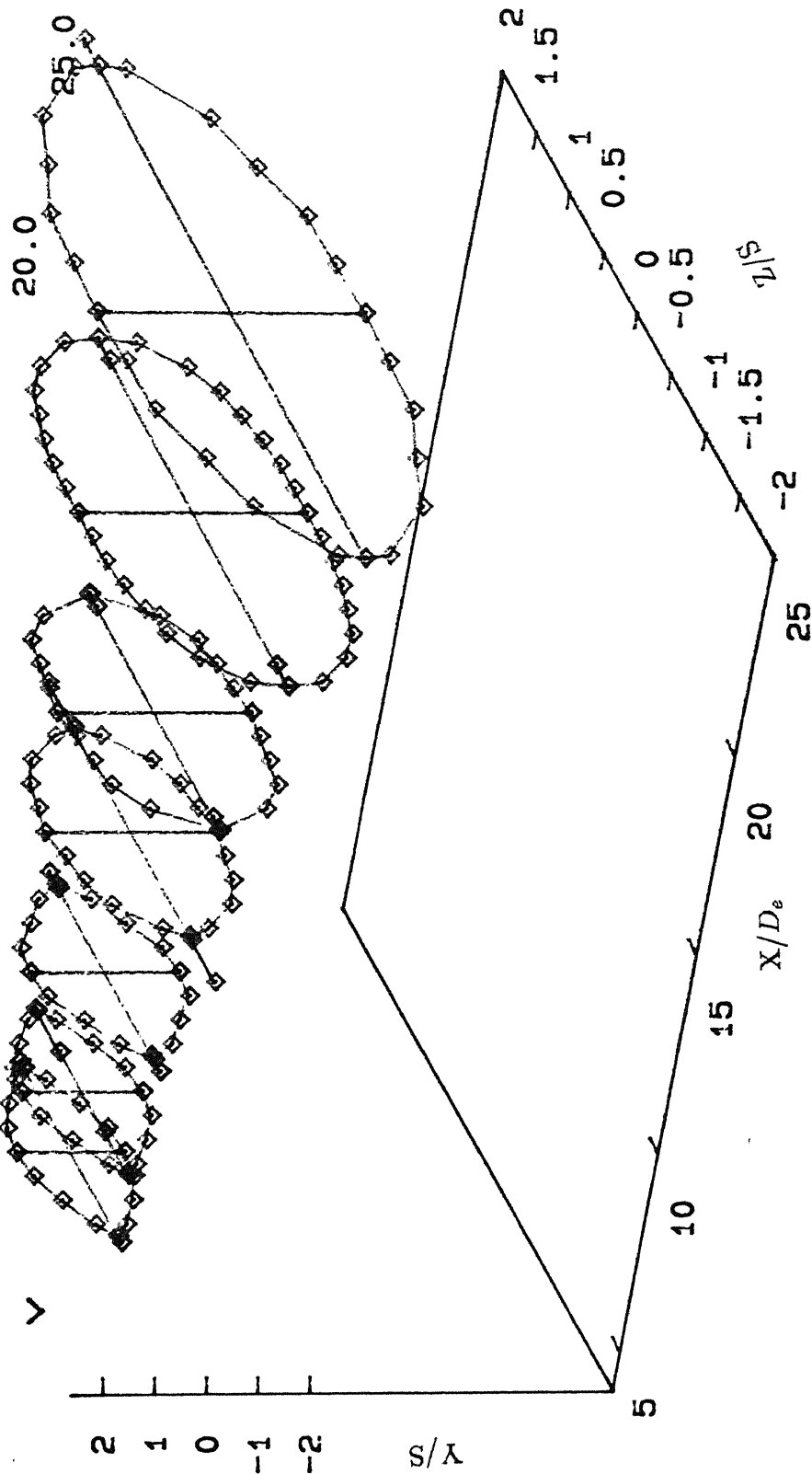
Twin elliptic jets, $M_e=0.2$, $AR=4:1$ $X/D_e=4$

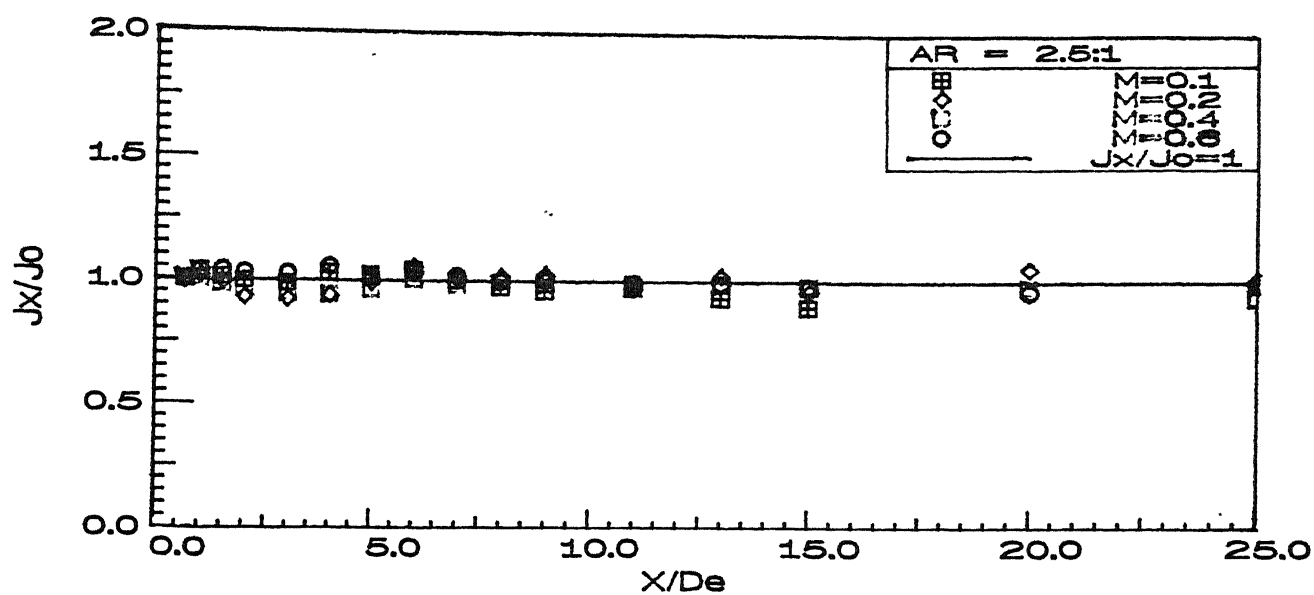
5.5

8.5

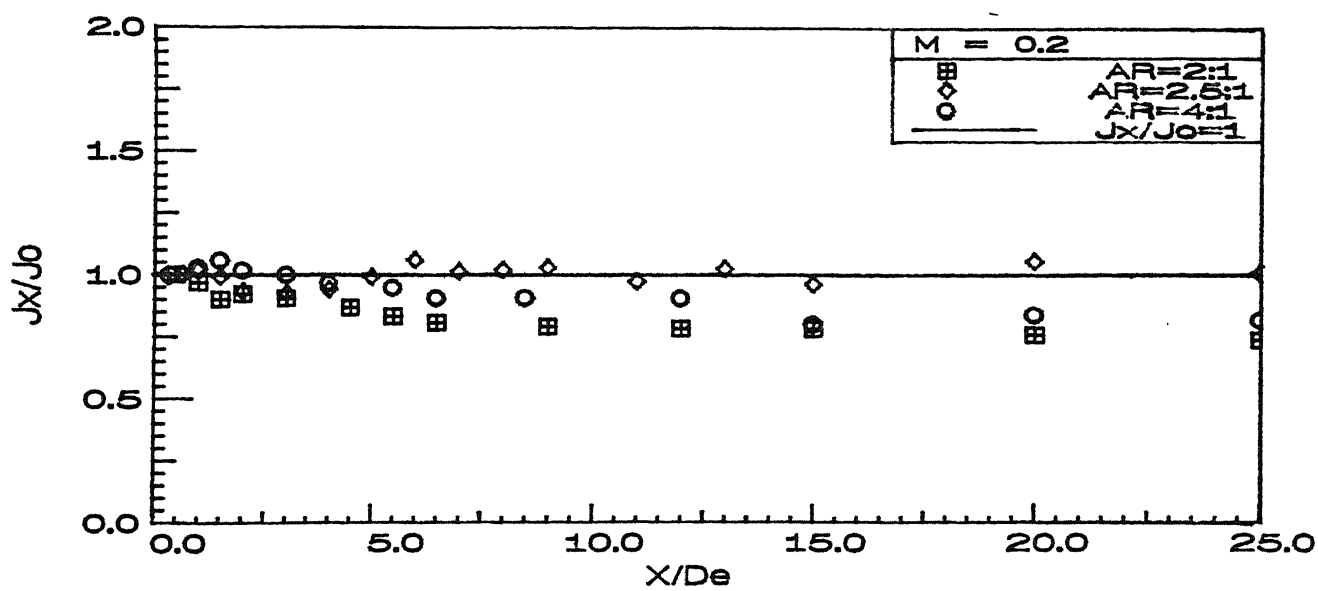
12.0

15.0

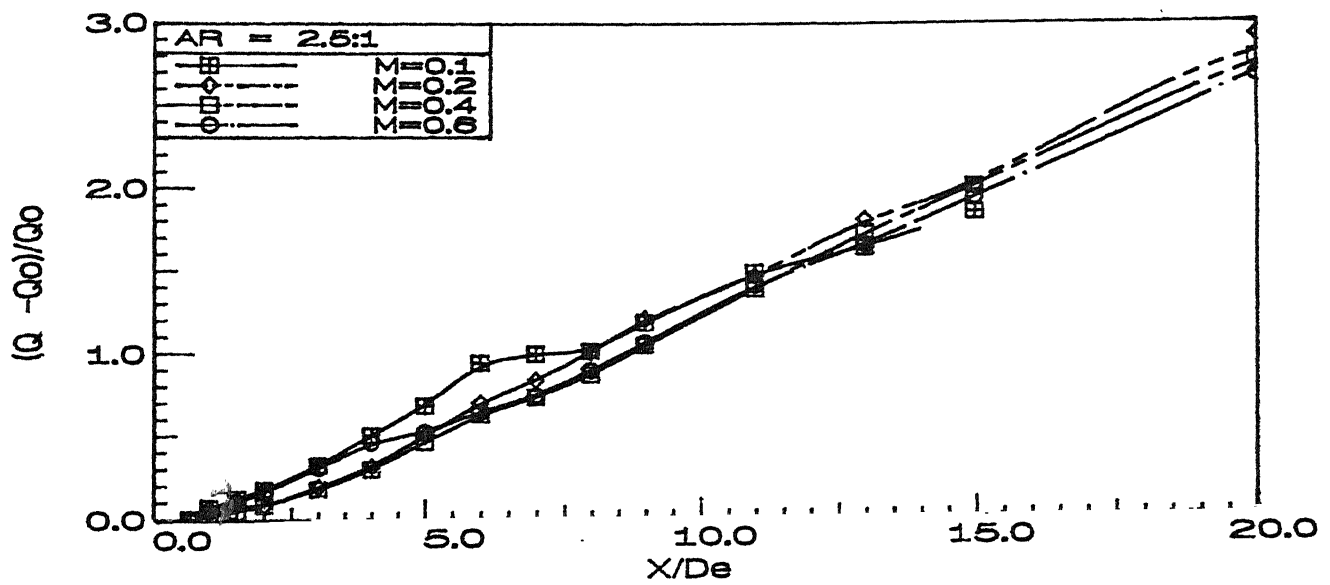
4.c Three Dimensional half width spread ($AR = 4$ $M_e = 0.2$)



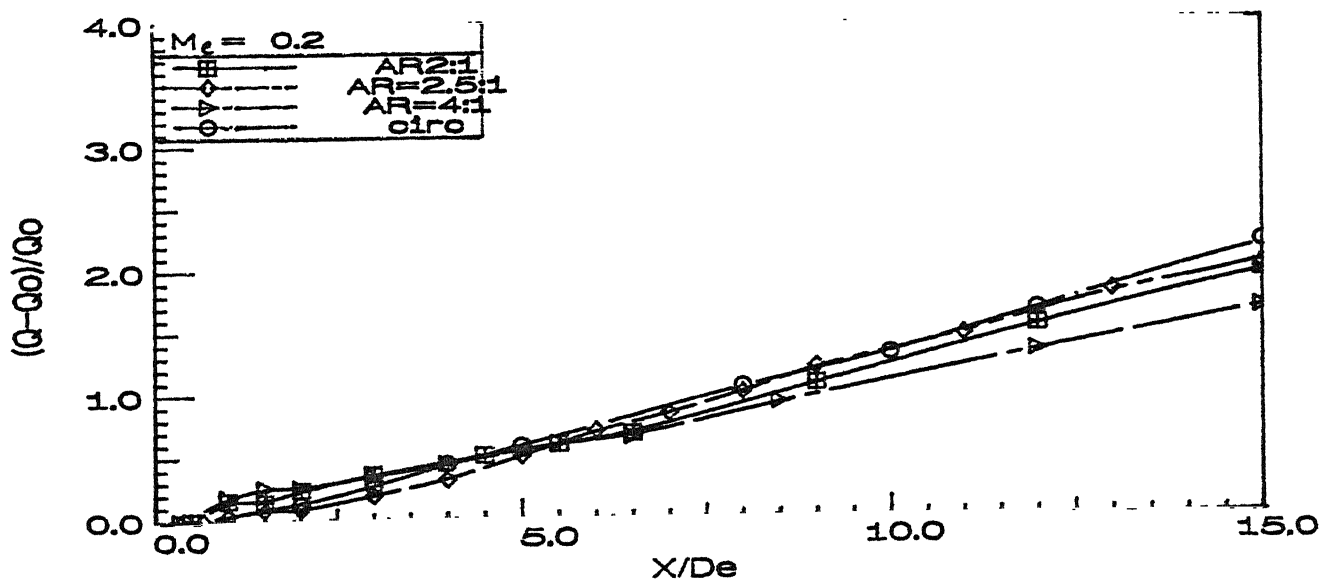
5.a Momentum flux for all Mach numbers ($AR = 2.5$)



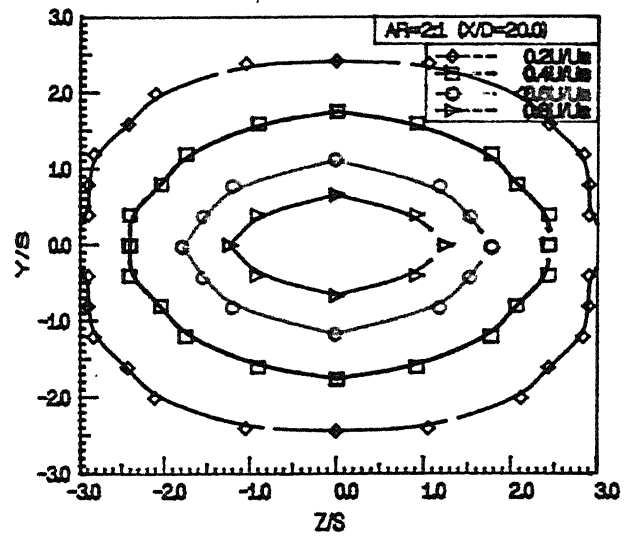
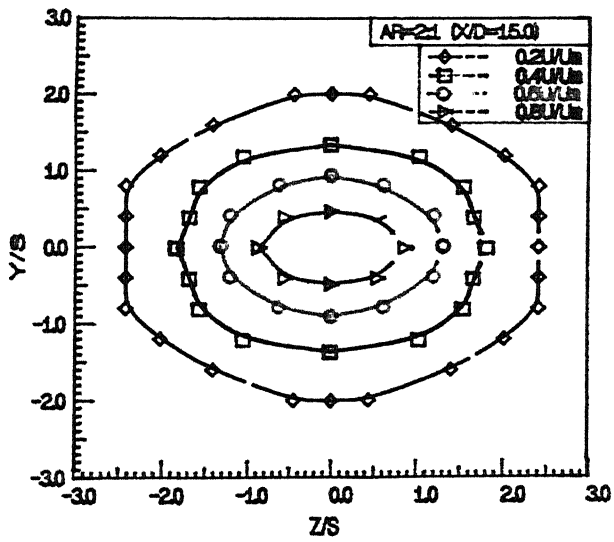
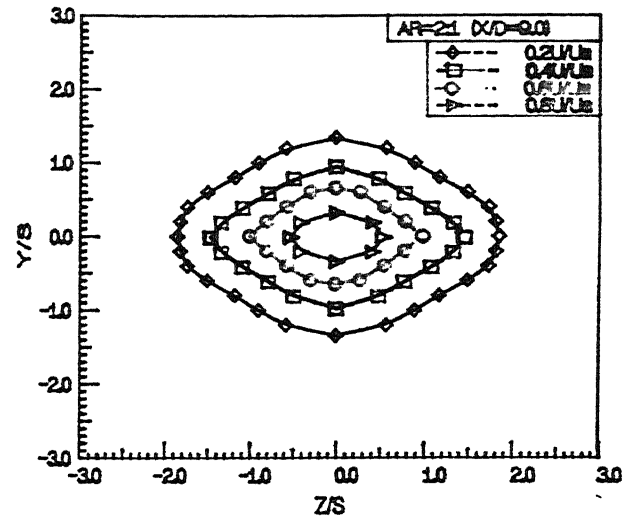
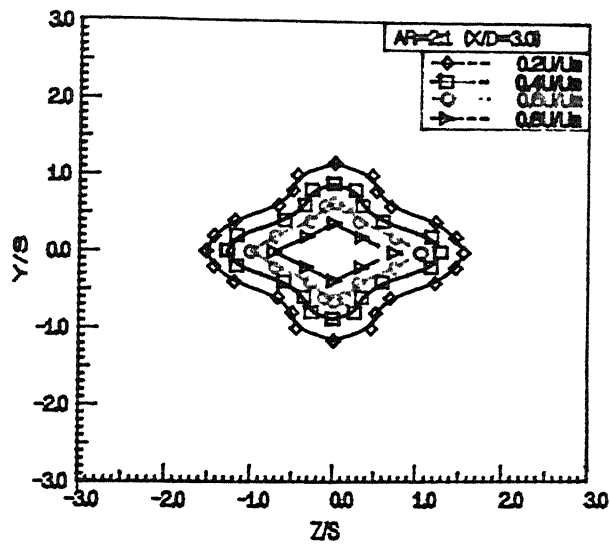
5.b Momentum flux for all aspect ratios



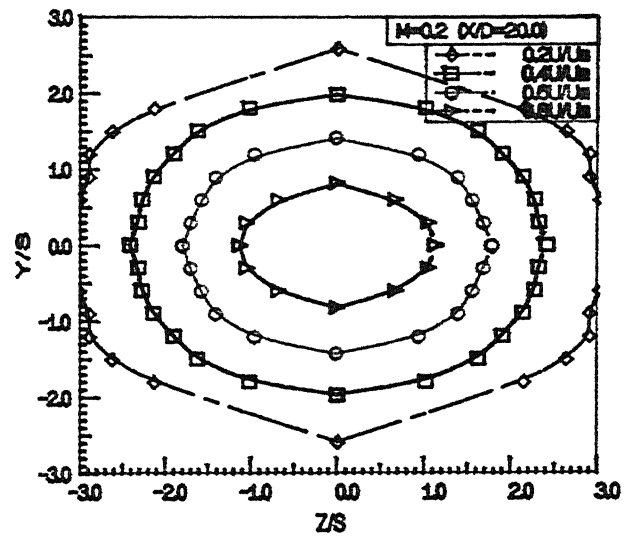
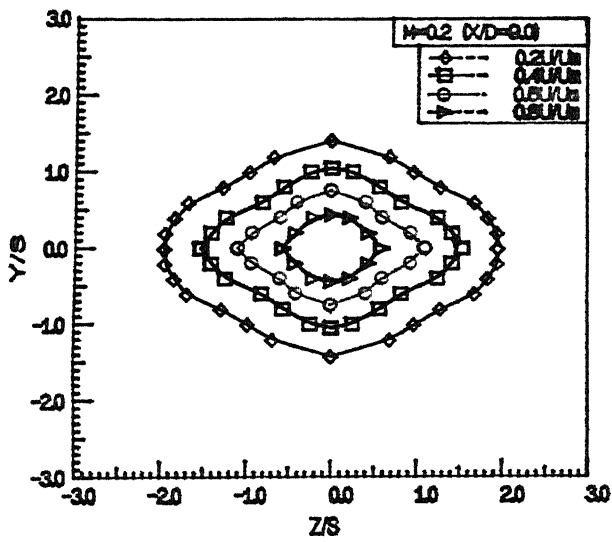
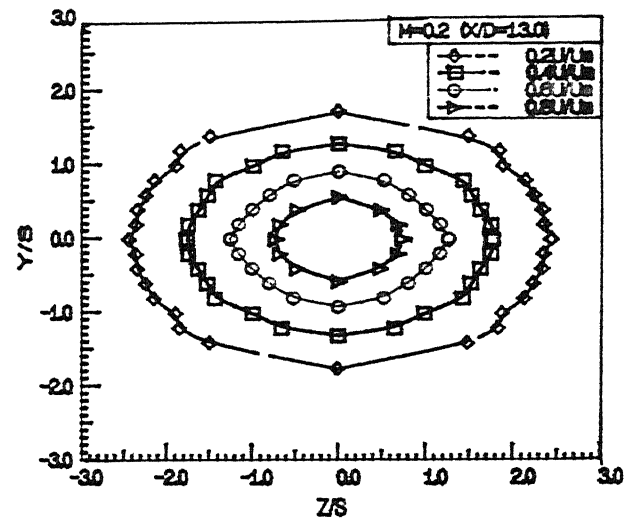
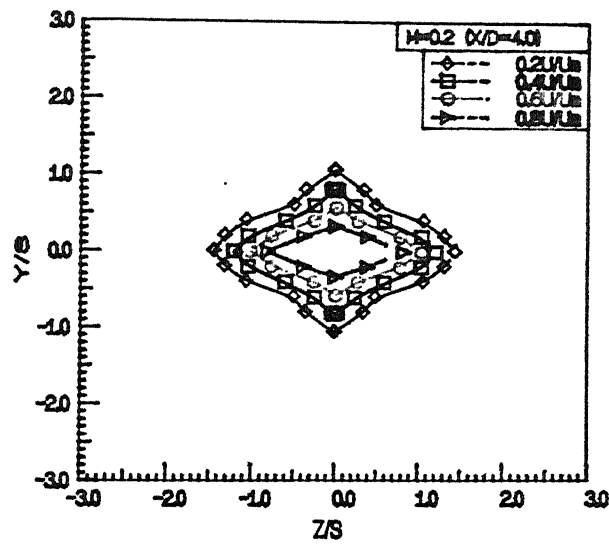
6.a Variation of entrainment with axial location ($AR = 2.5$)



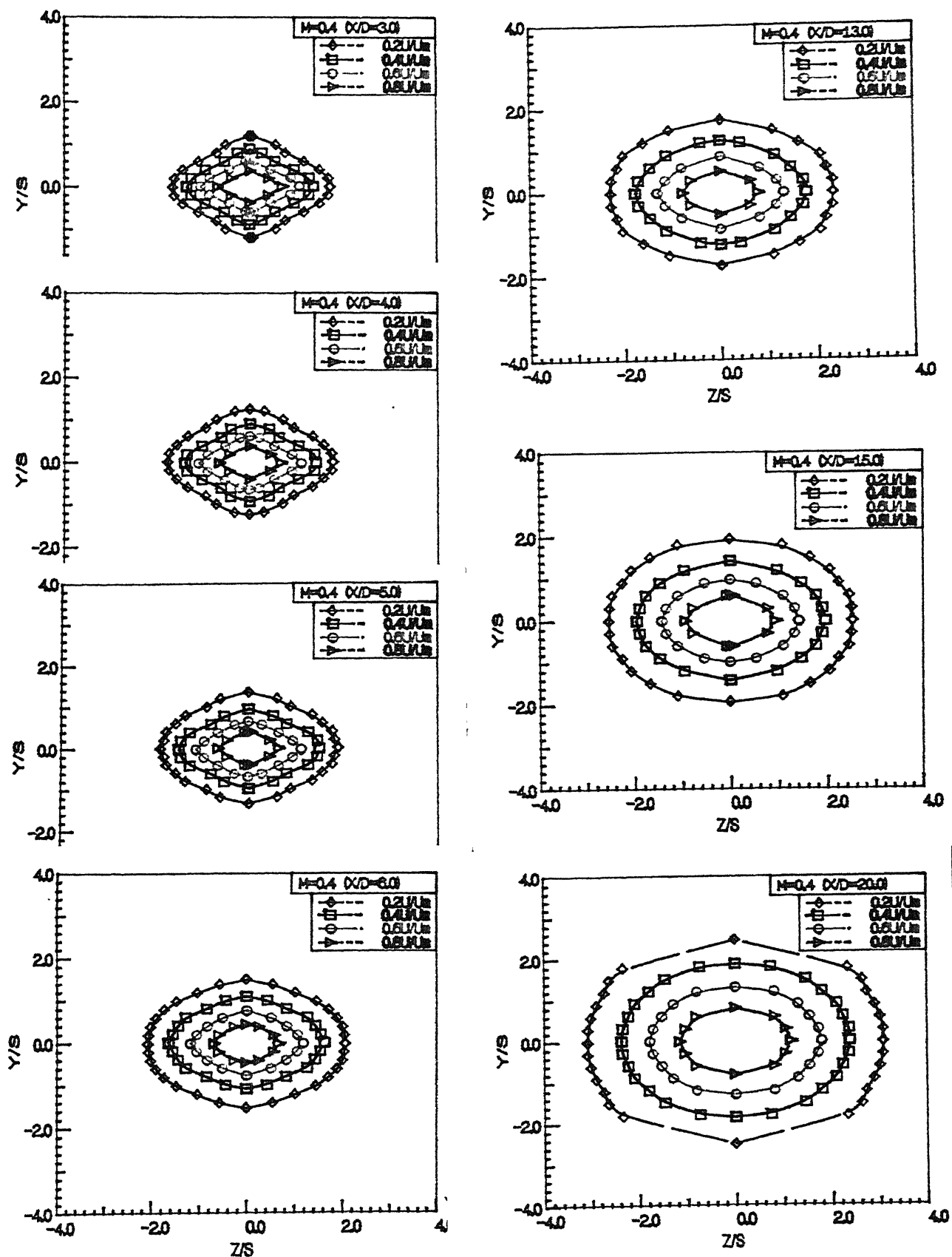
6.b Variation of entrainment with axial location ($Me = 0.2$)



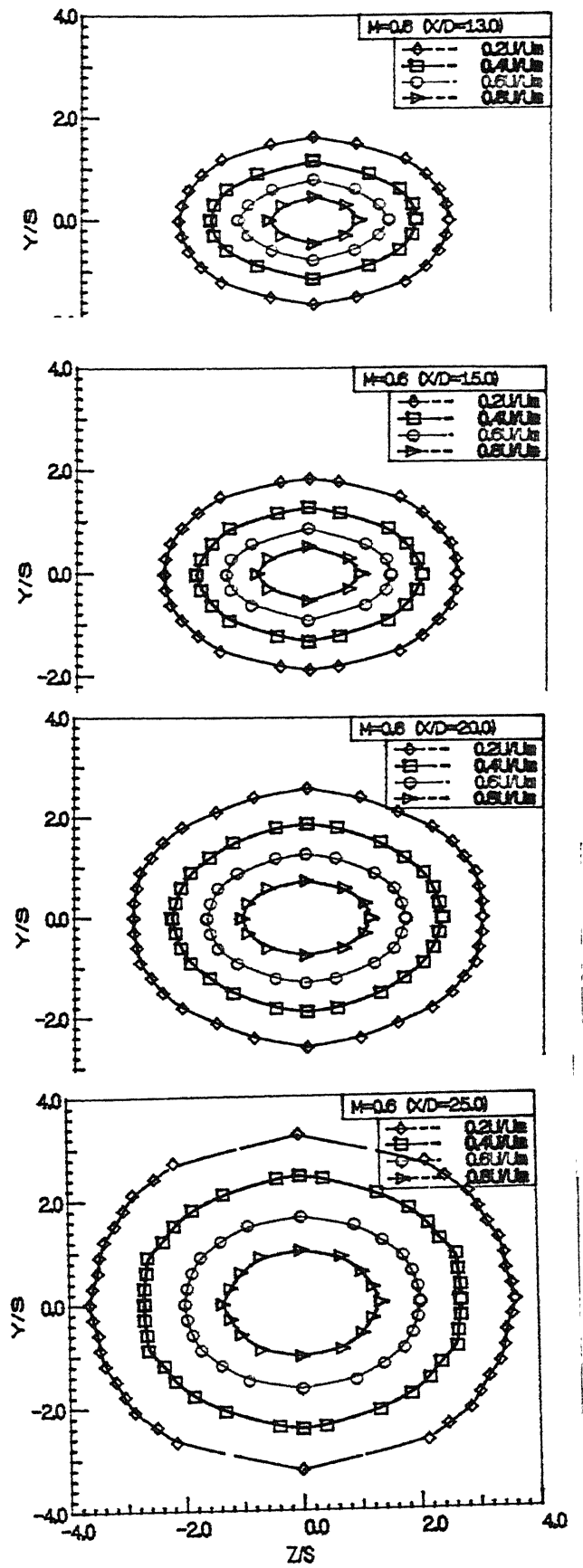
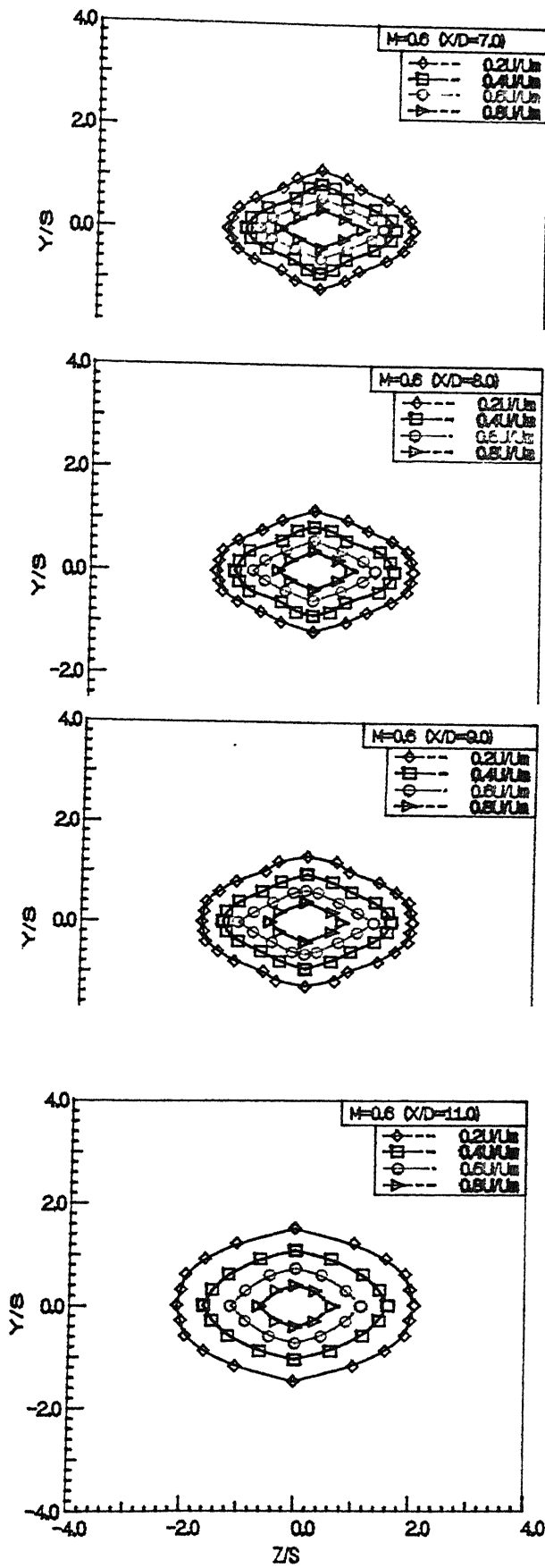
7.a Constant velocity contours ($AR = 2$, $M_e = 0.2$)

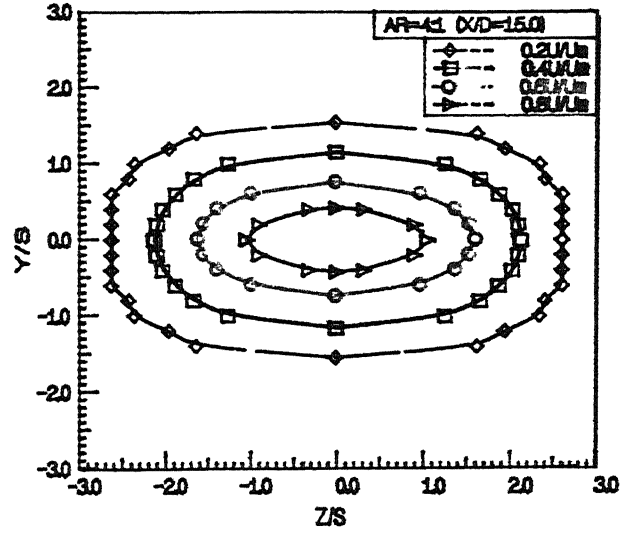
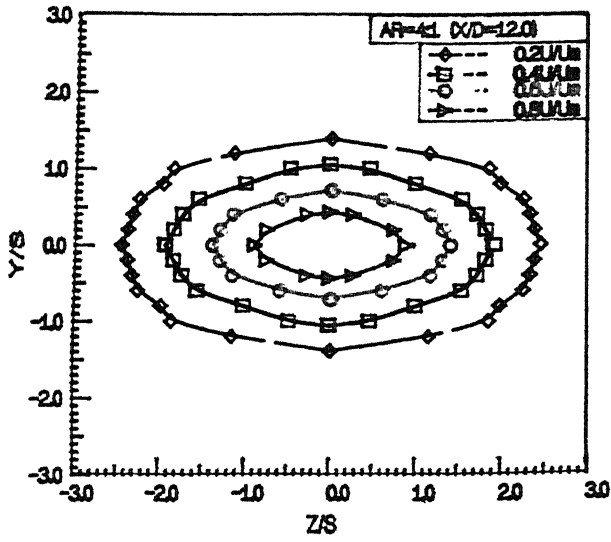
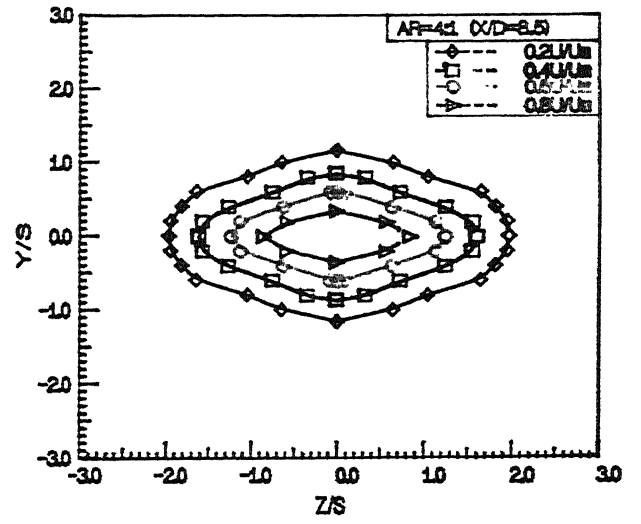
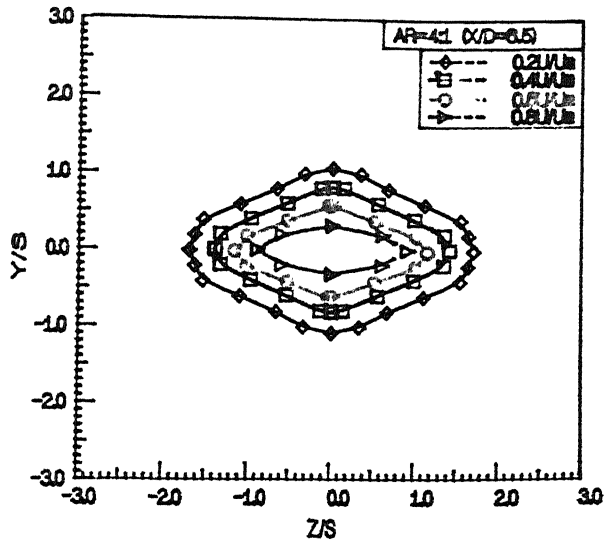


7.b1 Constant velocity contours ($AR = 2.5$, $M_e = 0.2$)

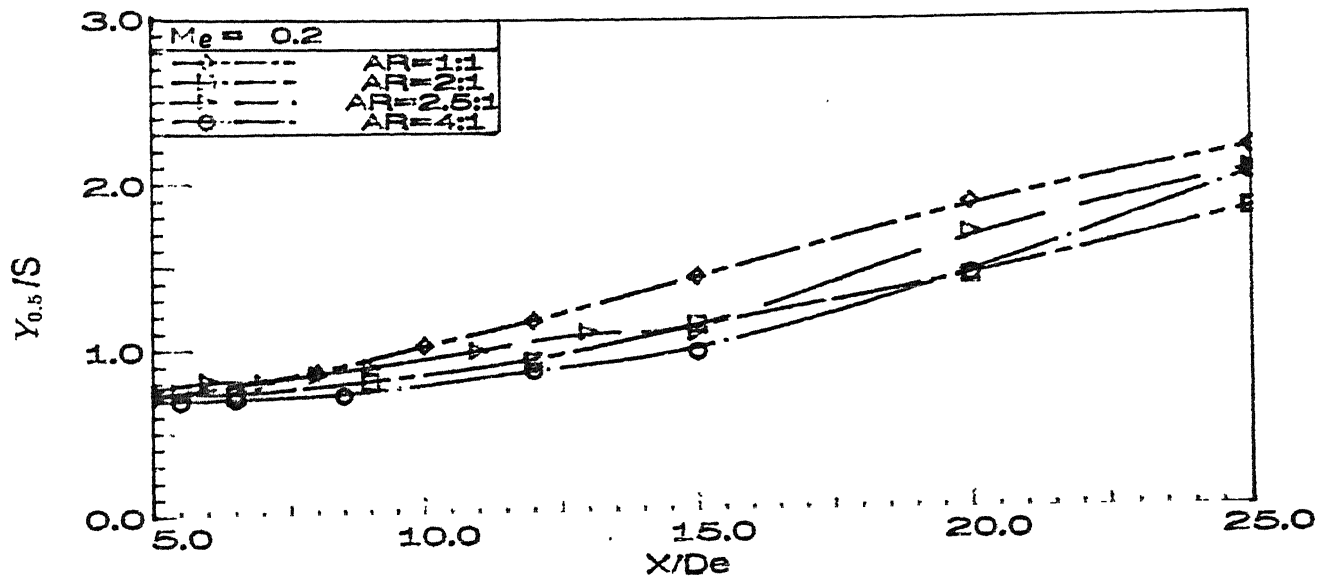


7.b2 Constant velocity contours ($AR = 2.5$, $M_e = 0.4$)

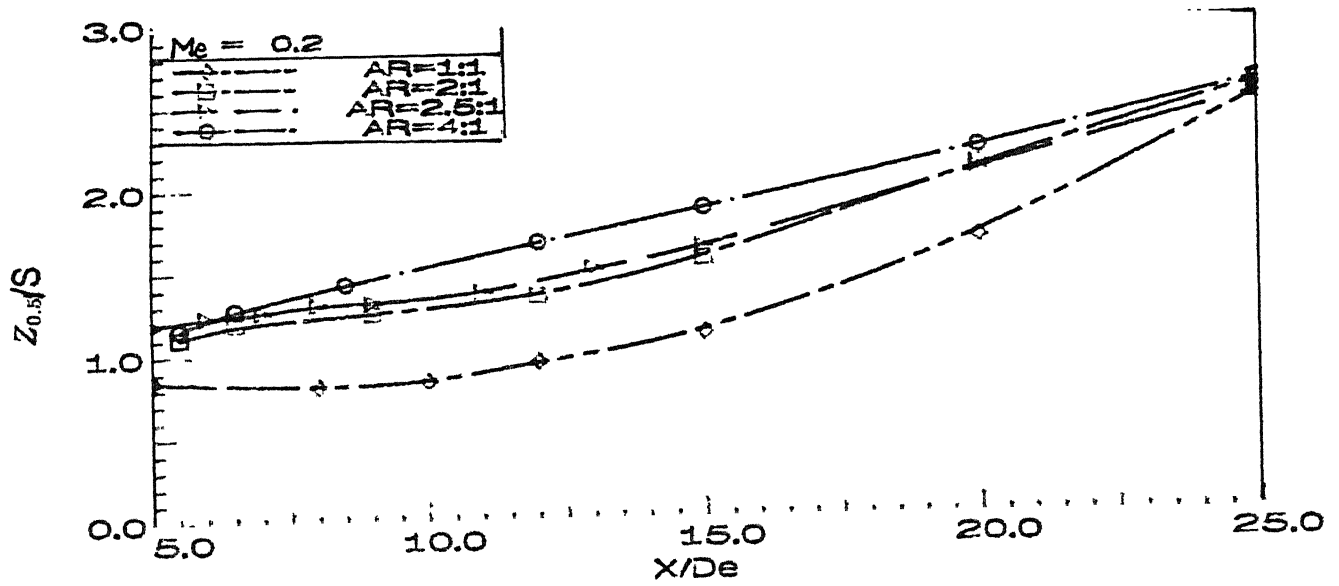




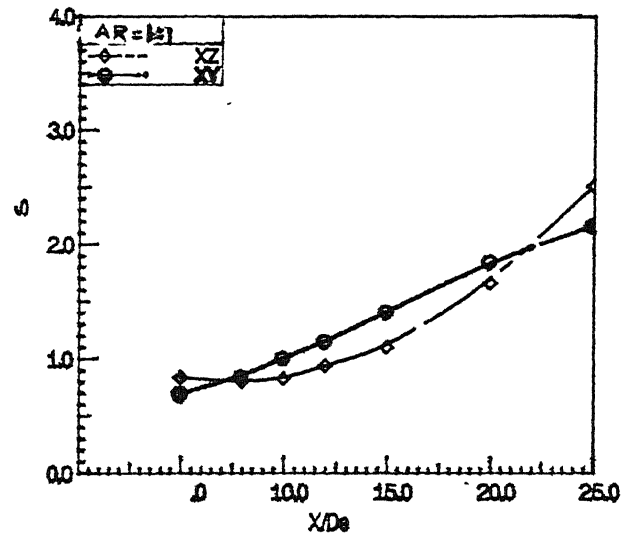
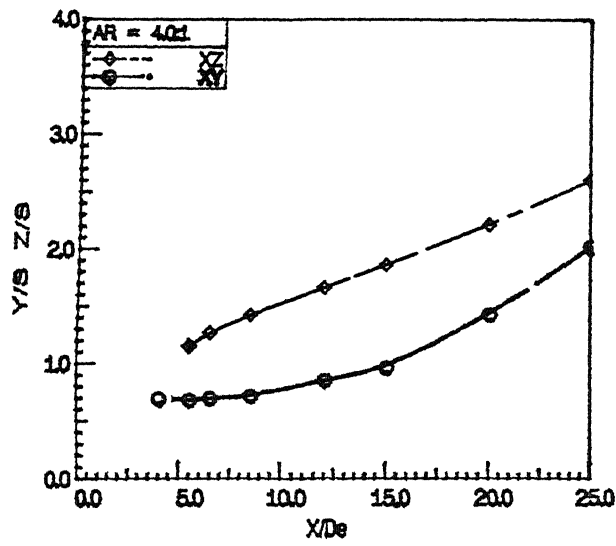
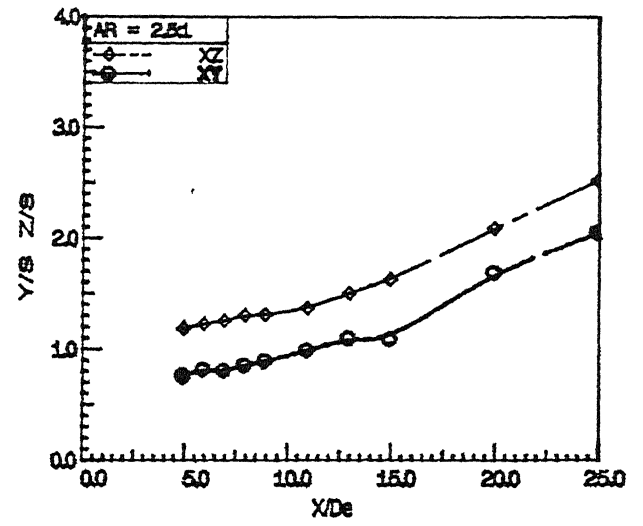
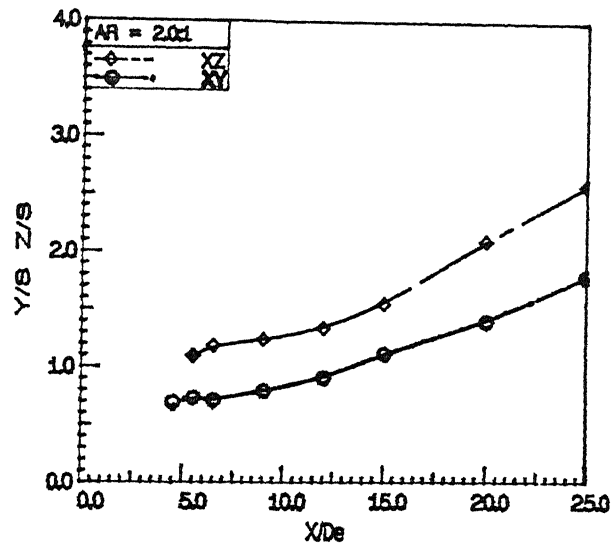
7.c Constant velocity contours ($AR = 4$, $M_c = 0.2$)



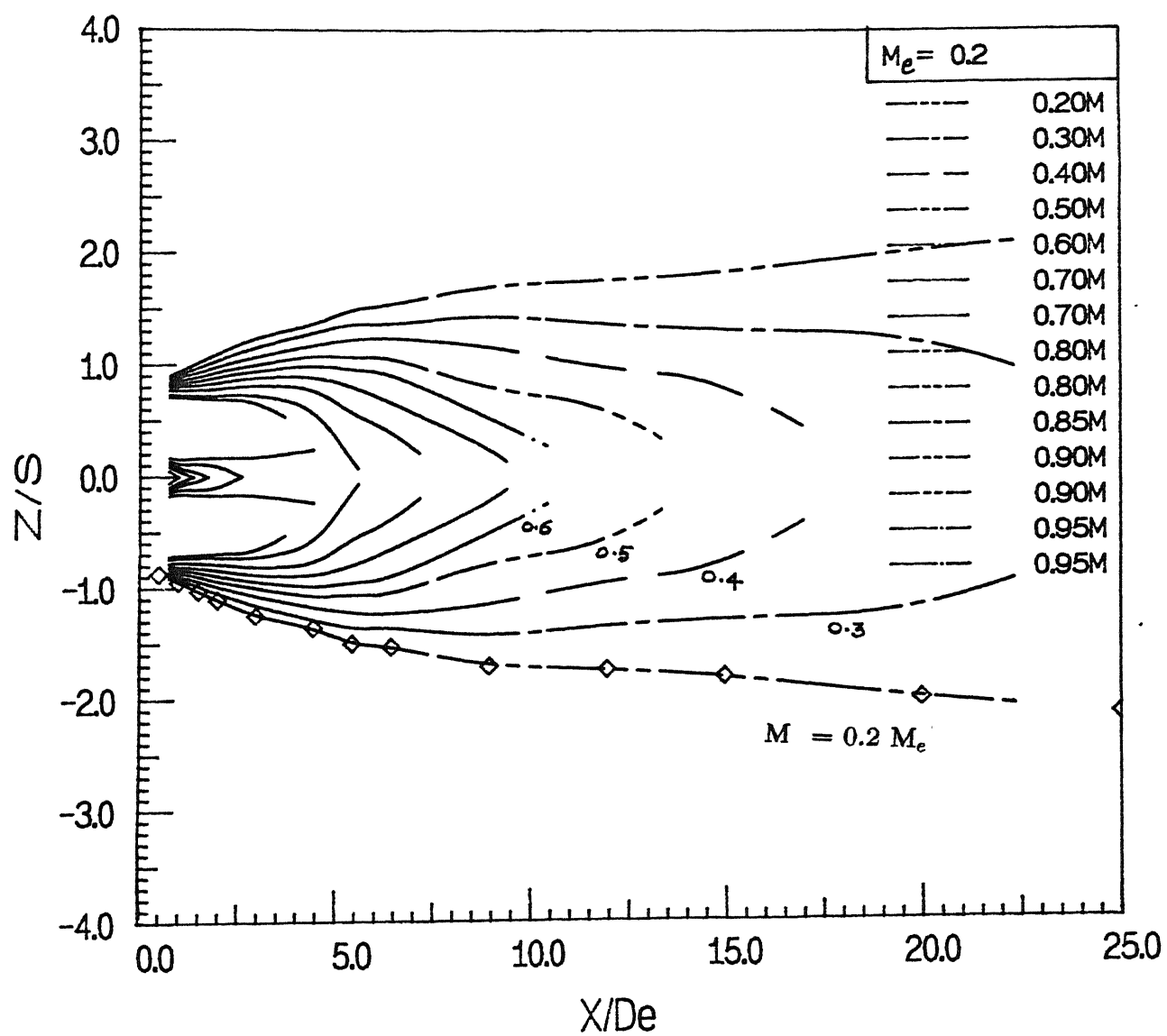
8.a1 Comparison of half width velocity in XY plane



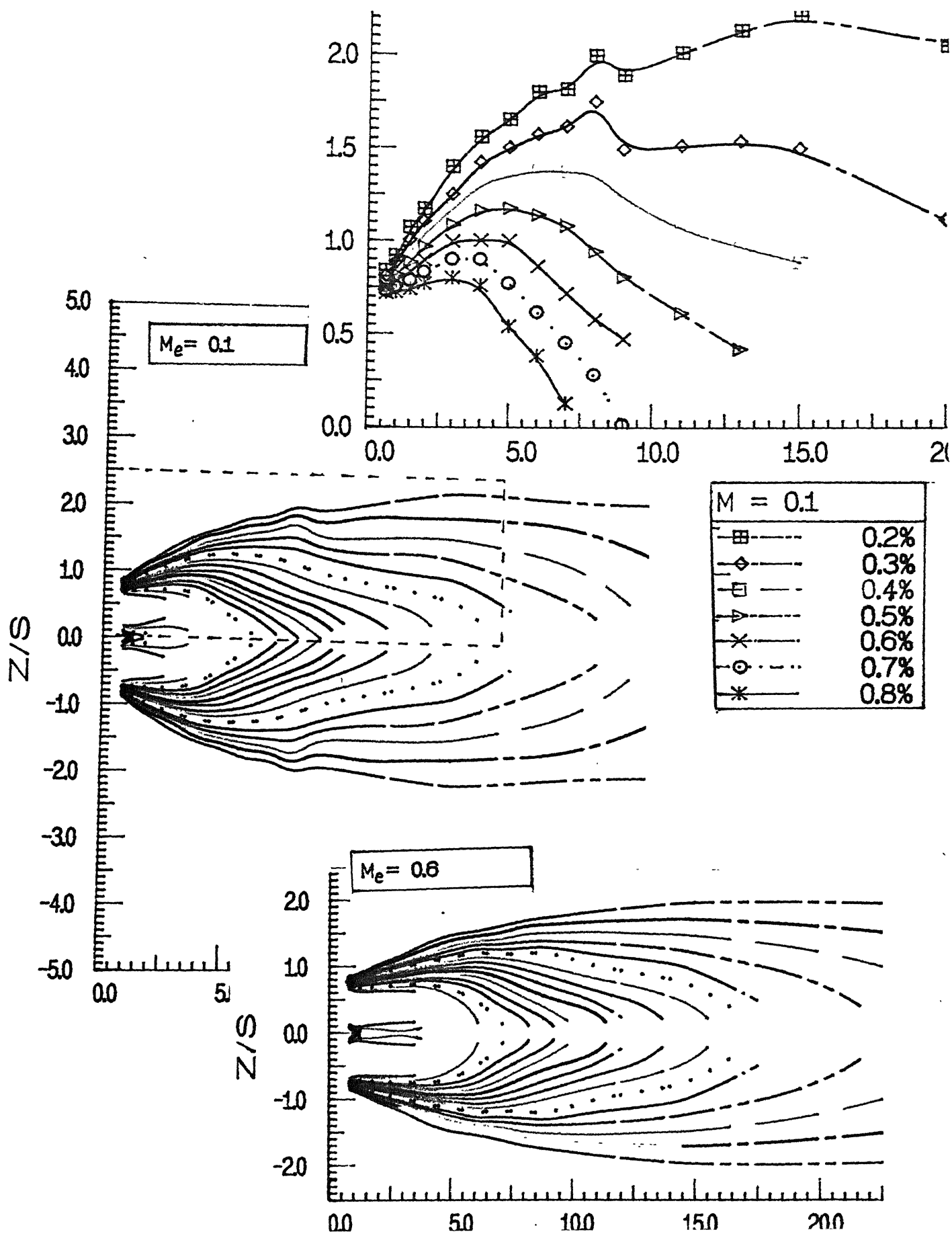
8.a2 Comparison of half width velocity in XZ plane

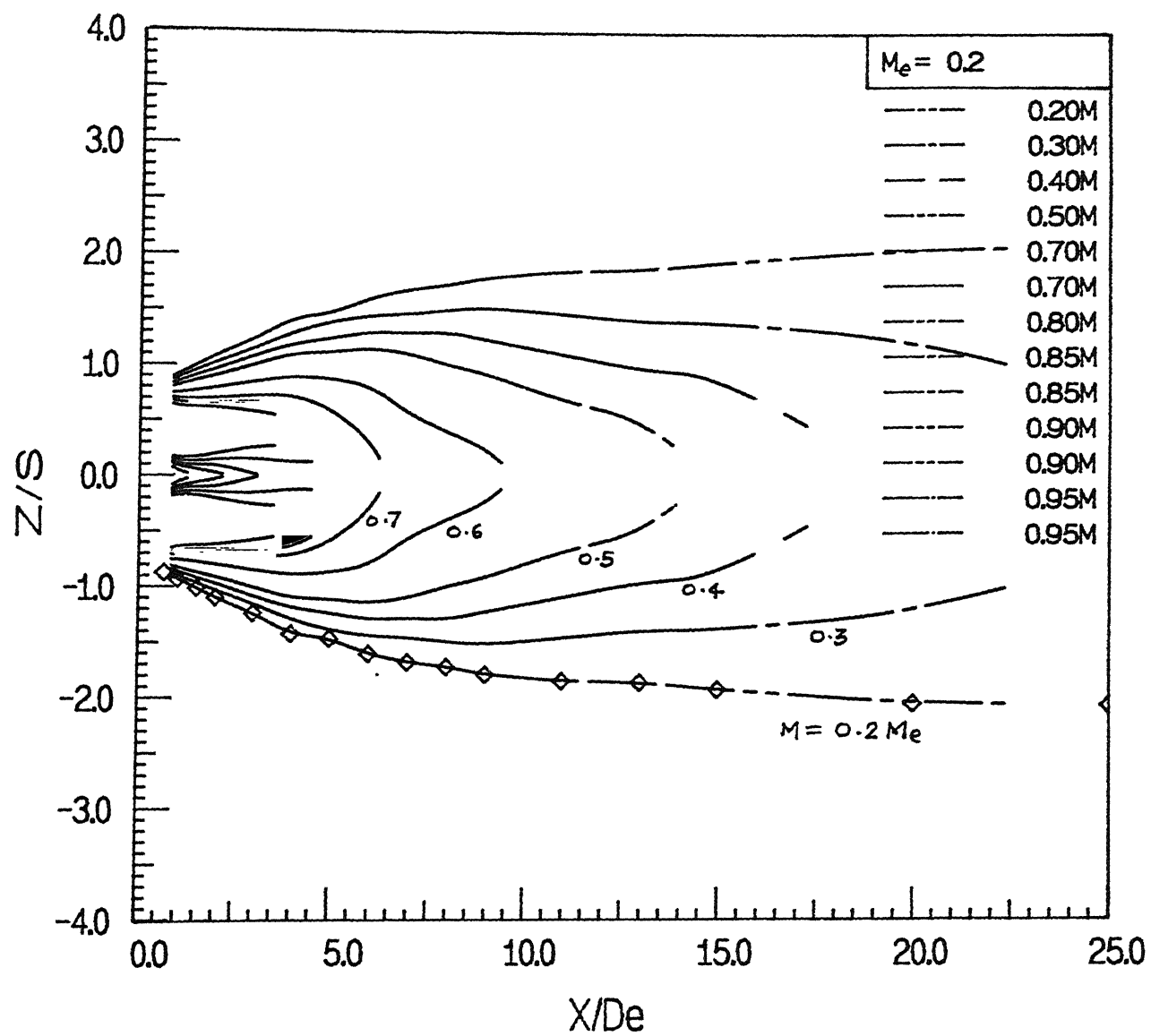


8.b Half spread lines in XZ and XY plane

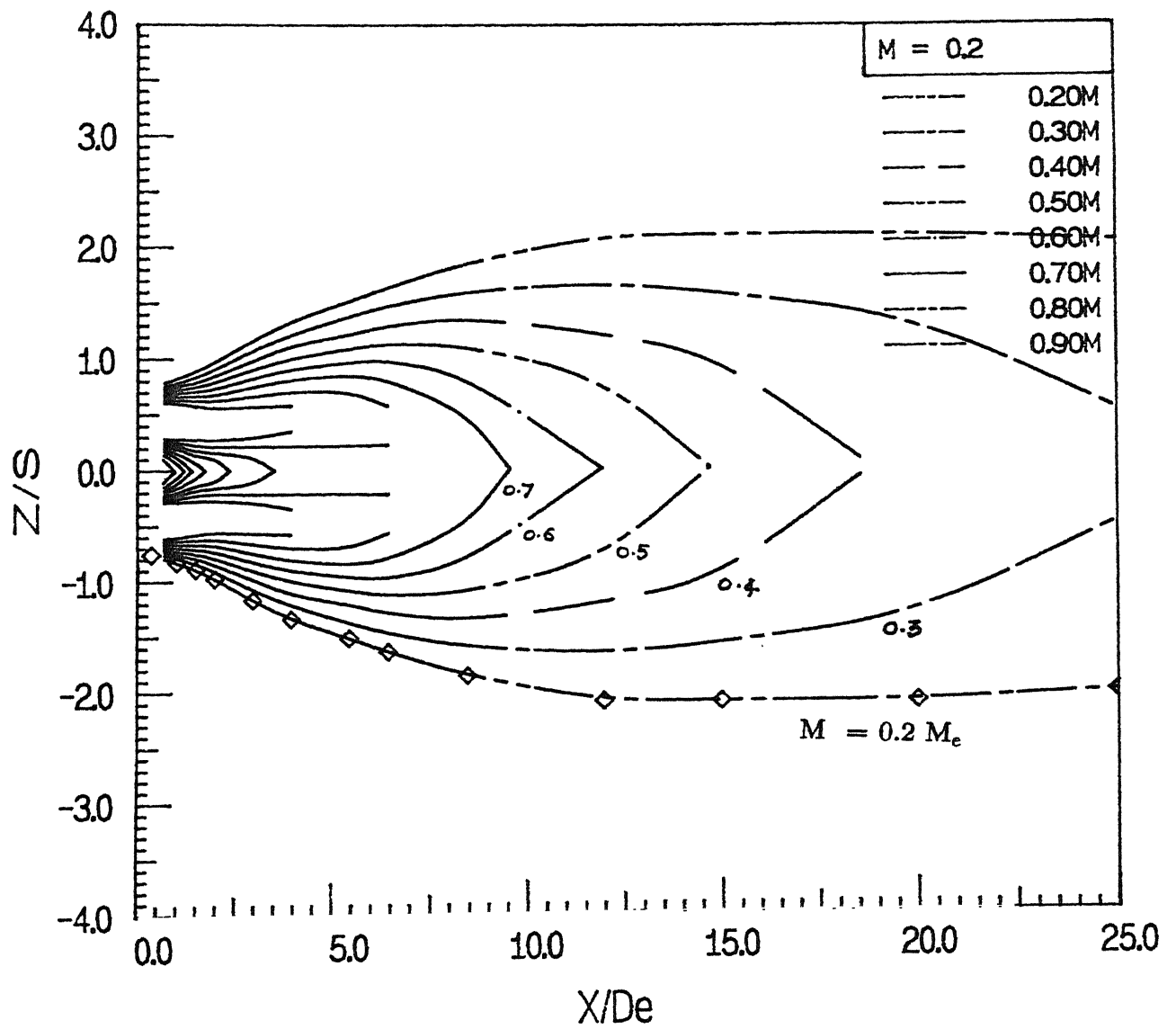


9.a Iso Mach profiles ($AR = 2$, $M_e = 0.2$)

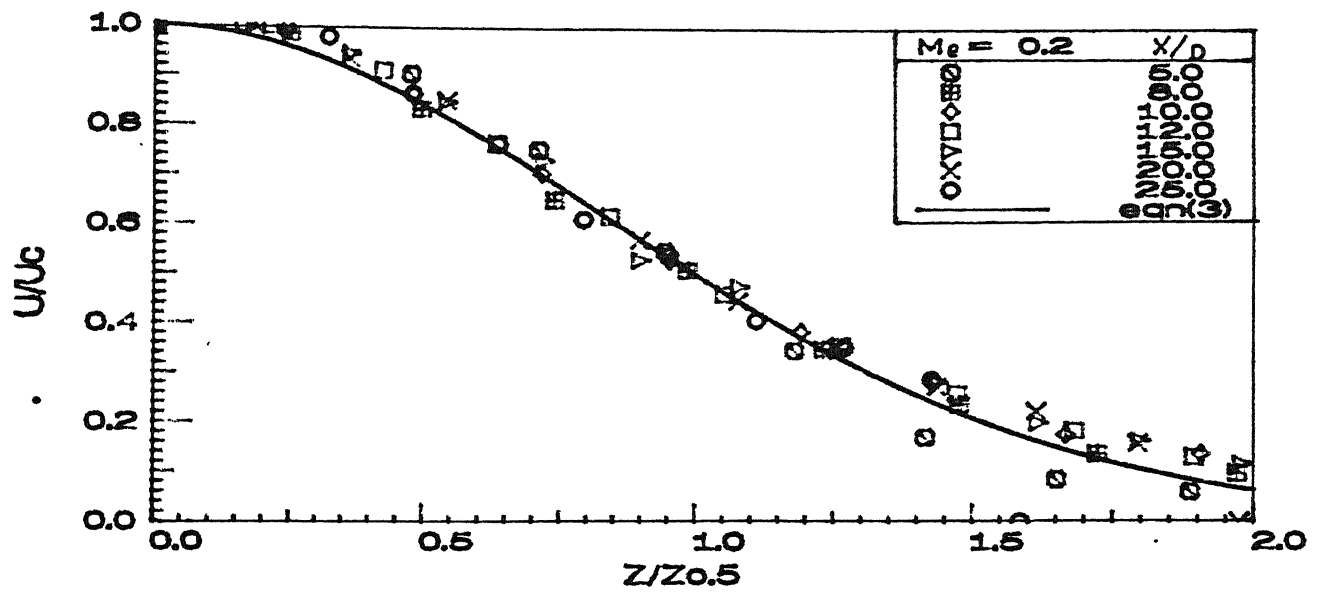




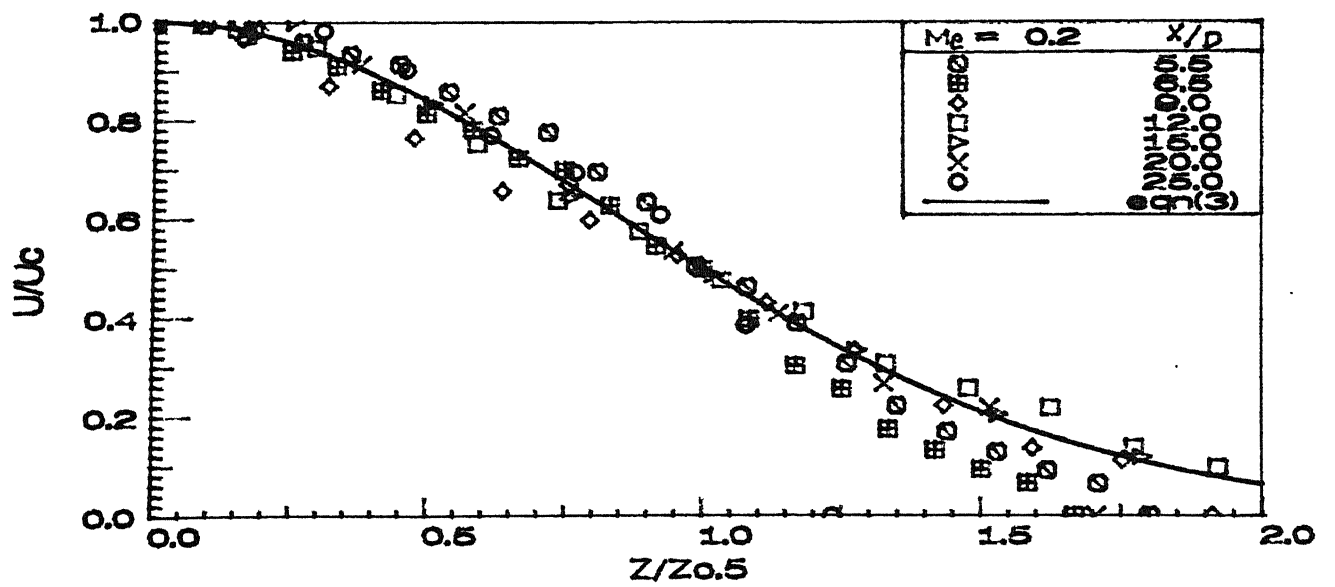
9.b2 Iso Mach profiles ($AR = 2.5$, $M_e = 0.2$)



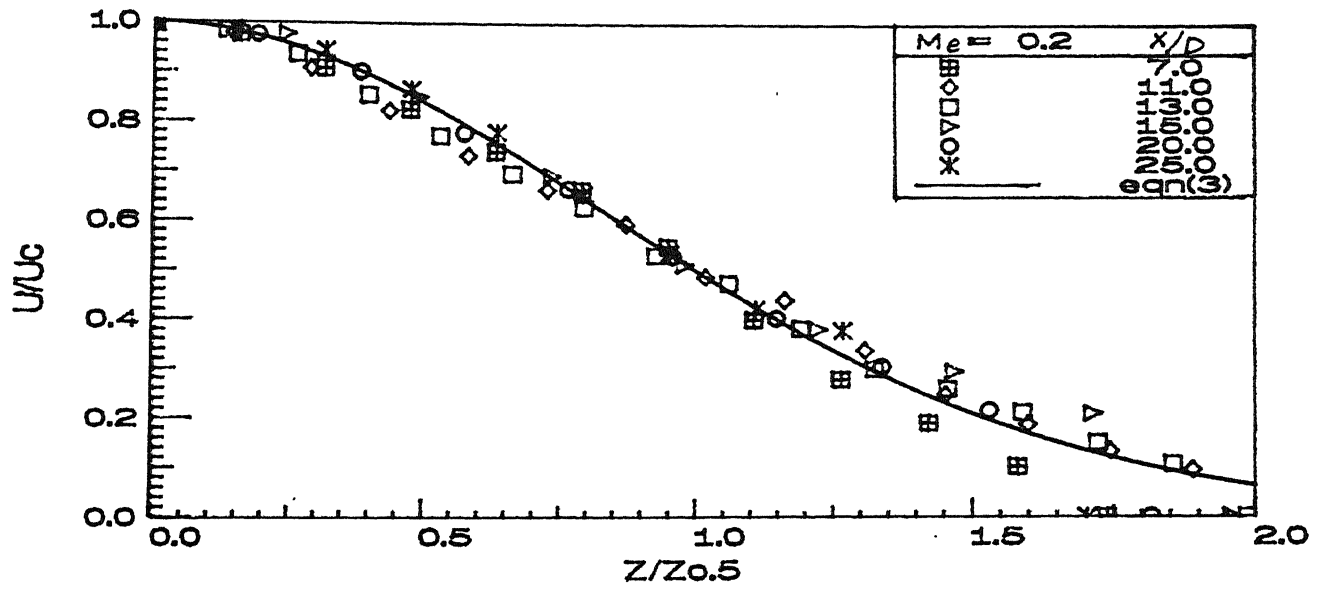
9.c Iso Mach profiles ($AR = 4$, $M_e = 0.2$)



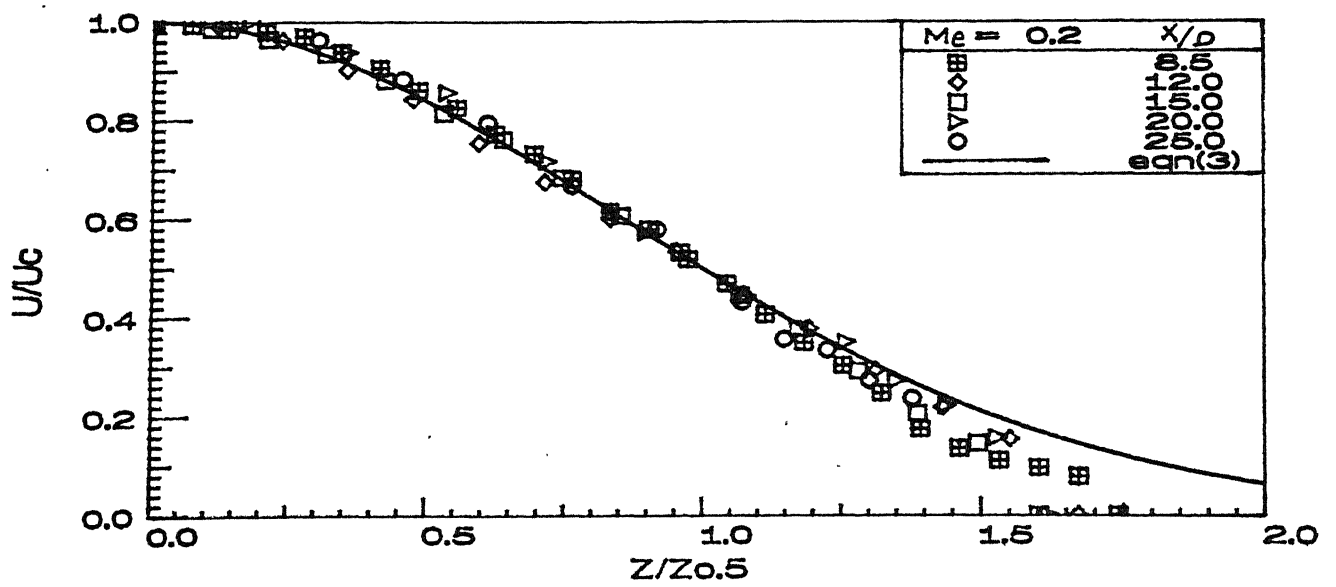
10.a Similarity profiles for AR 1:1



10.b Similarity profiles for AR 2:1



10.c Similarity profiles for AR 2.5:1



10.d Similarity profiles for AR 4:1